Alternative splicing as a regulatory mechanism of the NLRP3 inflammasome

Dissertation

zur

Erlangung des Doktorgrades (Dr. rer. nat.)

der

Mathematisch-Naturwissenschaftlichen Fakultät

der

Rheinischen Friedrich-Wilhelms-Universität Bonn

vorgelegt von

Florian Hoß

aus

Neuwied

Bonn, September 2018

Angefertigt mit Genehmigung der Mathematisch-Naturwissenschaftlichen Fakultät der Rheinischen Friedrich-Wilhelms-Universität Bonn

1. Gutachter: Prof. Dr. med Eicke Latz
2. Gutachter: Prof. Dr. med. Joachim L. Schultze

Tag der Promotion: 02.04.2019
Erscheinungsjahr: 2019

Table of Contents

1. Zusammenfassung

Wesentlicher Bestandteil des angeborene Immunsystems sind vererbbare Rezeptoren, die pathogene Muster oder Veränderungen der Zell-Homöostase erkennen. Nach Aktivierung durch Pathogene oder sterile Gefahrensignale können einige intrazelluläre Rezeptoren des angeborenen Immunsystems (z. B. NLRP3) multimere Signalübertragungsplattformen, sogenannte Inflammasome, bilden. Diese führen zur Aktivierung von Caspase-1, die sowohl einen pyroptotischen Zelltod, als auch die Aktivierung der Zytokine IL-1β und IL-18 induziert. NLRP3 spielt eine zentrale Rolle in kardiovaskulären, neurodegenerativen und entzündlichen Erkrankungen.

Ziel dieser Studie war es, zu erörtern, ob alternatives Splicing (AS) als regulatorische Instanz für die Aktivierung des NLRP3-Inflammasoms dient, ähnlich wie es für andere Immunrezeptoren oder pflanzliche Resistenzgene gezeigt wurde. Ich konnte zeigen, dass die NLRP3 LRR-Domäne von repetitiven, stark konservierten Exonen kodiert wird und dies eine Eigenschaft ist, die auch weitere LRR-kodierende Genfamilien besitzen. Diese strikte Modularität der LRR-Exone erlaubt AS, ohne strukturelle Schäden zu induzieren. Tatsächlich konnte ich AS mehrerer NOD-like Rezeptoren nachweisen, am prominentesten in NLRP3. Der häufigsten humanen alternativen NLRP3 Isoform fehlt Exon 5. In murinem NLRP3 konnte keine alternative Variante detektiert werden.

Mit Hilfe verschiedener Modellsysteme und Testmethoden konnte ich zeigen, dass NLRP3 Δ Exon 5 inert gegenüber gängigen Aktivatoren ist. Des Weiteren konnte ich aufzeigen, dass die Regulation der NLRP3 Isoformen auf Einzelzellebene stochastisch erfolgt. Die mechanistische Begründung der Inaktivität von NLRP3 Δ Exon 5 liegt im Verlust der Interaktionsfähigkeit mit NEK7. Unerwarteterweise konnte die Aktivierbarkeit von NLRP3 Δ Exon 5 durch eine Vorbehandlung von mehr als 10 Stunden mit einem entzündungsfördernden Signal wiederhergestellt werden. In Zusammenhang mit der stochastischen Prävalenz der NLRP3 Isoformen ergibt sich dadurch eine Untergruppe von Zellen, die in einer ersten Welle der NLRP3-Aktivierung nicht pyroptotisch wird und zu einem späteren Zeitpunkt unterstützend zum Entzündungsgeschehen beitragen kann.

Zusammengefasst zeigen die hier dargelegten Daten eine noch nicht beschriebene Art der Regulation des NLRP3-Inflammasoms durch alternatives Splicing und erlauben Einblicke in speziesspezifische regulatorische Mechanismen mit therapeutischem Potenzial, die nicht in Mausmodellen gefunden werden könnten.

2. Summary

The innate immune system relies on germ-line encoded pattern recognition receptors and is critically involved in the early sensing of pathogens and disturbances of cell homeostasis. Upon activation by pathogenic or sterile danger signals, several cytosolic receptors of the innate immune system (e.g. NLRP3) can recruit multi-protein signaling platforms, so called inflammasomes. Inflammasome formation leads to the activation of caspase-1, causing pyroptosis as well as maturation and release of IL-1β and IL-18. NLRP3 is critically involved in several cardiovascular, neurodegenerative and inflammatory diseases.

This study aimed to decipher whether alternative splicing (AS) might act as a regulator of NLRP3 inflammasome activation, similarly to what is described for other vertebrate immune receptors and plant R-proteins. I could show that the LRR of NLRP3 is encoded by multiple repetitive and highly conserved exons, a feature which is shared by other LRR encoding genes. This strict exonic modularity of LRR domains of several human gene families serves as a prerequisite for non-destructive AS. Indeed, I could show AS of the LRR of several NOD-like receptors, most prominently in NLRP3. Human NLRP3, but not mouse NLRP3, could be detected as two major isoforms: The fully active NLRP3 full-length variant and a variant lacking exon 5. By use of several different model systems and readouts, NLRP3 Δ exon 5 could be shown to be inert to common NLRP3 activators. Furthermore, I could show that alternative splicing is stochastically regulated on a single-cell level. Mechanistically, I could provide evidence that NLRP3 Δ exon 5 is inactive due to the absence of a necessary interaction surface for NEK7 binding, required for NLRP3 activation. Surprisingly, a prolonged priming for over 10 h rendered NLRP3 Δ exon 5 activatable. In combination with the stochastic isoform expression, this allows for a backup pool of cells, which do not become pyroptotic in the first round of NLRP3 inflammasome activation, but rather enable a sustained inflammatory response.

The data presented here provide evidence for a not yet described regulatory role of AS in NLRP3 inflammasome activation through differential utilization of highly conserved LRR modules. Moreover, the species differences described here might hold therapeutic potential that could not have been revealed in mouse models.

3. Introduction

3.1. The immune system

While the historic roots of modern medicine reach back several thousand years, immunology, the science of how an organism defeats infections, is relatively young. Although mankind always invented treatments against diseases, some of the biggest breakthroughs were based on immunological findings. At the end of the 18th century, Edward Jenner used cowpox to successfully vaccinate against smallpox. In the 19th century, Robert Koch proved microorganisms to be the cause of infectious diseases, and Pasteur and others extended the repertoire of available vaccinations. At the same time, two key findings already heralded the separation of the immune system (IS) into two branches, the adaptive and the innate IS: Kitasato, Ehrlich and von Behring discovered antibodies as specific circulating antitoxins, while Metchnikoff described macrophages as cells able to engulf and digest microbes. Since then, our knowledge of the IS has increased enormously and immunology has evolved into a flourishing field of research.

The first line of defense is provided by epithelial and mucosal tissues, which prevent the entry of pathogens and harmful substances. Below that layer, different cell types of the innate and adaptive IS are located to recognize and fight invading pathogens. Besides, specialized immune cells, located in other organs, can be recruited to the site of infection, and different soluble factors, such as antibodies or the complement system, contribute to clearance of the infection and recovery to homeostasis.

Simplistically, the innate IS constitutes a rather unspecific, but readily available task force, while the adaptive IS is composed of specialized immune cells which need to be educated before activation.

The major cell types of the innate IS are macrophages, monocytes, dendritic cells (DCs), granulocytes and mast cells, which are all derived from the myeloid linage, as well as natural killer cells derived from the lymphoid linage. The adaptive IS consists predominantly of T- and B-lymphocytes, which are selected for their highly specific antigen receptors and are able to either specifically kill infected cells or secrete highly specific antibodies against pathogens, respectively. Moreover, they can provide a long-lasting memory against pathogens after a first encounter, a mechanism utilized by vaccinations. The huge variety of the receptors of the adaptive IS is achieved via a complex gene-rearrangement process [1]. The two branches of the IS are highly dependent on each other. Mostly myeloid cells engulf and digest pathogens and

present the derived pathogen-specific peptides to T cells in order to educate them. Depending on an either pro- or anti-inflammatory environment so called T-helper cells can afterwards license B-lymphocytes for antibody production or cytotoxic T-killer cells [1].

The IS of higher vertebrates is a complex, non-spatial defined organ, which is distributed all over the body and does not act independently of other organs and tissues. Immune cells clear infections, remove harmful substances, play a role in wound healing and detect malignant tissue aberrations [2], but their function is fine-tuned by a pleiotropy of positive and negative signals from other non-immune tissues [3].

3.1.1. The innate IS

Cells of the innate IS are often the first to detect a threat and to initiate an immune response. Tissue-resident innate cells such as macrophages, DCs or mast cells are enriched at likely sites of infection and upon activation, recruit further cells by secreting cytokines and chemokines. The first wave of recruited cells consists of neutrophils and monocytes, which support the tissue-resident cells in phagocytosis of pathogens, followed by the release of antimicrobial peptides, proteases and reactive oxygen species. Professional antigen-presenting cells such as DCs, provide co-stimulatory interactions and secrete cytokines to induce a specific adaptive immune response. Following the immune response, cells of the IS are also responsible for the induction of tissue repair and re-establishment of homeostasis [1].

Although eosinophils and basophils have been phenotypically described for a long time, relatively little is known about their exact functions except for their role in the defense against multicellular pathogens [4]. Over the last years, it became evident that even platelets, which were previously only known for their role in coagulation, play a role in innate immunity [5].

Beside the cellular components, the innate IS consists of secreted factors known as acute phase proteins. These include C-reactive protein and complement factors, which work as opsonins and lytic agents, ferritin and haptoglobin, which inhibit bacterial iron supply, and coagulation factors, which lead to the trapping of pathogens within blood clots [4,6].

3.1.2. Pattern recognition receptors

Characteristically, innate immune cells, but also some non-immune cells express so-called pattern recognition receptors (PRRs), which can be activated by pathogen-associated molecular patterns (PAMPs) or damage-associated molecular patterns (DAMPs) [7–9]. In context of the discovered interplay between metabolism and immunity a new class of patterns was suggested to be added to the group of PRR activators, so-called homeostasis-altering molecular processes (HAMPs) [10].

In contrast to the receptors of the adaptive IS, PRRs are typically germline-encoded and their specificity cannot be altered by genomic reshuffling. Therefore, they can only detect conserved patterns [11]. To maximize their effectiveness PRRs mostly detect highly conserved pathogenic structures, which are very often integral to the pathogen's survival, replication or infectivity [11] (Figure 3-1).

PRRs can be subdivided into several sub-classes, of which the following represent the most prominent ones: Toll-like receptors (TLRs), retinoic acid inducible gene 1 (RIG-I)-like receptors (RLRs), C-type lectin receptors (CLRs), nucleotide oligomerization domain (NOD)-like receptors (NLRs) and N-terminal pyrin domain (PYD) C-terminal DNA-binding hematopoietic interferon-inducible nuclear protein (HIN) domain containing (PYHIN) family of receptors.

Vertebrate TLRs evolved to recognize mostly cell wall components and nucleic acids. Commonly used TLR agonists include Lipopolysaccharide (LPS) (TLR4), the triacylated lipopeptide Pam3CSK4 (TLR1/2) and the imidazoquinoline derivative resiquimod (R848, TLR7) [7]. TLRs are located either on the cell surface or within endosomal compartments, where they form either homo- or heterodimers. Upon activation, they can either induce the secretion of interferons via the Toll/ IL-1R homologous domain-containing adapter-inducing interferon-β (TRIF)/ tumor necrosis factor (TNF) receptor-associated factor (TRAF) pathway or they signal via the myeloid differentiation primary-response protein 88 (MyD88)/ IL-1R-associated kinase 4 (IRAK4) complex, which leads to nuclear factor kappa-light-chain-enhancer of activated B cells (NF-$_k$B) activation and the production of pro-inflammatory cytokines. Within the class of TLRs, TLR4 is unique, as it is able to induce both pathways [7,12].

The cytosolic RLRs induce a general anti-viral state of the cell and the production of type-I interferon upon sensing viral double-stranded (ds) RNA [13]. RIG-I, the namesake of this family, seems to mainly recognize the 5'triphospate signature of dsRNA [14].

CLRs are well known for their role in in anti-fungal immunity. However, they might also contribute to the defense of parasites, bacteria and viruses. Dectin-1, Mincle, mannose-receptor and DC-SIGN represent prominent members of the CLR family. Upon activation, they induce an antimicrobial response, pro- or anti-inflammatory cytokines and phagocytosis [4,15].

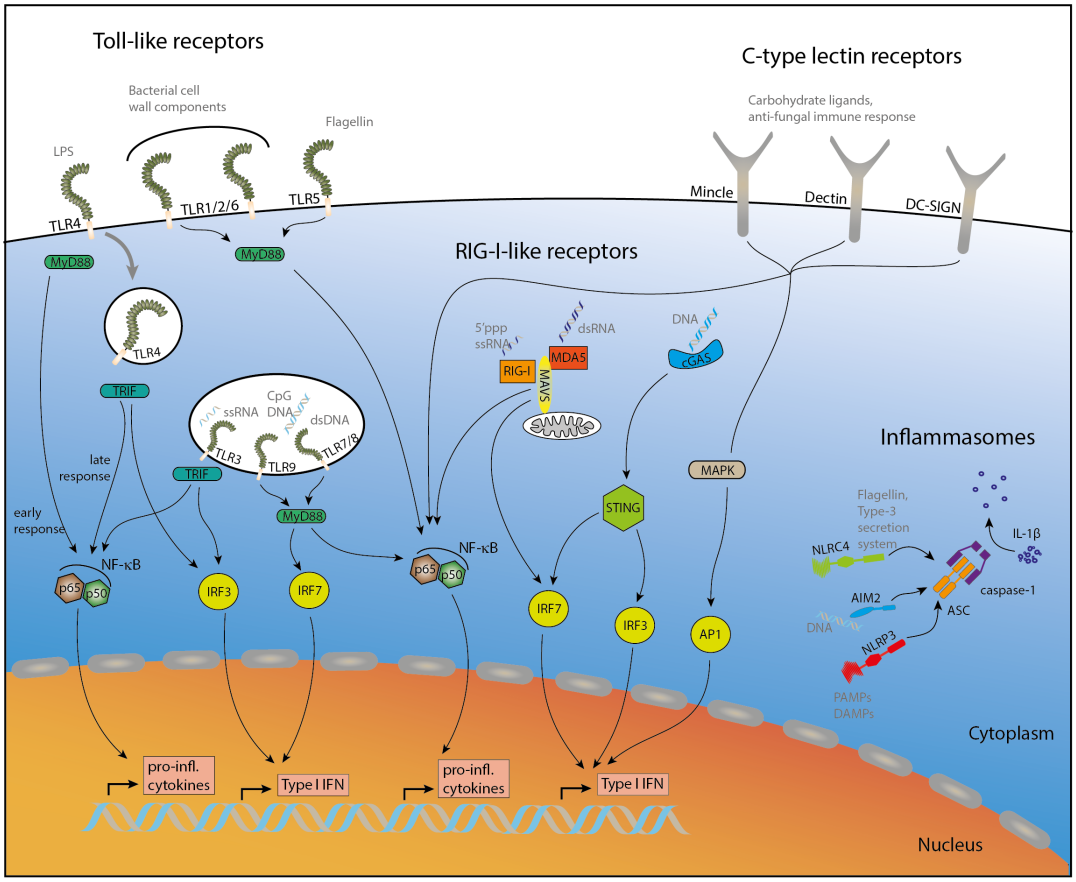

Figure 3-1 Pattern recognition receptors of the innate immune system
TLRs located on the cell surface mostly recognize components of bacterial cell walls and other directly extracellularly available microbial structures. Endosomal TLRs sense nucleic acids and molecules, which are only available after uptake and digestion. TLRs signal via MyD88 and TRIF to induce the NF-κB or IRF-dependent transcription of pro-inflammatory cytokines and type I IFNs. RIG-I and MDA5 act as cytosolic nucleic acid sensors preferentially detecting RNA, while cGAS/STING is the default cytosolic DNA sensor, inducing a potent type-I IFN response. C-type lectin receptors bind to carbohydrates and are predominantly involved in anti-fungal immune responses. AIM2, NLRP3 and NLRC4 are all capable of inducing inflammasome formation. Key events in inflammasome activation are ASC speck formation, caspase-1 self-activation and IL-1β maturation.
AP1: activator protein 1; AIM2: absent in melanoma 2; ASC: apoptosis-associated speck-like protein containing a caspase activation and recruitment domain; cGAS: cyclic GMP-AMP synthase; DC-SIGN: Dendritic cell-specific ICAM-grabbing non-integrin; IL: Interleukin; IRF: interferon regulatory factor; LPS: lipopolysaccharide; MAPK: mitogen-activated protein kinase; MAVS: mitochondrial antiviral signaling protein; MDA5: melanoma differentiation antigen 5; MyD88: myeloid differentiation primary-response protein 88; NF-κB: nuclear factor kappa-light-chain-enhancer of activated B cells; NLRC: nucleotide-binding oligomerization domain-containing protein with a caspase recruitment domain; NLRP: nucleotide-binding oligomerization domain -, leucine-rich repeat-, pyrin domain- containing; Pro-infl: pro-inflammatory; RIG-I: retinoic acid inducible gene 1; STING: stimulator of interferon genes; TLR: Toll-Like receptor; TRIF: TIR domain-containing adaptor protein inducing IFN.

NLRs are cytosolic PRRs, which are characterized by their NOD and their leucine-rich repeats (LRRs). Apart from the NLRs able to induce inflammasome formation (which I will describe in more detail below), NLRs can play multiple roles. NOD-1 and NOD-2 are able to activate the NF-$_k$B and mitogen-activated protein kinase (MAPK) pathways similar to TLRs [16] and NLR family caspase activation and recruitment domain (CARD) containing 5 (NLRC5) and class II major histocompatibility complex (MHC) transactivator (CIITA) act as transcriptional regulators of the MHC class II complex [17]. Absent in melanoma 2 (AIM2) and interferon gamma inducible protein 16 (IFI-16), the two members of the PYHIN family of receptors, sense cytosolic DNA and were described to induce inflammasomes similar to NLRs [18].

The most important sensor of cytosolic DNA, cyclic GMP-AMP (cGAMP) synthase (cGAS), is not a member of any of these subfamilies. Upon activation, cGAS produces the second messenger cGAMP, which triggers stimulator of interferon genes (STING) to induce an interferon response [19].

3.1.3. Inflammasomes

Inflammasomes are multimolecular signaling platforms that promote the cleavage of pro-caspase-1, and the maturation of the pro-inflammatory cytokines interleukin (IL)-1β and IL-18 in response to a range of danger signals derived from either pathogens or sterile cell damage [20]. The IL-1 family cytokines are potent pro-inflammatory mediators implicated in numerous metabolic and autoimmune diseases.

The inflammasome complex was discovered and named in 2002 [21]. However, there is not just one inflammasome, but several different receptors have been proposed to induce the assembly of an inflammasome complex. The most prominent inflammasome receptors include NLR family PYD containing 1 (NLRP1), NLRP3, NLRC4, AIM2 and Pyrin [22]. NLRP1B recognizes anthrax lethal toxin, NLRP3 a huge variety of DAMPS and PAMPs, NLRC4 associates with different NLR family apoptosis inhibitory proteins (NAIPs) and detects components of the bacterial type-3 secretion system and flagellin, AIM2 recognizes cytosolic DNA and Pyrin detects toxin-induced modifications of Rho GTPases [23]. While most inflammasome components are conserved between mice and humans, the function of human NLRP1 is not as clear and humans only express one NAIP. Beside these sensors, others have been reported to induce inflammasome formation. Yet, the exact

pathways for RIG-I, IFI-16, NLRP6, NLRP7 and NLRP12 are controversial or not well-defined [24].

Inflammasome assembly is organized in a hierarchy and requires, in most cases, a sensor protein, an adapter protein, and an effector protein [20,25]. The activated receptor recruits the adaptor apoptosis associated speck-like protein containing a CARD (ASC), which oligomerizes and mediates the interaction with the effector caspase-1. Consequently, pro-caspase-1 undergoes auto-catalytic maturation. The active hetero-tetramer of caspase-1 cleaves pro-IL-1β and pro-IL-18 and induces the release of their mature forms, which exert potent pro-inflammatory effects [20,25,26]. Furthermore, the activation of caspase-1 results in an inflammatory type of cell death termed pyroptosis, which requires gasdermin D (GSDMD) cleavage [27,28]. Although the different inflammasome sensor proteins enable a response to a diverse spectrum of DAMPs and PAMPs, the classical inflammasome pathways converge already on the level of ASC [29].

3.1.4. Structure and assembly of the inflammasome

The central adapter of inflammasome assembly is ASC. It is composed of an N-terminal PYD and a C-terminal CARD, connected by an unstructured linker region. Each of these two domains promotes homotypic interactions and links the PYD of the receptor to the CARD of the effector caspase-1 [30]. However, NLRC4 constitutes an exception to the rule. It can either directly interact with pro-caspase-1 via its own CARD or recruit pro-caspase-1 via the adapter ASC [20,31].

PYDs and CARDs both belong to the death-domain superfamily, one of the largest protein domain families. Death-domain family members participate in cell death and inflammation and characteristically form homotypic interactions. These interactions are typically not restricted to dimers, but rather give rise to oligomeric signaling platforms [32]. Although the sequence similarities between death-domain family members are limited, ASC-PYD, AIM2-PYD, NLRP3-PYD and others were shown to fold into a classical six helix-bundle [33–39].

Upon activation, the inflammasome receptor molecule either undergoes conformational changes enabling oligomeric self-interaction (e.g. NLRC4) [40] or several receptor molecules assemble in close proximity by binding to a common ligand (e.g. AIM2) [41]. Both mechanisms lead to DD homo-interactions of several receptors and a oligomeric PYD cluster acts as a seed to promote ASC-PYD filament formation [41] (Figure 3-2 A). Under homeostatic conditions, a high energy barrier

keeps ASC in a soluble form and prevents spontaneous oligomerization. The preformed seed recruits ASC and lowers the threshold for ASC polymerization by a prion-like propagation of conformational changes [42]. This process leads to the assembly of ASC PYDs into a hollow filament with a right-handed rotation, an inner diameter of 20 Å and an outer diameter of 90 Å [41,43]. Since PYD and CARD of ASC are orientated in a back-to-back orientation and are stabilized by the linker region, they are structurally independent from each other and the CARD does not influence PYD filament formation [4443]. Instead, the CARDs are located on the outside of the filaments and recruit pro-caspase-1 [43,45]. Similar to the PYDs, CARDs can assemble

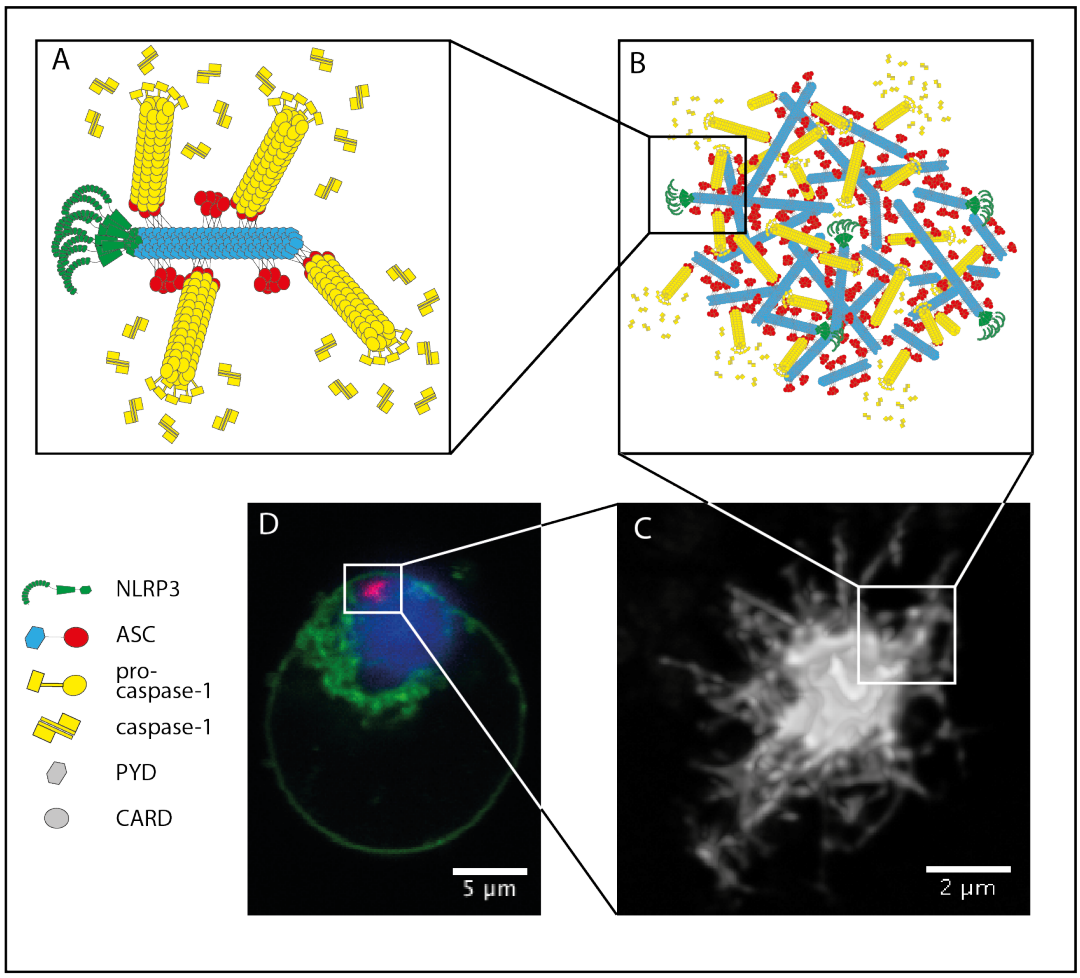

Figure 3-2 Inflammasome assembly
A Upon activation, NLRP3 *(green)* recruits ASC via its PYD. The ASC PYDs *(blue)* polymerize into filaments with their corresponding CARDs *(red)* to the outside. ASC-CARDs can cluster and form seeds for caspase-1 *(yellow)* polymerization. The caspase-1 filaments act as a platform for caspase-1 self-maturation. **B** Multiple ASC filaments can be cross-linked via CARD-CARD interactions. **C** High resolution stimulated emission depletion (STED) microscopic image of an ASC speck. **D** All ASC molecules of a cell are recruited into one speck per cell. Confocal microscopy image of an activated macrophage, expressing ASC-mCherry (red). Nuclei (blue) and membrane (green) were counterstained. ASC: apoptosis- associated speck-like protein containing a CARD; CARD: caspase recruitment domain; NLRP3: nucleotide-binding oligomerization domain, leucine-rich repeat, PYD containing 3; PYD: pyrin domain.
Modified from Hoss *et al.* 2016 [29]

filamentous structures which are mutually exclusive to PYD filaments [46,47] (Figure 3-2 A, B).

The overall inflammasome complex is assembled by multiple filaments, clustered together similarly to a bird's nest with a condensed globular core and single filaments extending into the periphery [46] (Figure 3-2C). Blocking the CARD interaction interface disables the crosslinking of ASC filaments [48]. This finding strongly supports the theory that ASC filaments are cross-linked via CARD-CARD interactions. Beside crosslinking ASC filaments, the CARDs can form seeds for further homotypic pro-caspase-1 CARD filaments [42,48,49]. Analysis of full ternary inflammasome complexes containing a receptor, ASC and pro-caspase-1 showed that pro-caspase-1 is even over-stoichiometric to ASC [41]. Taking the structure described above into account, this is not un-expected since the pro-caspase-1 filaments can emerge in a star shaped complex (seen from along the ASC filament) to all sides multiplying the number of involved pro-caspase-1 monomers. This architecture increases the local concentration of pro-caspase-1 and allows for caspase-1 activation by auto-proteolysis [21,45,50,51].

As soon as the inflammasome is activated, all ASC molecules from one cell are recruited into one speck following an energetic gradient (Figure 3-2D). The process is irreversible and once started no longer dependent on the initial starting signal, reminiscent of prionoid events [42]. This guarantees extreme sensitivity, since prionoid filament formation results in a potent signal amplification cascade [42].

3.1.5. Inflammatory caspases and cell death

Upon activation and auto-proteolysis of pro-caspase-1, a C-terminal 10 kDa and a 20 kDa fragment are released from the CARD domain forming the enzymatically active caspase-1 complex as a heterotetramer of two p10 and two p20 subunits [52,53]. However, a more recent study suggested that a p33 (CARD+p20)/p10 tetramer, still attached to the ASC speck, represents the predominant active species [54]. The active caspase-1 heterotetramer cleaves pro-IL-1β and pro-IL-18 into their active p17 and p18 forms, respectively [55–57]. The other major target of caspase-1 is the pyroptosis mediator GSDMD. In homeostatic cells, the auto-inhibitory C-terminus of GSDMD folds back on the N-terminus and inhibits its lytic activity. Upon cleavage, the N-terminal p30 fragment is released, localizes to membranes and forms functional oligomeric pores [58–60].

Although the best known substrates for caspase-1 are the IL-1 family cytokines and the pyroptosis effector GSDMD, many more proteins can be processed by caspase-1 [61,62].

Taking into account the tremendous effects of caspase-1 activation and the large number of activated caspase-1 molecules per cell [41], it is only reasonable that the active half-life of caspase-1 is restricted to a few minutes [62]. According to the p33/p10 model, once released from the speck by cleavage of the CARD linker, the locally increased concentration of the tetramer is lost and drops below the dissociation concentration, rendering caspase-1 quickly inactive [54].

3.1.6. Inflammasome Regulation

The ability for immediate response is a key characteristic of the innate IS. Such rapid responses involve events that may cause excessive and self-amplifying inflammation, causing severe damage to the host. Therefore, a multitude of checkpoints exists within this response in order to fine-tune, reduce or terminate it. This includes positive and negative feedback loops, protein-protein interactions, regulation of gene expression, posttranslational modifications and autophagy [63]. Furthermore, decoy receptors and programmed cell death are involved.

One way to regulate the inflammasome are so called pyrin-only proteins (POPs) and CARD-only proteins (COPs), which can act as decoy interaction partners for different inflammasome components relying on PYD or CARD homo-interactions [29]. Four different POPs were discovered in the human system, while there is no murine orthologous [64,65]. While the role the role of POP1 is controversial [29] and POP4 seems not to be involved in inflammasome regulation [66], POP2 and POP3 are widely accepted as inhibitors of the inflammasome. POP2 is proposed to bind as a competitive inhibitor to the inflammasome receptors NLRP3, NLRP1 and NLRP12 [65,67,68]. POP3 is genetically located within the same gene cluster as AIM2 and inhibits specifically AIM2 induced ASC speck formation [69]. In addition, POP1, POP2 and POP4 also regulate NF-kB signaling and thereby indirectly the expression of inflammasome components [66,67,70,71]. Additionally, some viruses express POP-like proteins in order to evade the recognition by the innate IS [29].

Not only the inflammasome seed formation is inhibited, but also caspase-1 activation as the common downstream event with potentially detrimental outcomes. COPs are restricted to the genomes of primates [65], but it is speculated that a splice forms of ASC (ASC-c) adopts their function in mice [72]. The COPs CARD16, CARD17 and

CARD18 are highly homologous to the CARD of pro-caspase-1 and have most likely derived from gene duplication events [65]. CARD17 has been shown to bind to the tips of pro-caspase-1 filaments, preventing further polymerization and activation [73,74]. The experimental evidence for the function of CARD16 and CARD18 is not as clear. Both have been shown to either promote or inhibit inflammasomes in different assays [29].
A closely related mechanism of regulation is alternative splicing of ASC, resulting in up to 4 different isoforms of ASC. The role of ASC-b, which lacks the flexible linker, is controversial but most likely the stiff connection between PYD and CARD reduces the efficiency of inflammasome formation [72]. ASC-c lacks most of the PYD and inhibits IL-1β maturation [72]. ASC-b and ASC-c are both LPS-inducible and detectable in human macrophages [72].
Remarkably, the effects of the released pro-inflammatory IL-1 cytokines are even regulated downstream of the inflammasome. The IL-1 receptor 2 acts as a decoy receptor without a signaling domain, the IL-1 receptor antagonist (IL-1Ra) binds the IL-1 receptor, but prevents its activation, and IL-18 binding protein is a secreted decoy interaction partner of IL-18 [75].

3.1.7. NLRP3

NLRP3 consists of three functional domains, the N-terminal PYD, the NOD (also known as NACHT) and the C-terminal LRR. The exact overall structure of NLRP3 is not yet known. However, the structure of NLRP3 PYD was successfully solved by X-ray crystallography [34] and the LRR of NLRP3 is highly canonical, which allows for a reliable modeling based on the structure of ribonuclease inhibitor [106, see as well Results]. Moreover, the crystal structure of a related inflammasome sensor, NLRC4, was solved [40]. The LRR was shown to fold back onto the NOD and to sequester NLRC4 in the monomeric state. During activation, a dramatic conformational change opens up the self-inhibited NLRC4 and allows for its oligomerization [49,77]. Similarly, NLRP3 is assumed to be kept inactive by its LRR. Upon activation, NLRP3 clusters via the NODs and brings the PYDs close enough together to act as a seed for ASC polymerization [41].
Activation of the NLRP3 inflammasome is tightly regulated and requires at least two independent signals: in a first priming or licensing step, PRRs or cytokine receptors trigger the activation of NF-kB that induces the expression of NLRP3 and pro-IL-1β. A second stimulation step is required to induce the assembly of the inflammasome [78] (Figure 3-3).

Some reports indicate, however, that NLRP3 cannot only be primed by de novo transcription, but also via post-translational modifications (PTMs). A fast licensing step of already translated NLRP3 protein via de-ubiquitination is dependent on BRCC3 [79,80]. In human monocytes, an extracellular signal-regulated kinase 1 phosphorylation-dependent priming process, which takes place within minutes after stimulation with LPS, was postulated as well [81]. Moreover, nitrosylation was reported to inhibit NLRP3 activation [82–84].

PTMs can modulate protein function in diverse ways and their roles depend on the modified residue and on the type of PTM. Ser-5 phosphorylation within the PYD of NLRP3 can block inflammasome activation, most likely by blocking a PYD-PYD interaction surface [85]. Other phosphorylation sites described to inhibit NLRP3 include Ser-295 and Tyr-861 [86,87].

Compared to other inflammasome receptor molecules, NLRP3 has a special role. It senses a range of very diverse stimuli, such as bacterial toxins, ATP, crystals and metabolic changes. Thus, it seems inconceivable that they would all bind directly to NLRP3 and therefore the term sensor should be preferred over receptor. The best-characterized activators can be summarized as either phago-lysosomal disruptive (crystals) or as causing changes in ion homeostasis (ATP/ bacterial toxins) (Figure 3-3). There are some suggestions for common upstream activating events, but none is able to integrate all known activators. Mitochondrial damage and release of cardiolipin, mtDNA and ROS were discussed as common upstream events in the NLRP3 activation [88–90]. However, it was shown that although these events co-occur, only potassium ion (K^+) efflux activates NLRP3 [91].

The cytosolic concentration of K^+ is much higher than in the extracellular space. An electrochemical gradient and active transport via the Na^+/K^+ pump keep the K^+ gradient preserved in homeostatic cells [92]. Several classical NLRP3 activators disrupt this gradient by allowing for net K^+ efflux [93]. The ATP receptor P2X7 works as a ligand-gated cation channel, which allows for the exchange of K^+ against Na^+ or H^+ [92]. The bacterial toxin gramicidin acts as a channel ionophore as well, allowing for a flux of monovalent cations [94], whereas valinomycin and nigericin work as carrier ionophores, selectively binding and transporting K^+ out of the cell [95]. However, the exact NLRP3 activation mechanism downstream of K^+ efflux remains elusive. Other ion fluxes have been associated with NLRP3 activation as well, but their role is not as clear. Some reports claim a significant role for Ca^{2+} mobilization, while the overall evidence rather suggests that an elevated intracellular Ca^{2+} concentration is not involved in NLRP3 activation [92].

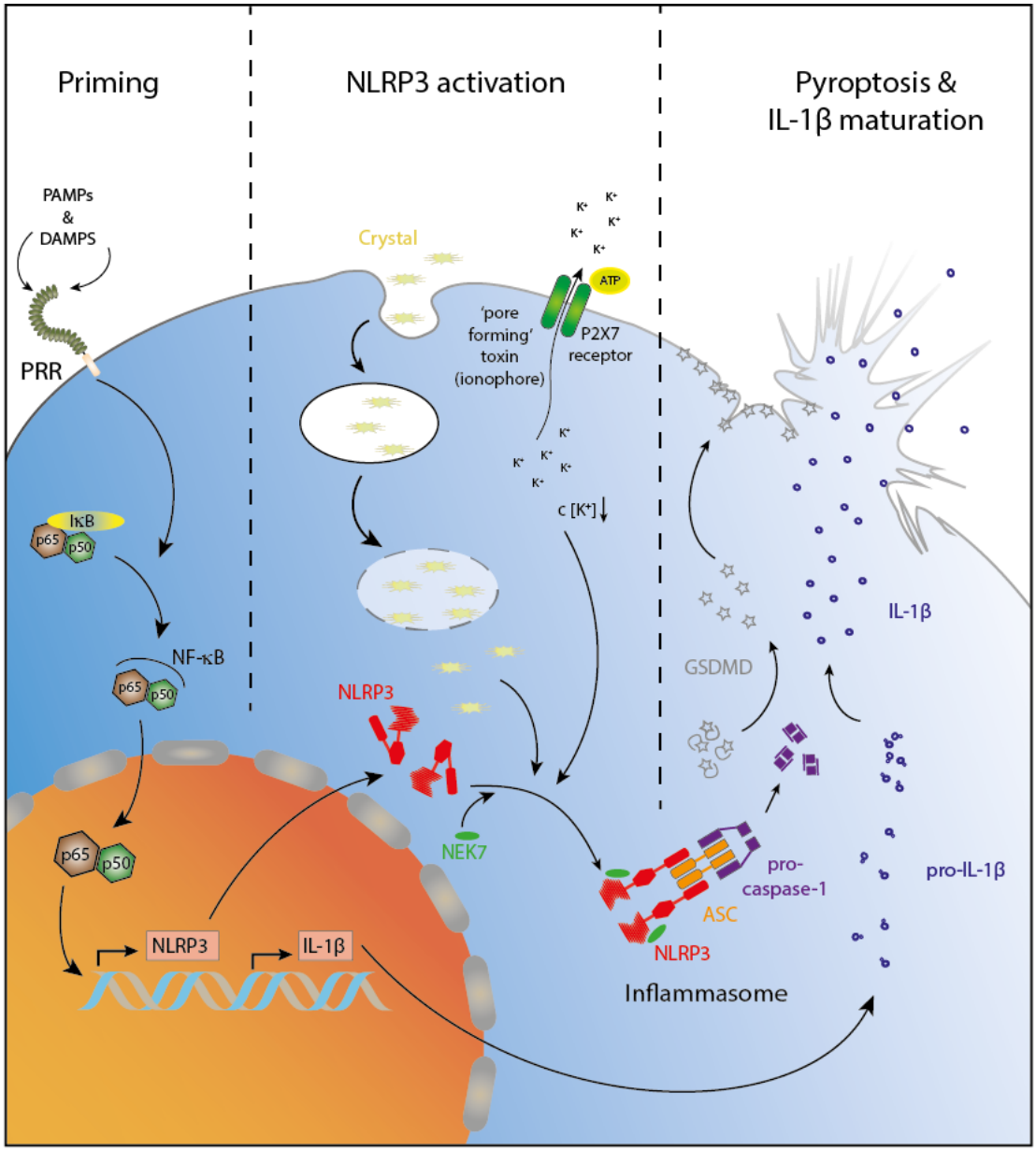

Figure 3-3 NLRP3 inflammasome activation

The NRP3 inflammasome is regulated on multiple layers. Most importantly, NLRP3 and pro-IL-1β expression need to be induced in most cells. This priming signal can be derived from PRR signaling or pro-inflammatory cytokines, which activate the NF-κB pathway. NLRP3 can be activated by a diverse set of stimuli, including lysosomal rupture by phagocytosed crystals or potassium efflux via pore-forming toxins or ion channels. NEK7 binding to NLRP3 is considered as a prerequisite for inflammasome formation. Upon activation, NLRP3 recruits ASC, which recruits pro-caspase-1. After proximity-induced self-activation, caspase-1 is capable of processing pro-IL-1β and GSDMD into their bioactive forms. The N-terminal GSDMD fragment forms pores in the cell membrane, resulting in pyroptotic cell death and IL-1β release.

ASC: apoptosis- associated speck-like protein containing a caspase activation and recruitment domain; DAMP: Damage-associated molecular pattern; IκB: Inhibitor of κB; IL: Interleukin; NEK7: never in mitosis related kinase 7; NF-κB: nuclear factor kappa-light-chain-enhancer of activated B cells; NLRP3: nucleotide-binding oligomerization domain, leucine-rich repeat, pyrin domain containing 3; P2X7: Purinergic Receptor P2X, Ligand Gated Ion Channel 7; PAMP: Pathogen-associated molecular pattern, PRR: Pattern recognition receptor.

Modified from Grebe, Hoss and Latz, 2018 [96]

NIMA-related Kinase 7 (NEK7) was found in three independent screens to interact with NLRP3 as a prerequisite for NLRP3 inflammasome activation [97–99]. It still needs to be determined how the interaction between NLRP3 and NEK7 is regulated. It was shown that the catalytic domain of NEK7, but not its kinase activity, is required for the interaction with the NLRP3 LRR domain [99]. Additionally, the interaction is dependent on the phosphorylation of NEK7, although the kinase NEK9, known to phosphorylate NEK7, is dispensable [97,99]. NEK7 has been linked previously to the formation of centrosomes and mitosis and the requirement for NEK7 results in the mutual exclusion of NLRP3 activation and mitosis [97].

Beside the classical NLRP3 inflammasome activators, NLRP3 can be activated via a non-canonical pathway: Murine caspase-11 directly binds to cytosolic LPS and activates the NLRP3 inflammasome independent of TLR4 [100,101] and human caspase-4 and -5 were found to be the functional homologues of murine caspase-11 [102,103]. It is believed that caspase-11 initiates a K^+ efflux, which in turn activates NLRP3. However, two different mechanisms are described: First, caspase-11 cleaves pannexin-1, which forms a pore for ATP to be released from the cell, and ATP then activates the P2X7 receptor upstream of NLRP3 [104]. Second, caspase-11 cleaves GSDMD, which induces pore formation leading to pyroptosis, but also K^+ efflux activating NLRP3 [27]. Which of these mechanisms is of higher relevance or whether they might act in concert requires further investigation.

In addition to the non-canonical inflammasome, the ‘alternative inflammasome’ was proposed. This pathway is suggested to be unique in human monocytes, does not induce ASC speck formation (although it is dependent on NLRP3, ASC and caspase-1) and pyroptosis, and is independent of K^+ efflux. Here, the activation of NLRP3 is gradual and occurs via a TLR4-RIPK1-FADD-caspase-8 axis [105]. Another inflammasome pathway exclusively described in human monocytes, explains the recognition of cytosolic DNA via cGAS/STING, which drives NLRP3 activation and renders NLRP3, instead of AIM2, the default inflammasome sensor for cytosolic DNA in this cell type [106]. Similar to the alternative inflammasome, the activation of NLRP3 via inhibition of hexokinase followed by its release from the mitochondria is reported to be independent of pyroptosis and K^+ efflux. Bacterial N-acetylglucosamine, metabolic inhibitors or negative feedback loops can inhibit hexokinase and activate NLRP3 [107]. On the one side, this defines a metabolic enzyme as a PRR, on the other side, it promotes the idea that NLRP3 can act as general sensor for HAMPs and does not rely on a specific pathogen-derived ligand [10]. However, some conflicting data on this topic is published. According to older publications, mTORC1- and PKM2-

dependent induction of glycolysis via hexokinase-1 is required for NLRP3 activation [108,109].

Other studies provided evidence for an intense crosstalk between metabolic conditions and NLRP3 activation as well. β-hydroxybutyrate, a ketone metabolite, produced during starvation or low carbohydrate prevalence, acts as a potent inhibitor of NLRP3 [110] and omega-3 fatty acids were also shown to act as negative regulators of the NLRP3 inflammasome [111].

Other circulating molecules can also regulate the NLRP3 inflammasome. The neurotransmitter dopamine induces ubiquitination and degradation of NLRP3 upon binding to the dopamine D1 receptor [112]. Type-1 interferons (IFNs) can dampen the inflammasome response via several mechanisms: Type-1 IFN-induced STAT-1 signaling directly inhibits NLRP3 and NLRC4 activity and induces an autocrine IL-10 STAT3 signaling loop restricting pro-IL-1β expression [113]. Additionally, IFN-β induces IL-1RA secretion [114]. However, IFNs are not exclusively negative regulators of the inflammasome. IFN-induced guanylate binding proteins and the immunity-related GTPase family member b10 are required to liberate ligands of cytosolic bacteria for sensing by the non-conical NLPR3 or the AIM2 inflammasome [115–117].

Although the (NLRP3) inflammasome is widely recognized as a feature of the innate IS, future studies will be needed to shed light on the effects it might have on the adaptive IS. For example, an intracellular complement-driven pathway was described that induces ROS and NLRP3 activation in CD4 T-cells as an integral component of a normal adaptive T-cell response [118].

Independent of its role as an inflammasome sensor, NLRP3 was shown to act as a transcription factor for T_H2 differentiation of CD4 T-cells as well [119]. While it binds as a transcription factor to the *IL-4* promotor, IL-4 was shown to suppress NLRP3 activation post-transcriptionally [120].

3.1.8. NLRP3-associated diseases

Diseases linked to or caused by the innate immune system are generally termed autoinflammatory. Both inherited or newly acquired specific mutations as well as misbalanced regulation of inflammatory processes can cause autoinflammatory diseases. They are not to be confused with autoimmune diseases, which are caused by auto-antibodies or other mis-regulated effectors of the adaptive IS [63].

Mutations in NLRP3, NLRC4 and pyrin were reported to cause inflammasome-dependent autoinflammatory diseases due to gain-of-function mutations. Mutations

within the *NLRP3* gene (also known as *CIAS1*) cause a spectrum of different inflammasome-dependent diseases, which are summarized as cryopyrin-associated periodic syndromes (CAPS) and cause generalized painful rashes and fevers. Some subtypes are also associated with neurosensory hearing loss, bony overgrowth of the knees, central nervous system inflammation and amyloidosis [63]. Mutations within *MEFV*, the gene coding for pyrin, cause familial Mediterranean fever (FMF) the most common autoinflammatory disease and NLRC4 mutations were described as a cause for autoinflammatory diseases as well [121,12263].

Except for inflammasome-triggered autoinflammatory diseases, a multitude of diseases is not intrinsically caused by the NLRP3 inflammasome but closely linked and often aggravated by NLRP3, rendering NLRP3 activation a serious health issue. Whenever crystalline material enters the body, macrophages try to clear it by phagocytosis. However, if they fail to digest the crystals, this crystalline material may cause phago-lysosomal rupture, ROS production and NLRP3-dependent inflammasome activation. NLRP3 is triggered by asbestos, silica and other crystals, leading to progressive pulmonary fibrosis [123–125]. Even everyday inhaled particulate matter airway pollution causes NLRP3 activation [126] and most likely contributes significantly to the high numbers of chronic inflammatory airways diseases. In gout, uric acid crystals are deposited within joints, where they are also phagocytosed by macrophages, leading to the same phago-lysosomal destabilization pathway and NLRP3-dependent inflammasome activation. The symptoms are pain and swelling of the joints [127].

Gout is not the only metabolic disease linked to NLRP3 activation. Saturated fatty acids were shown to activate NLRP3 and to promote type 2 diabetes (T2B) [128]. T2B in general is associated with increased inflammatory cytokine levels, including IL-1β [129]. It was also shown that pancreatic islet amyloid polypeptide, which is co-secreted with insulin, forms aggregates which induce NLRP3-dependent cell death of β-cells [130,131]. Atherosclerosis is another diet-induced NLRP3-dependent disease. Cholesterol crystals deposited within atherosclerotic plaques are strong inflammasome activators, leading to inflammation, swelling of the plaque and eventually rupture and thrombosis [96,132,133].

Moreover, neurodegenerative diseases such as Alzheimer's disease, Parkinson's disease and multiple sclerosis are strongly influenced by NLRP3. Amyloid-β plaques in Alzheimer's disease or α-synuclein aggregates in Parkinson's disease are NLRP3 inflammasome activators promoting inflammation and cell death [26]. Mice lacking NLRP3 showed a delayed development, less inflammation and weaker symptoms in

a murine model for multiple sclerosis (experimental autoimmune encephalomyelitis) [26].

Although NLRP3 seems to be rather detrimental to the host, an evolutionary beneficial role can be assumed. The above-mentioned diseases were most likely of no evolutionary impact, as they just started to exponentially gain significance when people became older and adopted a modern life style. Western-diet further aggravated the negative impact of NLRP3 since people started to suffer population-wide from the above-mentioned metabolic disorders.

Most likely, a key factor for the conservation of NLRP3 is its role in the immune response against influenza. Upon challenge with influenza viruses, NLRP3-, ASC- or caspase-1-deficient mice showed a diminished immune response and an increased mortality [134]. However, another study showed that NLRP3 was obligatory for inflammasome formation in certain cell types, but only ASC and caspase-1 were required to mount an adaptive immune response [135]. In conjunction with this, the necessity for the IL-1 signaling axis in establishing an anti-influenza CD8 T-cell response was shown [136]. Proposed modes for the detection of viral RNA by NLRP3 are via RNaseL [137] or DHX33 [138].

3.2. The leucine-rich repeat motif

The leucine-rich repeat (LRR) motif is a widespread structural feature of many proteins, including the innate IS receptors TLRs and NLRs. As many as 500 human genes encode for LRR-containing proteins and hundreds of protein structures containing LRRs have been solved [76]. The three-dimensional structure of LRRs was first determined by crystallization of the ribonuclease inhibitor [139]. It is defined by the specific amino acid pattern LxxLxLxxNx(x/-)L (with L being Leu, Ile, Val, or Phe and N being Asn, Thr, Ser, or Cys) followed by a variable sequence. Together, one repeat unit consists of 20 to 30 amino acids [140]. The overall structure of LRRs is (depending on the number of repeats) horseshoe-like, with parallel β-strands forming the inner concave surface and α-helices building the outer convex surface. The xxLxL stretch defines the β-sheet, which is followed by a flexible loop as a connection to the α-helix. Another flexible loop links back to the next β-strand [76] (Figure 3-4).

The LRR is a versatile structural element, which enables interactions with a broad spectrum of ligands including proteins [141,142], lipids [143], nucleic acids [144] and bases [145,146] and is therefore very suitable as a receptor domain. The LRR motif is not only

part of TLRs and NLRs, but it is also an integral components of plant resistance proteins [147] and in jawless vertebrates, a complete adaptive immune system is based on recombination of LRR fragments [148]. The LRR gene conversion-derived variable lymphocyte receptors of jawless vertebrates functionally resemble T-cell and B-cell receptors of jawed vertebrates [148].

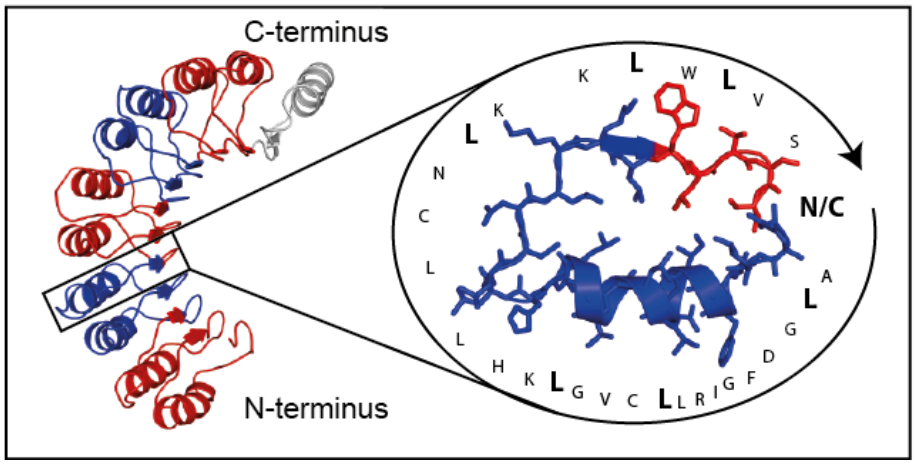

Figure 3-4 The leucine-rich repeat fold is defined by a consensus sequence
The leucine-rich repeat domain of NLRP3 (encoded by exons 5 to 10, bottom to top) was modeled based on the human ribonuclease inhibitor (RI) crystal structure by R. Brinkschulte. Different colors indicate different exons. One repeat is defined by a β-sheet and an α-helix connected via flexible linkers. This fold is defined by the LRR consensus sequence (bold letters). The N- to C-terminal direction of a single repeat is indicated on the right side by a surrounding arrow.

3.3. Splicing

In contrast to bacterial genes, which typically consist of a continuous protein-coding nucleotide sequence, eukaryotic genes are built up by coding and non-coding stretches, exons and introns, respectively. RNA splicing of freshly transcribed pre-mRNA removes these intronic sequences. Only after splicing is completed and a 3' poly-A tail and a 5' cap is added, an mRNA molecule is considered mature and exported from the nucleus. It is assumed that early during evolution, self-splicing introns, as they still exist in chloroplasts, mitochondria and phages, developed. Later on, splicing became much more complex, but also more flexible. Today's eukaryotic splicing machinery consists of 5 additional small nuclear RNAs (snRNAs) (U1, U2, U4, U5, U6) and as many as 200 proteins [149]. Although protein splicing factors regulate and simplify the splicing reaction, the spliceosome depends on the RNA moieties and is a ribozyme. Since the biochemical reaction of group II self-splicing introns and the eukaryotic spliceosome is very similar, it is assumed that the snRNAs

took over the structural and catalytic roles of group II introns. Thereby, conservation pressure was relieved from the introns and the number of spliceable RNAs increased dramatically [150].

3.3.1. The splice reaction

The splice reaction itself takes place as two energy-neutral transestrerifications. However, the spliceosome complex, which catalyzes the reaction and positions the pre-mRNA accordingly, requires ATP as a source of energy.

To remove one intron, the 2'-hydroxy group of a specific adenine at the 3' end of that intron attacks the phosphate at the 5' splice site. As a result of this reaction, the intron is cleaved from the 5' exon and the 5' end of the intron is covalently linked to the branch point adenine forming a lariat. Then, the 3'-hydroxy group of the detached exon attacks the phosphate at the 3' end of the intron. Thereby, the two exons become joined and the intron, which remains a lariat, is released [151] (Figure 3-5).

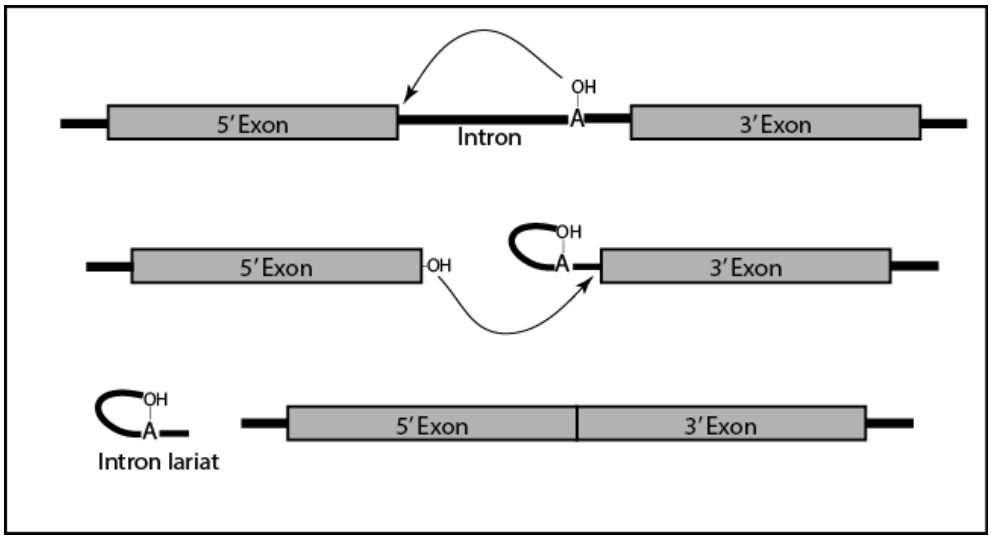

Figure 3-5 Splice reaction
During the splice reaction, the 2'-hydroxy group of the branch point adenine in the intron attacks the phosphate at the 5' splice site. The 5' exon is released from the intron and the intron forms a lariat. Next, the 3'-hydroxy group of the 5' exon attacks the phosphate at the 3' end of the intron, the two exons join and the intron lariat is released.

3.3.2. The spliceosome and splice regulation

In order to catalyze and regulate the reaction, the spliceosome has to recognize three positions within the pre-mRNA for each splicing event: The 5' splice junction, the branch point and the 3' splice junction are mostly identified by base-pairing of pre-mRNA and snRNAs. During the splicing process, several complementary

interactions are necessary to break, shift or substitute, which allows for re-checking of the consensus sites as well as spatial rearrangement, facilitating the chemical reaction [150]. Many of the spliceosomal proteins are DEAD/H-box RNA-dependent ATPases/helicases, most likely to facilitate all the necessary alterations in base-pairing which occur during the splicing process [152].

Typically, U1 and U2 bind first to the pre-mRNA, although their binding is only productive in rare cases at the first attempt. U1 binds to the 5' exon-intron junction and U2 binds the intronic branch point. Next, a heterotrimer of U4/U5/U6 is recruited. U6 replaces U1, and U1 and U4 are released. U2 and U6 interact via base-pairing and form the catalytically active core of the spliceosome. The complex disassembles after the intronic lariat formation and joining of the exons [149].

Beside the proteins making up the spliceosome itself, many additional proteins act as regulators (Table 3-1). Although many factors involved in the regulation have been discovered, the overall regulation is not yet well understood and needs further investigation [153]. Three classes of regulators mainly influence the splicing: Serine-arginine repeat (SR) factors, heterogeneous nuclear ribonucleoproteins (hnRNPs), and tissue-specific RNA-binding proteins [149]. Dependent on the localization within the RNA and the local environment, including cooperative binding partners, they can either promote or inhibit splicing. However, the strongest effect is attributed to so-called exonic or intronic splicing enhancer or silencer sites, defined regions within the pre-mRNA acting as binding sites for splice factors [149,153].

	Exon inclusion	Exon exclusion
Conserved consensus splice site sequence	++	-
Exonic Splice Enhancer (ESE)	++	-
Intronic Splice Enhancer (ISE)	++	-
Exonic Splice Silencer (ESS)	-	++
Intronic Splice Silencer (ISS)	-	++
Serine-arginine repeat (SR)-proteins	++	+
heterogeneous nuclear ribonucleoproteins (hnRNPs)	+	++
Cis-acting RNA-RNA base pairing	Selection of a single alternative exon from a cluster	
Transcriptional speed	++/--	++/--
Histone modifications	Influences transcriptional speed, recruit pos. /neg. splicing factors	
Nucleosome occupancy	+	
RNA pol II C-terminal domain (CTD) phosphorylation	++	+

Table 3-1 Multiple factors influence alternative splicing

A diverse set of factors is described to regulate and influence alternative splicing. While a few features as the conservation of the consensus splice site and ESE motives can be associated relatively well with exon inclusion, most other factors are described to influence splicing either in one or the opposite direction dependent on the context of other factors and the gene specific environment.

Similar to other RNA maturation processes, splicing mostly takes place co-transcriptionally and the C-terminal heptad repeat domain (CTD) of RNA polymerase II (Pol II) seems to be involved in the temporal-spatial coupling of transcription and splicing [154,155]. The speed of transcription influences the exon inclusion, and nucleosome occupancy and histone modifications affect the speed of Pol II [155].

3.3.3. Alternative splicing

Alternative splicing (AS) occurs when not only an intron is removed from the pre-mRNA, but an intron-exon-intron stretch. Thereby, the functionality of gene products can be changed dramatically without the necessity of an increased number of genes. Indeed, the increased complexity of higher-order organisms is mostly achieved by a more diverse AS pattern, not by more coding genes. While *C. elegans*, mice and humans carry around 20,000 protein-coding genes, they express about 50,000, 100,000 and 200,000 different isoforms, respectively [149]. In humans, more than 95 % of multi-exonic genes are alternatively spliced [156,157]. This is possibly due to a higher conservation of the consensus splice-sites in lower-order organisms and

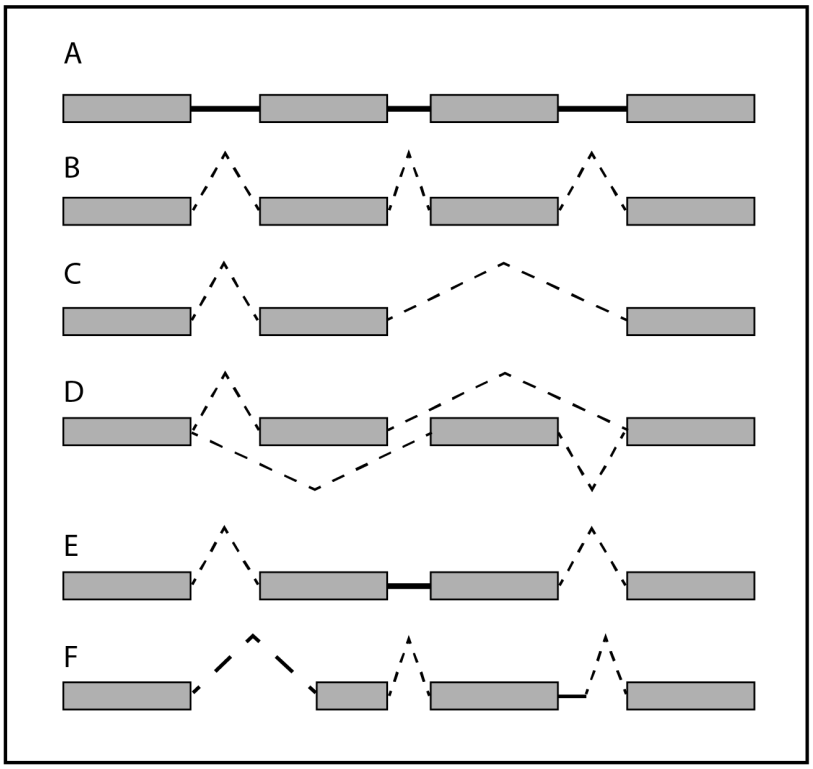

Figure 3-6 Principles of alternative splicing
A Schematic drawing of the exon-intron structure of a gene. **B** Splicing removes introns. **C** to **F** Different kinds of alternative splicing: **C** Exon removal, **D** mutually exclusive exons, **E** intron retention, **F** usage of non-canonical splice sites within introns or exons.

a higher number of regulating splice factors in complex organisms [149]. AS is especially prevalent in the nervous and immune systems [153,158] and increasing evidence suggests that AS contributes to the complexity of immune responses not only in humans [159]. However, AS can also contribute to the development of various diseases [160].

AS may not only delete functional domains, but it may also shift the reading frame of the mRNA, resulting in a new protein product or a premature stop codon. In general, one or several exons can be spliced out, exons can be mutually exclusive, introns can be retained, or non-canonical splice sites within exons or introns can be used [151,153] (Figure 3-6). Although it is possible that AS leads to nonsense-mediated decay, most splicing events seem to retain the reading frame [156]. Surprisingly, different isoforms of the same gene can behave like unrelated proteins and are characterized by significantly different interaction profiles [161]. Moreover, AS seems to be regulated in an on/off fashion for most genes in a specific cell type [162].

Over the last years, improvements in transcriptomics led to the discovery of an increasing number of new transcript variants. However, these data should be treated with caution since bioinformatic analysis of nucleic acid amplification assays can easily overestimate AS diversity [163 153]. The regulation of AS is not perfect and just by chance, every exon-skipping event will take place at a very low incidence, inducing a stochastic noise [164]. The average erroneous mis-splicing rate was determined to be 0.7% per intron. Given that a median gene contains four exons, roughly 2% of every transcript will be mis-spliced [165]. Taking into account the further increasing sensitivity of transcriptomics and that large-scale proteomic experiments support only a fraction of the transcript variants documented on RNA level [166], newly obtained data providing evidence of new AS products should be carefully evaluated for their biological relevance. The same is true for annotated isoforms, which were predicted from single expressed sequence tags (ESTs) in the beginning of the sequencing era and never systematically re-evaluated. Furthermore, over the last years it became evident that bioinformatics analysis of nucleic acid amplification assays can easily overestimate AS diversity [153,163]. This is further supported, as large-scale proteomic experiments support only a fraction of the transcript variants documented on RNA level [166,167]. Therefore it is of foremost importance to prove the existence of a splice isoform not only on nucleotide but as well on protein level.

3.3.4. Splicing in immunity

Alternative splicing is a mechanism widely used to regulate immune responses. Upon activation of T- and B-cells AS can regulate gene sets that are not altered at transcriptional level [153]. For example, different isoforms of CD45 homo-dimerize with different affinities to shape T-cell receptor signaling [168] and the expression of CD3ζ, which corresponds to the ability of a T-cell to be activated during antigen presentation, is significantly regulated by AS of CD3ζ exon 8 [153].

Not only the adaptive IS is regulated by AS, but also PRRs are known to be regulated by AS. Upon activation of TLRs, IL-6 or IFN signaling, a short isoform of MD-2 (MD-2s) lacking exon 2 is upregulated. MD-2s acts as a negative regulator of TLR4 activation by LPS [169]. An alternative isoform of STING, named MRP, differentially suppresses the IFN signaling branch of STING, but keeps the NFκB signaling unaffected [170]. Inflammasome activation can be regulated by AS of the adapter ASC, resulting in up to 4 different isoforms, of which two are LPS inducible and act as negative regulators. While ASC-c lacks most of the PYD and is a clear inhibitor of IL-1β secretion via a competitive mechanism, ASC-b only lacks the flexible linker between PYD and CARD and reduces the efficiency of inflammasome speck formation [72]. Resistance proteins in plants are structural and functional homologous of vertebrate NLRs. Interestingly, AS has been reported as a key feature in plant defense against pathogens and in stress situations [171,172]. Moreover, human NLRP3 mRNA can be alternatively polyadenylated in order to remove regulatory sites. This results in a shortened 3'UTR, which lacks the binding site for the negative regulators miRNA-223 and tristetraprolin [173].

3.4. Scope of this study

NLRP3 is a key component of the inflammasome pathway, driving caspase-1-dependent pyroptosis and IL-1β maturation in numerous metabolic and inflammatory diseases. Due to the high pro-inflammatory impact, NLRP3 activation is tightly regulated on multiple levels. Alternative splicing is known to drive functional diversity of proteins, and alternative splicing events have been described for some inflammasome components. However, alternative splicing of NLRP3 and related proteins has never been systematically investigated. Understanding the role of alternative splicing in inflammasome activation and the inherent mechanistic differences of alternative isoforms might help to expand the knowledge of basic NLRP3 activation and pave the way for novel treatments of inflammatory diseases.
Therefore, the aim of this study was to evaluate whether the structural prerequisites for alternative splicing are present in NLR genes, and to determine whether alternative splicing is a conserved feature across related proteins. Furthermore, alternative NLRP3 variants were to be described with regard to their frequency and potential regulation of the frequency, as well as the isoform distribution on single-cell level. Finally, this study aimed to investigate the molecular mechanisms of how alternative splice variants of NLRP3 might influence inflammasome activation and regulation.
The following objectives were formulated to meet these goals:

(1) To assess the spliceability of NLRP3 and related proteins *in silico*.
(2) To determine the prevalence of alternative splicing of NLR genes by deep RNAseq followed by hit validation and further qPCR analysis.
(3) To clone and express NLRP3 splice variants in different cell types.
(4) To analyze the different NLRP3 isoforms for their impact on inflammasome activation in primary human cells and in *in vitro* models.
(5) To assess the NLRP3 isoform distribution on single-cell level by qPCR.
(6) To decipher the molecular mechanisms of differential activity of different NLRP3 isoforms using structure-guided mutagenesis.

4. Materials and Methods

4.1. Materials

4.1.1. Devices

Product	Supplier
Blotting system Xcell II Blot Module	Invitrogen
Centrifuges	Eppendorf
Confocal microscope Leica SP5 AOBS with SMD	Leica Microsystems
Counting chamber Neubauer	Brand
DNA gel electrophoresis system PerfectBlue	Peqlab
Electronic E4 XLS+ multichannel pipets	Mettler Toledo
Epoch Microplate Spectrophotometer	BioTek
Flow cytometer Canto II	BD
Flow cytometer MACS Quant VYB/Analyzer 10	Miltenyi Biotechnology
Flow cytometric cell sorter Aria III	BD
Freezing containers	True North
Gel electrophoresis chamber Novex mini cell	Invitrogen
Gel Imaging system VersaDoc	Bio-rad
Heatblock Thermomixer	Eppendorf
HiSeq2500	Illumina
Incubator for tissue culture	SANYO Biomedical
MacBook Pro	Apple
MACS mix for rotation	Miltenyi Biotechnology
Magnet for Dynabead immunoprecipitation (IP)	Invitrogen
Molecular Immager VersaDoc	BioRad
Pipettes (0.1 µL – 1 ml)	Mettler-Toledo
Pipetting device Pipet boy acu	Integra Biosciences
Plate reader SpetraMax i3	Molecular Devices
Plate shaker DOS-10L	neolab
QuadroMACS separator	Miltenyi Biotechnology
QuantStudio 6 Flex	Thermo Fischer
Qubit 3.0	Thermo Fischer

Rotator for immunoblotting RM5	Ingenieurbüro CAT M. Zipperer
Sterile tissue culture hood	Fischer Scientific
Tapestation	Agilent
Thermocycler T3000	Analytica Jena
Thermocycler Tadvanced (96-well)	Biometra
Tissue culture microscope Leica DMIL LED	Leica
UV table for DNA imaging UVstar	Biometra
Western Blot reader Odyssey	LICOR Biosciences
Wide-field fluorescent microscope Zeiss Observer.Z1	Carl Zeiss Jena

4.1.2. Disposables

Product	**Supplier**
0.45 µm filters, 0.22 µm filters	Millipore
14 ml tubes for cultivating bacteria	VWR
15 ml, 50 ml tubes	Greiner bio-one
384-well clear plate (LDH)	Thermo Fischer
384-well qPCR plate	Applied Biosystems
384-well Small volume HTRF Plate	Labomedic
5 ml, 10 ml, 25 ml pipettes	Greiner bio-one
6-well plate Nunc delta surface (for hMDMs)	Thermo Fischer
96-well PCR plate	4titutde
Cell scrapers	Sarstedt
Cell strainer 70 µm	Greiner BioOne
Enzyme linked immunosorbent assay (ELISA) plates maxisorp	Nunc
MACS MS columns	Miltenyi Biotechnology
Microcentrifuge tubes	Eppendorf
Needles	Braun Melsungen
Opti-Seal Optical Disposable Adhesive	Bioplastics
PCR Stripes	Sigma
Pipet tips (0.1 µL – 1 ml, filtered and unfiltered)	Mettler-Toledo
Scalpel	Feather
Syringes	BD Bioscience
Tissue culture plasticware (flasks, plates)	Greiner bio-one

4.1.3. Reagents and Kits

Product	Supplier
10% NuPage Bis-Tris gels	Life Technologies
10x PBS (2 g Potassium chloride, 2 g Potassium dihydrogen phosphate, 80 g Sodium chloride, 11.5 g di-Sodium hydrogen phosphate anhydrous per 1 l)	Pan Biotech
10x reducing agent (500 mM dithiothreitol in stabilized form)	Life Technologies
10x Tris glycine (0.025 M Tris, 0.192 M glycine, pH 8.5 when diluted to 1x)	Thermo Scientific
16% formaldehyde, methanol-free	Life Technologies
20x MES buffer	Life Technologies
20x MOPS buffer	Life Technologies
20x TBS (400 mM Tris, 3 M NaCl, pH 7.4)	Santa Cruz Biotechnology
37% formaldehyde, methanol stabilized	Sigma
4-12% NuPAGE Bis-Tris gels	Life Technologies
4x LDS sample buffer (8% LDS, 40% glycerol, 2.04 mM EDTA, 0.88 mM SERVA Blue G, 0.7 mM Phenol Red, 564 mM Tris, pH 8.5)	Life Technologies
AF488 mAb labeling kit	Invitrogen
Agarose	Biozym
Ampicilin	Sigma
AmpliTaq Gold™ DNA Polymerase	Thermo Fischer
Anthrax lethal factor	List Biological Laboratories
Anthrax protective antigen	List Biological Laboratories
ATP	Sigma
Bichoninic acid (BCA) assay	Thermo Scientific
Blasticidin	Invivogen
Bovine serum albumin (BSA)	Roth
CD14 MicroBeads UltraPure, human	Miltenyi Biotechnology
Chloroform	Merck
Cholera toxin B subunit (CTB)	Sigma
CloneJE PCR Cloning Kit	Thermo Fischer
cOmplete protease inhibitor	Roche
CRID3	Pfizer

Curdlan	Invivogen
D1000 ScreenTape, Sample buffer, Ladder	Agilent
Dexamethasone	Sigma
DMEM	Life Technologies
DMSO	AppliChem
DNase I	Invitrogen
dNTP mix (10 mM)	Thermo Fischer
DOTAP	Roche
Doxycyclin	Sigma
DRAQ5	eBioscience
Dynabeads Protein A	Life Technologies
Dynabeads Protein G	Life Technologies
easysep human neutrophil enrichment kit	StemCell
EconoTaq PLUS GREEN 2 x Mastermix	BioCat
ELISA substrate solution BD Opteia	BD Biosciences
Endoporter	Geen-tools
Ethylenediaminetetraacetic acid (EDTA) solution 0.5 M, pH 8.0	Life Technologies
Ficoll-Paque PLUS	GE Healthcare
Genejuice	Milipore
Glycerol	Roth
Goat serum	Life Technologies
GoTaq Probe qPCR Master Mix	Promega
HEPES	Gibco
Hoechst34580	Life Technologies
Human IL-1β ELISA	R&D Systems
Human IL-1β HTRF	Cisbio
Human TNFα HTRF	Cisbio
Hygromycin B	PAA
Isopropanol	Roth
L-Glutamine	Life Technologies
LB agar (Lennox L agar) (10 g Peptone 140, 5 g Yeast Extract, 5 g NaCl, 12 g Agar per 1 l)	Life Technologies
LB Medium (Luria/Miller) (10 g Tryptone, 10 g Yeast Extract, 10 g NaCl per 1 l)	Roth
LDH cytotoxicity assay	Thermo Fischer

LeuLeuO-Me	Chem -Impex
Lfn-PrgI	Geyer-Lab
Lipofectamine 2000	Thermo Fischer
LPS ultrapure EB	Invivogen
Methanol	Roth
Mouse IL-1β ELISA	R&D Systems
Mouse IL-1β HTRF	Cisbio
Mouse TNFα ELISA	R&D Systems
Mouse TNFα HTRF	Cisbio
NaCl	Roth
Nigericin	Invitrogen
Nonidet-P40 (NP-40)	AppliChem
OptiMEM	Invitrogen
Pam3CSK4	Invivogen
pDC isolation kit II, human	Miltenyi Biotechnology
Penicillin/ Streptomycin	Thermo Fischer
PeqGreen	PeqLab
PFU Ultra II HS 2x Master Mix	Agilent
PGN from S. aureus	Invivogen
Phorbol-12-myristate 13-acetate (PMA)	Sigma
PhosSTOP	Roche
PMSF	Applichem
Poly (dA:dT)	Invivogen
Poly I:C	Invivogen
Poly-L-Lysine	Sigma
Polybrene	Sigma
Polymorphprep	Progen
PureLink Quick Gel Extraction Kit	Life Technologies
PureLink Quick Plasmid Maxiprep Kit	Life Technologies
PureLink Quick Plasmid Miniprep Kit	Life Technologies
PVDF membrane Immobilon-FL	Millipore
Qubit HS dsDNA assay kit	Thermo Fischer
Qubit HS RNA assay kit	Thermo Fischer
R837	Invivogen
R848	Invitrogen
Random Hexamers	Thermo Fischer

Restriction enzymes	Fermentas
rhGM-CSF	Immunotools
rhIFN-α	PeproTech
rhIFN-β	Immunotools
rhIFN-γ	Immunotools
rhIL-10	PeproTech
rhIL-18	Invivogen
rhIL-1β	R & D Systems
rhIL-3	Immunotools
rhIL-4	Immunotools
rhM-CSF	Immunotools
rhTNFα	R & D Systems
RNA ScreenTape, Sample buffer, Ladder	Agilent
RNase Inhibitor	Thermo Fischer
RNeasy mini kit	Quiagen
RPMI-1640	Life Technologies
Sense mRNA library Prep Kit	Lexogen
Silica	US Silica
Sodium hydroxide solution 5 M	Merck
Sodium Pyruvate	Life Technologies
Superscript III reverse transcriptase	Thermo Fischer
T4 DNA Ligase, HC	Fermentas
TAE buffer 50x (2 M Tris, 1 M acetic acid, 50 mM EDTA, pH 8.5	Roth
taqman gene expression assay human 18s RNA (Hs99999901_s1)	Invitrogen
TaqMan Gene Expression Assay human Hprt (Hs02800695_m1)	Invitrogen
Tris HCl pH 7.4	Roth
Tris HCl pH 8.0	Roth
Triton X-100	Roth
Trypsin	Invitrogen
Tween 20	Roth
Wheat germ agglutinin (WGA)-AF633	Invitrogen
zVAD-FMK	MBL
β-Estradiol	Tocris

4.1.4. Buffers and media

Name	Composition
1x TBS	100 ml 10x TBS, water to 1 l
1x TBST	100 ml 10x TBS, 1 ml Tween 20, water to 1 l
2x freeze mix	60 % FCS, 20 % Medium, 20 % DMSO
Blocking buffer	3% BSA in TBS
Complete DMEM	DMEM supplemented with 10% FBS, 100 U/ml penicillin, 100 µg/ml streptomycin
Complete RPMI	RPMI supplemented with 10% FBS, 100 U/ml penicillin, 100 µg/ml streptomycin, 1mM L-Glutamine, 0.5 mM sodium pyruvate
IP-buffer	50 mM Tris (pH 7.8), 50 mM NaCl, 0.1% NP-40, 10 % Glycerol add fresh: cOmplete protease inhibitor, PhosSTOP inhibitor, PMSF 0.2 mM
MACS buffer	PBS, 0.5% BSA and 2 mM EDTA
NP-40 buffer	20 mM Tris-HCl (pH 7.4), 150 mM NaCl, 1 mM EDTA, 1% Nonidet P-40, 10% glycerol, add fresh: cOmplete protease inhibitor, PhosSTOP inhibitor, PMSF 0.2 mM
Permeabilization/ blocking buffer	PBS, 10% FBS, 0.5% Triton-X100, Privigen 1:66
WB buffer	3% BSA in TBST
WB transfer buffer	100 ml 10x Tris-glycine, 150 ml methanol, water to 1 l

4.1.5. Antbodies

Immunoblot

Primary antibodies (clone, species)	Dilution	Supplier
ASC (polyclonal (AL-177), rabbit)	1:1000	Adipogen
GFP (JL-8, mouse)	1:1000	Clonetech
IL-1β (detection AB human ELISA kit, biotinylated)	1:250-500	R&D Systems
IL-1β (detection AB mouse ELISA kit, biotinylated)	1:1000	R&D Systems
Mouse caspase-1 (sc-514, rabbit)	1:200	Santa Cruz

NEK7 (EPR4900, rabbit)	1:500-1:2000	Abcam
NLRP3 (Cyro2, mouse)	1:2000-1:5000	Adipogen
tagRFP (polyclonal, rabbit)	1:5000	Evrogen
β-Actin (rabbit/mouse)	1:1000	Licor

Immunoprecipitation

Primary antibodies (clone, species)	**Dilution**	**Supplier**
GFP (96-well plate GFP-trap coated)	---	Chromotek
NLRP3 (D4D8T, rabbit)	1:100-200	Cell Signaling
tagRFP (polyclonal, rabbit)	1:220	Evrogen

Immunocytochemistry

Primary antibodies (clone, species)	**Dilution**	**Supplier**
ASC (TMS1, mouse), labeled with AF488	1:200	Biolegend

Secondary antibodies

Primary antibodies (clone, species)	**Dilution**	**Supplier**
Anti-mouse IRDye 680 RD	1:25000	LICOR
Anti-mouse IRDye 800 CW	1:25000	LICOR
Anti-rabbit IRDye 680 RD	1:25000	LICOR
Anti-rabbit IRDye 800 CW	1:25000	LICOR
Streptavidin IRDye 680 RD	1:30000	LICOR

4.1.6. Plasmids

The complete annotated plasmid sequences can be retrieved from the Latz lab Geneious-database using the indicated IDs. Protein sequences for the artificially created NLRP3 variants can be found in the appendix (section 12.4).

Plasmid ID	**Description**	**Backbone**
56	CMV VSV-G	pCMV
57	CMV Gag-Pol	pCMVR8.74
486	CMV Flp recombinase	pOG44

565	CMV 5' LTR hNLRP3 S5 (wt)-mCitrine, 3' LTR	pR
688	CMV 5' LTR hNLRP3 S5 (delta exon 5)-mCitrine, 3' LTR	pR
714	CMV 5' LTR hNLRP3 S5 (2x exon 6)-mCitrine, 3' LTR	pR
722	CMV 5' LTR hNLRP3 S5 (delta exon 5)-tagRFP, 3' LTR	pR
739	CMV 5' LTR hNLRP3 S5-tagRFP, 3' LTR	pR
785	CMV Tet. ind.-NLRP3-tagRFP, PGK-hASC-mTurquoise, FRT, hygromycin resistance	pcDNA5-FRT
801	CMV Tet. ind.-NLRP3(delta exon 5)-tagRFP, PGK-hASC-mTurquoise, FRT, hygromycin resistance	pcDNA5-FRT
978	CMV 5' LTR hNLRP3 S5 (double exon 6, rescue all surface)-mCitrine, 3' LTR	pR
1069	CMV 5' LTR hNLRP3 S5 (exon5 all surface to exon 6)-mCitrine, 3' LTR	pR

4.1.7. Cell lines

Unmodified/ received from collaborators

Cell line	**Source**
A431	Received from Tomasz Próchnicki
BLaER1 caspase-4$^{-/-}$ NLRP3$^{-/-}$	Gaidt *et al*. 2016 [105]
E. coli DH5α	Life Technologies
ECV-304	Received from P. Langhof
Flp-In 293 T-REx	Life Technologies
HEK 293T	ATCC
HEP-G2	Received from S. Schmidt
Murine Balb/c immortalized macrophages (iMo) NLRP3$^{-/-}$	Latz Lab, UMASS Worcester, USA, produced as Hornung *et al.* 2008 [124]
SW-620	Received from P. Langhof
THP-1	ATCC

Generated cell lines

Cell line	Parent cell line	Insert	Technique
BLaER1 NLRP3 Δ exon 5	BLaER1 caspase-4$^{-/-}$ NLRP3$^{-/-}$	722	Retro-viral
BLaER1 NLRP3 full-length	BLaER1 caspase-4$^{-/-}$ NLRP3$^{-/-}$	739	Retro-viral
Flp-In 293 NLRP3 Δ exon 5	Flp-In 293 T-REx	801	Flp-In
Flp-In 293 NLRP3 full-length	Flp-In 293 T-REx	785	Flp-In
iMo NLRP3	iMo NLRP3$^{-/-}$	565	Retro-viral
iMo NLRP3 Δ exon 5	iMo NLRP3$^{-/-}$	688	Retro-viral
iMo NLRP3 2x exon 6	iMo NLRP3$^{-/-}$	714	Retro-viral
iMo NLRP3 2x exon 6 surface rescue	iMo NLRP3$^{-/-}$	978	Retro-viral
iMo NLRP3 double expressing high	iMo NLRP3	722	Retro-viral
iMo NLRP3 double expressing high-intermediate	iMo NLRP3	722	Retro-viral
iMo NLRP3 double expressing low	iMo NLRP3	722	Retro-viral
iMo NLRP3 double expressing low-intermediate	iMo NLRP3	722	Retro-viral
iMo NLRP3 exon 5 surface to exon 6	iMo NLRP3$^{-/-}$	1069	Retro-viral

4.1.8. Oligonucleotides

Assay	Target	Sequence
LRR PCR	hNLRP3 exon 4 fwd	GCTGCAGATCCAGCCCAGCCAG
LRR PCR	hNLRP3 exon 10 rev	GTGGTCTTGGCCTGGATGGATCGC
LRR PCR	mNLRP3 Exon 4 for	GCTGCAGTGGCAGCCCAGCCAAC
LRR PCR	mNLRP3 Exon 10 rev	CCCTATACCAGAAGAGCCTCGGCTG
LRR PCR	pNLRP3 Exon 4 for	GCTACAGATTGAGCCCAGCCAGC
LRR PCR	pNLRP3 Exon 10 rev	ACATTGGCGTCTGACAGCCTTGG
LRR PCR	LRR PCR human exon 7/8 rev	CCAGAATTCACCAACCCCAGTTTCTG CAGGTTACACTGTGGATTC
qPCR	HPRT fwd	TCAGGCAGTATAATCCAAAGATGGT

qPCR	HPRT rev	AGTCTGGCTTATATCCAACACTTCG
qPCR	hNLRP3 exon 4/5 fwd	TGCCTGTTCTCATGGattggtg
qPCR	hNLRP3 exon 5/6 rev	AGCGCCCCAACcacaatctc
qPCR	hNLRP3 exon 4/6 fwd	CTGTTCTCATGGgttggggc
qPCR	hNLRP3 exon 6/7 rev	GCAGCTGACCAACcagagc
qPCR	hNLRP3 exon 6/8 rev	GCCAGAATTCACCAACcagagc
qPCR	hNLRP3 exon 6 rev	GAGTGCTGCTTCGACATCTCC
sc-pre-amp	HPRT fwd	ATTTATTTTGCATACCTAATCATT
sc-pre-amp	HPRT rev	GTAATCCAGCAGGTCAGCAAAGAA
sc-pre-amp	hNLRP3 full-length fwd	TTTTTGCCGGGGCCTCTTTTC
sc-pre-amp	hNLRP3 full-length rev	AGGAGATGTCGAAGCAGCACTC
sc-pre-amp	hNLRP3 ∆ exon 5 fwd	AGGCCGACACCTTGATA
sc-pre-amp	hNLRP3 ∆ exon 5 rev	ACAGAAGTCTGATTCCGAAGTCAC
sc-PCR	hNLRP3 full-length fwd	GACCCAGGGATGAGAGTGTTGT
sc-PCR	hNLRP3 full-length rev	CCCAACCACAATCTCCGAAT
sc-PCR	hNLRP3 full-length probe	AACGCTCCAGCATCCTGGCTGTAACA
sc-PCR	hNLRP3 ∆ exon 5 fwd	CAAGCTCCTCTCATGCTGCC
sc-PCR	hNLRP3 ∆ exon 5 rev	GAGATGTCGAAGCAGCACTCAT
sc-PCR	hNLRP3 ∆ exon 5 probe	TTCTCATGGGTTGGGGC
SSO	hNLRP3 intron 4/ exon 5 morpholino	GCTGTTCACCAATCTAGGAATTAGA
SSO	Std. ctr. morpholino	CCTCTTACCTCAGTTACAATTTATAT

4.1.9. Software

Software	**Supplier**
CellProfiler (version 2.1.1)	Carpenter *et al.* 2006[174]
FACS Diva	BD
Fiji (version 2.0.0)	Schindelin *et al.* 2012[175]
FlowJo V10	FlowJo
Gel scan Quantity One (version 4.6.9)	Bio-rad
Geneious R11	Biomatters
Illustrator CS6	Adobe
ImageStudio (version 4.0)	LI-COR Odyssey
ImmunoSpot analysis	CTL europe
MacPyMol	Schrödinger LLC

Mendeley Desktop	Mendeley
Office 2011	Microsoft
Photoshop CS6	Adobe
Prism 7	GraphPad
QuantStudio 6 and 7 Software	Life Technolgies
SoftMax Pro (version 6.3)	Molecular Devices
ZEN (version 2.0)	Carl Zeiss Jena

4.2. Methods

4.2.1. Molecular Biology

Generation of plasmids

New plasmids were either created by restriction digest/ ligation of existing plasmids or by overlap extension PCR and synthetic fragments. Non-project specific plasmids were not newly generated but taken from the Latz laboratory plasmid repository. R. Stahl helped with generation of plasmids.

Restriction digest

3 µg of insert or 6 µg of vector were digested with 2 µL of each enzyme in a volume of 50 µL for 60 min at 37 °C. Enzymes with STAR activity where only incubated for 30 min and inactivated for 5 min at 80 °C. Reaction products were separated on a 1-2 % agarose gel with PeqGreen (1:20000) in TAE buffer. Respective bands were visualized and sliced out on a UV-table. DNA was isolated from gel fragments using PureLink Quick Gel extraction kit according to the manufacturer's instructions.

Overlap extension PCR

Synthetic fragments were ordered via GeneArt (Thermo Fisher). Overlapping primers were used to create fragments, which could be fused by splice PCR and ligated into the respective vector.

Ligation

Purified vector and insert were combined in a molar ration of 1:3 (200 ng vector) with 4 µL 5x ligation buffer and 1 µL ligase. The reaction was carried out in a volume of 20 µL for 30 min at 22°C.

Transformation

20 µL of competent bacteria (DH5α) were thawed on ice, 3 µL ligation mix were added and cells were incubated for 30 min on ice before heat shock at 42°C for 45 s. Then bacteria were incubated for another 2 min on ice and allowed to grow for 1 h at

37 °C in 150 µL LB medium at 750 rpm. Pre-culture was streaked out on an LB agar plate with selection antibiotic and incubated at 37 °C over night.

Plasmid preparation

For plasmid preparation, a single clone was picked from an LB plate or a culture was inoculated from a clonal glycerol stock. Miniprep cultures were grown in 4 mL LB medium, maxiprep cultures in 100 mL LB medium with 100 µg/ mL ampicillin overnight shaking at 37 °C. Plasmid preparations were performed with the PureLink Quick Miniprep/ Maxiprep kit according to the manufacturer's recommendations.

Plasmid verification

Each newly created plasmid was controlled by test digestion to verify successful ligation. Positive clones were Sanger-sequenced (GATC Biotech, Konstanz) over the insertion/ mutation sites. Received DNA sequences were aligned against the *in silico* created vector in Geneious software using pairwise alignment.

RNA extraction

A confluent 12- or 6-well was used for RNA extraction. Cells were primed as indicated in the figures. Afterwards, cell culture supernatants were discarded and cells were washed once with PBS. RNA isolation was performed using the RNeasy mini kit according to the manufacturer's recommendations. Cells were lysed in 350 µL RLT lysis buffer supplemented with 1% β-mercaptoethanol. Lysates were stored at -80 °C. A DNase I digest on columns was performed for 15 min at RT. Eluted RNA was spectroscopically quantified (260 nm) and analyzed for contaminations (260:280 <2 for proteins, 260:230 for organic solvents). RNA was stored at -80 °C.

cDNA transcription

The amount of RNA used for cDNA transcription was adjusted between samples of one experiment (between 250 ng to 1 µg of RNA). The volume of RNA was adjusted with RNase-free water to 12.9 µL. 1 µL of oligo-dT(18) primer was added and samples were heated up to 65 °C for 5 min. Then, the samples were transferred to ice and 4 µL 5x reaction buffer, 1 µL 10 mM dNTPs, 1 µL 0.1 M DTT and 0.1 µL SuperScript III were added to each sample. A pooled control without reverse

transcriptase (noRT) reaction was performed as well. Reverse transcription was conducted at 50 °C for 50 min and terminated by heating to 85 °C for 5 min. cDNA samples were diluted 1:10 to 1:20 for use in qPCR and stored at -20°C.

LRR PCR

PCRs of the whole NLRP3 LRR were performed to detect all possible isoforms. 2 µL of cDNA were mixed with 12.5 µL EconoTaq Plus 2x mix, 0.4 µL of an exon 4 binding fwd primer and an exon 10 binding rev primer. The reaction volume was adjusted to 25 µL with water.

The following PCR program was used:

1. 94°C 1 min
2. 94°C 30 s
3. 58°C/65°C 30 s
4. 72°C 3 min ->34x back to 2.
5. 72°C 10 min

Human- and mouse-specific primers were annealed at 65 °C, pig-specific primers at 58 °C.

Afterwards, the PCR products were separated on a 1 % agarose gel stained with PeqGreen and bands were visualized using VersaDoc Molecular Imager.

Sanger sequencing of LRR PCR Products

NLRP3 LRR PCR products were generated as described above, with the only modification that a Pfu proofreading polymerase was used. All fragments lacking one or more exons were isolated from the gel, purified and blunt-ligated into pJet vectors, using CloneJET PCR Cloning Kit. Bacteria were transformed, single clones were picked and plasmids were isolated. Afterwards, the inserted PCR fragment was sent for Sanger sequencing (GATC Biotech, Konstanz). Sequencing results were pairwise-aligned against NLRP3 (NM_004895) using Geneious software to determine which exon was spliced out.

Sybr Green qPCR for NLRP3 isoform abundance

Quantitative realtime PCRs were performed in 384 well plates on a Quant Studio 6. 2 µL of cDNA were mixed with 5 µL Sybr Green mastermix, 2 µL of 2 µM forward/reverse primer mix and 1 µL water.

40 PCR cycles were performed, starting with an initial denaturation at 95 °C for 10 min followed by cycles of denaturation at 95 °C for 15 s annealing/elongation phase at 60 °C for 1 min (1.6 °C/s). After the last cycle, a meltcurve analysis was performed, ranging from 60 °C to 95 °C with 0.05 °C/s.
The primer efficiency was determined for each primer pair. Therefore. highly concentrated cDNA from different samples was pooled and used for all primer pairs. cDNA was diluted 1:3 over 8 steps in triplicates. The efficiency was calculated from the slope of the standard curve ($e=10^{(-1/slope)}$). Primer specificity within the highly repetitive sequence of the NLRP3 LRR was controlled by Sanger sequencing of the PCR fragments.

NLRP3 isoform abundance calculation

To calculate the relative abundance of each splice variant, the following equation was developed:
Starting with the basic equation of PCR kinetics

(#1) $N_c = N_0 * E^c$

N_c -> amount of amplicon after c cycles

N_0 -> amount of target at reaction start

E -> efficiency

Within the log-linear phase of the PCR reaction this can be reformulated to calculate the starting concentration

(#2) $N_0 = N_t / E^{c(t)}$

N_t -> amount of amplicon at threshold

C(t) -> fractional cycle to reach threshold

The abundance of one isoform (independent of transcriptional regulation of the gene) can be calculated as a fraction of the sum of all isoforms

(#3) $R_A = N_{0A} / \sum_{i=A}^{X} N_{Oi}$

N_{0A} -> Starting concentration of isoform A

N_{0B} -> Starting concentration of isoform B

….

N_{0x} -> Starting concentration of Isoform X

R_A -> relative abundance of isoform A

Taking (#2) the equation can be transformed into

(#4) $R_A = (N_{tA} / E_A^{C(t)A}) / \sum_{i=A}^{X}(N_{ti} / E_i^{C(t)i})$

For a given fixed threshold for all isoforms ($N_{tA} = N_{tB} = \ldots = N_{tX}$) applies

(#5) $R_A = (1 / E_A^{c(t)A}) / \sum_{i=A}^{X}(1 / E_i^{C(t)i})$

(#6) $R_A = E_A^{-c(t)A} / \sum_{i=A}^{X}(E_i^{C(t)i})$

It was further taken into account that two primer pairs had to be designed in a way that they could also detect a minor additional splice variant. The primer pair exon 4/5 to 5/6 designed for the full-length variant would also detect a exon 7 missing variant and the primer pair 6 to 6/8 would not only detect exon 7 missing but also exon 5 and 7 missing. To correct for this, the respective $E^{-c(t)}$ of the respective minor variant was subtracted.

Single-cell semiquantitative PCR

The single-cell semiquantitative PCR protocol was developed with the help of G. Seifert.

Human GM-CSF derived macrophages were LPS-primed for 3 h with 2 ng/ mL LPS. Cells were washed with PBS to remove LPS and non-adherent cells (not properly differentiated/activated). Cells were trypsin-harvested, washed in media and Propidium iodide (PI)-stained 1:500 for 5 min (to discriminate dead cells). Cells were washed in medium once more, resuspended at a density of around $2*10^6$ cells/ mL and passed through a 70 µm cell strainer. Single PI-negative cells were sorted into 96-well PCR plates containing 5 µL of PBS using the BD FACS Aria III cell sorter in the flow cytometry core facility. Before every sort, the droplet deposition in the middle of wells was controlled to prevent cells from being positioned outside of the PBS and subsequent desiccation. Plates were sealed, immediately frozen on dry ice and stored at -80°C until further use.

Cells were lysed by thermal shift from -80 °C to 65 °C (2 min). Afterwards, plates were placed on ice and reverse transcription mastermix was added.

2 µL 5x buffer (Superscript)
0.5 µL dNTPs (10 mM)
1 µL DTT (100 mM)
0.25 µL random hexamers (50 µM)
0.01 µL RNase inhibitor
0.25 µL Superscript III (200 U/ µL)
1 µL water

After a short centrifugation step, the plate was incubated at 37 °C for 60 min, followed by an enzyme inactivation phase for 3 min at 95 °C. Targeted pre-amplification was performed with the whole input cDNA in the same well by expanding the volume. The pre-amplification mix contained primers for NLRP3 full-length, NLRP3 Δ exon 5 and HPRT.

5.625 µL 10x Ampli taq gold mix
5.625 µL $MgCl_2$ (25 mM)
1.125 µL dNTPs (10 mM)
6x 1.125 µL primer (10 µM)
0.5 µL Ampli taq gold
25.375 µL water

The content was mixed on a PCR plate shaker and spun down. The following pre-amplification PCR protocol was used

1	95 °C	10 min	
2	94 °C	25 s	
3	45 °C	2 min	
4	72 °C	25 s	5x to 2
5	94 °C	25 s	
6	47 °C	45 s	
7	72 °C	25 s	15x to 5
8	72 °C	7 min	
9	10 °C	--	

Detection of pre-amplified cDNA species was performed using taqMan assays for NLRP3 full-length, NLRP3 Δ exon 5, HPRT and 18S RNA on a QuantStudio 6 Flex system in 384-well setup. Every reaction was performed in duplicates.

NLRP3 variants	HPRT/ 18S
1.8 µL water	3.75 µL water
5 µL universal GoTaq Pro Mastermix	5 µL GoTaq qPCR MM
1 µL fwd primer (10 µM)	0. 25 µL HPRT TaqMan assay
1 µL rev primer (10 µM)	1 µL pre-amplified cDNA
0.2 µL probe (5 µM)	
1 µL pre-amplified cDNA	

NLRP3 primers were annealed at 55 °C, HPRT and 18S primer at 60 °C.

1	95 °C	2 min	
2	95 °C	15 s	
3	60 °C/55 °C	60 s	40x to 1

Positive control cDNA from bulk cells was created using respective higher concentrations of PCR components suitable to reverse-transcribe more RNA.

0.5 µg RNA
4 µL 5x buffer (Superscript)
2 µL dNTP (10 mM)
2 µL random hexamers (50 µM)
1 µL Superscript III
2 µL DTT (100 mM)
fill up to 20 µL with water

Library Prep RNA Seq

Human GM-CSF-derived macrophages were primed for 3 h with 2 ng/ mL LPS. RNA was isolated and stored at -80 °C. RNA integrity was checked for every sample before library preparation using an RNA ScreenTape on a Tapestation. RNA content and DNA contamination of samples were quantified using a Qubit device.
2 µg of total RNA were used as input material. RNA Seq library was generated using 'SENSE mRNA-Seq Library Prep Kit V2' according to the manufacturer's recommendation with the following details: For reverse transcription and ligation, the RTL buffer was used to generate rather bigger fragments. To further adjust the size of the library fragments during the purification after second strand synthesis 14 µL

PB and 2 µL PS were used. Before library amplification and adapter attachment, a test amplification was performed to prevent over- or under-amplification of the library. The library was amplified over 12 cycles using the i7 index primers 7001, 7002, 7004, 7005 and 7007 to maintain the best possible color-balance during the first cycles of RNA Seq.
The fragment size of the generated library was controlled using a Tapestation D1000 Screen Tape.

RNASeq

RNA sequencing was performed on an Illumina HiSeq high output flow cell using V4 chemistry in the Next Generation Sequencing (NGS) Core Facility of the Medical Faculty of the University of Bonn. Sequencing was aimed at 200 M paired-end reads per sample (2*125 bp). RNA libraries from 5 donors were pooled and distributed on 4 lanes.

RNASeq analysis

Analysis was performed by F. R. Ringeling and S. Canzar (Gene Center, Ludwig-Maximilians-Universität München).
Sequencing reads were aligned to the human genome (build GRCh38/hg38) using STAR aligner [176] with default settings and transcript annotations from Ensembl GRCh38.90:
> STAR --runThreadN 3 --genomeDir /genome/human/staridx_primary/ --sjdbGTFfile /annotation/Homo_sapiens.GRCh38.90.chr.gtf --readFilesIn Donor*_1.fastq Donor*_2.fq --outSAMtype BAM SortedByCoordinate
Transcript abundances for all samples were quantified using Kallisto [177] with default settings
> kallisto quant -i Homo_sapiens.GRCh38.cdna.all.gene.kidx -o $outdir -t 3 Donor*_1.fastq Donor*_2.fq
and then summarized to gene level abundances using the tximport Bioconductor Package [178].
Sashimi plots were generated using the sashimi_plot utility from the MISO software [179], and exon-skipping events were quantified using MISO “exon-centric” percentage-spliced-in analysis. Soft-clipped adapter sequence was removed from all STAR aligned samples and reads were subsequently trimmed to a uniform length of 91

bases per read, using in-house developed scripts. MISO was run with the following command:

> miso --run ./index_dir/ ./bams/Donor*.sorted.bam --output-dir miso_out --read-len 91

4.2.2. Cell culture

Isolation and differentiation of human primary cells

Human blood and cells freshly isolated from human blood were always handled with special care and were treated as potentially infectious until all tests by the blood donation service were passed.

Human and pig peripheral blood mononuclear cells (PBMCs) were isolated from blood cell concentrates from the blood donation service of the University Hospital Bonn or heparin anti-coagulated full blood from pigs (received from the UKB animal facility, taken from surgery-training animals pre-euthanasia). Blood was diluted 1:1 with PBS before being layered over Ficoll. Samples were centrifugated for 20 min at 700 x g without brake. The PBMC layer was collected, re-diluted in PBS to wash away remaining contaminations of Ficoll and platelets, and pelleted at 340 x g for 10 min. The wash step was repeated once and if necessary, red blood cells were lysed. The lysis was not performed if PBMCs were further used for a CD14 monocyte selection.

Human monocytes were positively selected using CD14 MACS beads and magnetically sorted according to the manufacturers recommendations.

In order to generate human monocytes derived macrophages (hMDMs), 10^7 cells were seeded per 6 well delta surface plates in 5 mL complete RPMI with 55 ng/ mL rhGM-CSF or rhM-CSF (100 ng/ mL) and incubated at 37 °C in a humidified incubator with 5% CO_2. Cells were used at day 3 and 4 as M0 macrophages or further differentiated into M1 or M2 macrophages. Cells were scrape-harvested, counted and re-seeded as before and incubated for another 3 days with GM-CSF + IFNγ (200 U/ mL) for M1 or GM-CSF + IL-4 (1000 U/ mL) for M2 macrophages.

Neutrophils were obtained by enrichment of polymorphonuclear cells from fresh drawn blood using polymorhprep followed by negative selection for neutrophils (easysep human neutrophil enrichment kit. pDCs were isolated from PBMCs using the pDC isolation kit from Miltenyi.

Generation of BMDMs

6 - 8 week old WT C57BL/6 mice (Charles River) were sacrificed, femurs and tibias were isolated and muscle and tissue was removed. Bones were cut off adjacent to the joints and bone marrow was flushed out with PBS. The cell suspension was pipetted up and down to prepare a single-cell suspension and passed through a nylon filter (70 µm) to a new falcon tube. Cells were pelleted (300 x g 5 min) once and resuspended in DMEM supplemented with 20% L929-conditioned supernatant. BMDMs were differentiated over 6 days in 5x 10 cm dishes in 10 mL of media at 37 °C, 5% CO_2 in a humidified incubator. Adherent BMDMs were harvested by removing media, washing cells in PBS and then incubating cells at 4°C for 10 min in cold PBS supplemented with 2 % FCS and 2 mM EDTA. Plates were tapped and still adherent cells were gently scraped. Cells were collected, pelleted (5 min at 340 x g) and resuspended in DMEM.

Culturing of immortalized murine macrophages

Immortalized murine macrophages (iMos) were cultured in complete DMEM at 37 °C and 5% CO_2 in a humidified incubator. Cells were passaged every second day at a ratio of 1:10 to 1:20. Therefore, medium was aspirated, cells were washed with PBS and harvested with trypsin. Cell suspension was diluted in complete DMEM and cells were pelleted at 340 x g for 5 min and reseeded in fresh medium.

Culturing of HEK293T cells

HEK 293T cells and Flp-In 293 TREx cells were cultured in complete DMEM at 37°C, 5% CO_2 in a humidified incubator. Cells were passaged every second to third day at a ratio of 1:5 to 1:15. Therefore, medium was aspirated, cells were washed with PBS and harvested with trypsin. Cell suspension was diluted in complete DMEM and cells were pelleted at 340 x g for 5 min and reseeded in fresh medium.

Culturing of THP-1 cells

THP-1 monocytes were cultured in suspension flasks in complete RPMI at 37 °C, 5% CO_2 in a humidified incubator. Cells were passaged to maintain a density of $3x10^5$-$8x10^5$ cells/ mL. Before experiments, cells were differentiated in complete RPMI with 500 nM PMA overnight. The next day, cells were washed and left to rest for another 24 h in fresh complete RPMI before experiments were performed.

Culturing of BLaER1 cells

BLaER1 cells were cultured in complete RPM in suspension flasks at 37 °C, 5% CO_2, in a humidified incubator. For experiments, cells were trans-differentiated into monocytes. $7*10^5$ cells were seeded in 100 µL RPMI supplemented with 10 ng/ mL of hrIL-3, 10 ng/ mL hrM-CSF and 100 nM β-Estradiol per 96-well for 6-7 days at 37 °C, 5% CO_2, in a humidified incubator.

Culturing of further cell lines

A-431, HepG2 and SW-620 cells were cultured in complete DMEM, ECV-304 were cultured in 199-Medium supplemented with 10% FCS.

Freezing and thawing of cells

Cells were harvested and resuspended in fresh medium at a density of 1 $x10^6$ to $10x10^6$ cells. 500 µL of cell suspension were mixed with 500 µL of 2x freeze mix in cryo-tubes. Vials were frozen down in isopropanol freezing containers at -80 °C to ensure a slow and continuous temperature drop. After one day, cells were transferred to -150 °C for permanent storage. Cells were thawed in a water bath at 37°C. As soon as nearly all ice was melted, cell suspension was mixed with 10 mL pre-warmed medium to dilute the DMSO. Cells were pelleted, resuspended in fresh medium and plated.

Transient transfection of cells

Cells were seeded and allowed to settle down. DNA was diluted in serum-free Opti-MEM medium. Transfection reagent (Genejuice or Lipofectamin 2000) was also diluted in serum-free Opti-MEM medium according to the manufacturers recommendations. After 5 min, DNA and transfection reagent were mixed and incubated for another 15 min before addition to cells.

Splice-switching oligos

Day 3 differentiated hMDMs were seeded with rhGM-CSF (55 ng/ mL) in complete medium and were allowed to settle before transfection. Morpholinos were heated up

to 65 °C before use to recover full activity. Morpholinos and Endoporter were premixed and carefully added to the cells to a final concentration of 6 µM each, or respective concentrations during the titration experiment. Cells were LPS-primed 39 h after transfection.

Viral transduction and fluorescent cell sorting

Virus-related work was exclusively performed in S2 areas and only after extensive training.

Viral vectors for retroviral transduction of target cells were produced in HEK 293T cells. To prevent further reproduction of the virus, the viral vector was created by transfecting 3 separate plasmids into HEK 293T cells: The gene of interest in a retroviral vector plasmid, a gag-pol packaging plasmid and vesicular stomatitis virus (VSV)-G plasmid for virus entry into cells.

$0.6*10^6$ HEK 293T cells were seeded per 6 well in DMEM in the evening before transfection and incubated at 37 °C, 5% CO_2 in a humidified incubator. The next day, 2 µg of retroviral vector construct, 1 µg of *gag-pol* plasmid *and* 100 ng of VSV-G plasmid were transfected using GeneJuice. Medium was replaced with 30 % FCS containing DMEM (for iMos) or RPMI (for BLaER1, THP-1) 24 h after transfection. For transduction of iMOs, arround $0.1*10^6$ immortalized macrophages were seeded as target cells. Another 24 h later, the viral vector-containing supernatant was harvested and filtered through a 0.45 µm filter to exclude cellular contamination of the target cells. Media was removed from the target cells and replaced with filtered supernatant.

Suspension cells were spin-transduced. 10^5 cells were resuspended in filtered supernatants with 8 µg/ mL (THP-1) or 2 µg/ mL (BLaER1) polybrene. Cells were pelleted at 800 x g for 50 min at 32 °C. Cells were carefully resuspended and further incubated at 37 °C, 5% CO_2 in a humidified incubator.

The viral vector-containing media was removed 24 h after infection. Cells were kept for 3 further passages before being moved to the normal cell culture or FACS sorting facility.

Most transduced genes of interested were fused to fluorescent reporter tags which were used to select for positively transduced cells and to sort cell lines of one experiment to a comparable expression level. FACS sorts were performed with assistance of the staff of the flow cytometry core facility of the University Clinics Bonn.

Flp-In

Flp-In 293 TREx cells were used to generate NLRP3-expressing ASC reporter cells. The Flp-In system was chosen to ensure that every cell contains exactly one copy of the genes of interest. By combining NLRP3 and ASC into one Flp-In vector, it was ensured that all cells were double positive. NLRP3 expression was strongly suppressed by the Tet-repressor to prevent overexpression-induced activation of the NLRP3 inflammasome. Cells were selected over 3 passages with 15 µg/ mL blasticidin before transfection to select for the expression of TetR.

$7.5*10^4$ cells were seeded in 0.6 mL complete DMEM and co-transfected with a vector encoding Flp recombinase and an FRT-site containing vector encoding tetracycline-inducible NLRP3-tagRFP, ASC-mTurquoise and a hygromycin resistance using GeneJuice transfection reagent. Medium was changed after 12 hours, and one day post transfection, hygromycin B (150 µg/ mL) selection was started. The following 3 days, medium was changed every day, afterwards as necessary. Hygromycin selection was performed for two to three weeks.

Activation of cells

$0.7*10^5$ to10^5 cells were seeded for activation assays per 96 well or $2*10^6$ per 6 well in the evening before. Medium was changed before stimulations. Cells were activated in 100 µL per 96 well or 1 mL per 6-well. If not indicated differentially, the following concentrations and time points were used: Human cells were primed with 2 ng/ mL LPS, mouse cells with 200 ng/ mL LPS for 3 h, R848 1 µg/ mL for 3 h, Pam3CSK4 1 µg/ mL for 3 h. 50 µL of supernatant were taken worth after priming to determine TNF levels. Inflammasome activators were afterwards added as 50 µL 2x concentrate per 96-well. The NLRP3 inflammasome was activated with 10 µM nigericin for 60 to 90 min, 5 mM ATP for 60 min, 1 mM LeuLeuO-Me for 4 h, Silica 1000 µg/ mL for 6 h, R837 20 µg/ mL for 1.5 h, PGN 25 µg/ mL for 20 h, the non-canonical NLRP3 inflammasome was activated with cytosolic LPS, delivered with Cholera toxin subunit B (20 µg/ mL + 2 µg/ mL LPS) or with DOTAP (3.75 µg/ mL + 750 ng/ mL LPS); the NLRP1B inflammasome with 1 µg/ mL Anthrax lethal factor + 1 µg/ mL protective antigen (PA) for 4 h; the NLRC4 inflammasome in mouse cells with LFn-PrgI (4 µg/ mL)+ PA (1 µg/ mL) for 4 h and in human cells with LFn-PrgI 3 ng/ mL and PA 1 µg/ mL for 2.5 h; the AIM2 inflammasome with poly (dA:dT) (200 ng transfected with 0.5 µL Lipofectamine 2000 per 96-well).

4.2.3. Microscopy and Flowcytometry assays

Expression analysis (flow cytometry)

To verify equal expression of recombinant proteins with fluorescent color tags in stable cell lines, cells were harvested, resuspended in PBS and passed through a 70 µm cell strainer to ensure a single-cell suspension before analysis at a MACSquant (VYB/ Analyzer10) or Canto II flow cytometer. Debris was excluded by gating in the FSC/SSC. Next, doublets were excluded by plotting SSC-A vs. FSC-W. All remaining events were considered cells and analyzed for their intensity in the respective fluorescent channel.

ASC speck assay (microscopy)

To ensure a good attachment of cells to the bottom of the well, plates were pretreated with poly-L-lysine for 5-10 min at 37 °C and washed afterwards with PBS before cells were seeded.

Flp-In 293 TREx cells expressing NLRP3 variants were either activated using nigericin or doxycycline-induced overexpression of NLRP3 variants was used to induce ASC speck formation. Cells were seeded the evening before and were stimulated with 10 µM and lower doses of nigericin for 2.5 h. For doxycycline-induced overexpression activation, cells were treated for a minimum of 8 h with doxycycline doses between 100 and 0.05 ng/ mL.

After the activation was completed, all cell types were fixed with 2% formaldehyde and nuclei were stained using DRAQ5 for 30 min at RT. Cells were washed once in PBS before imaging. hMDMs were stained in permeabilization/ blocking-buffer at 4 °C overnight with anti-ASC-AF488 antibody.

Cells were imaged using a Zeiss Observer.Z1 epifluorescence microscope. Five to nine images were taken per well. Images were quantified using Fiji software (using find maxima function) [175] or Cell Profiler [174] software, based on a pipeline created by G. Horvath.

ASC speck assay (flow cytometry)

Cells were harvested and $5*10^4$ cells were resuspended in 500 µL HEPES-buffered DMEM containing 20 µM zVAD-FMK. Cells were activated in suspension for 3 h with nigericin in a shaking heat block at 37 °C. Cells were fixed with 4 % formaldhyde and analyzed on a CANTO II flow cytometer. Data was analyzed using FlowJo software.

Confocal microscopy

iMos were primed with LPS. Caspase inhibitor VX-765 (30 µM) was added 20 min before the addition of nigericin to prevent pyroptosis. Cells were pulsed with nigericin (20 µM) in the presence of the membrane dye WGA-Alexa Fluor 633 (25 ng/ mL) and the nuclear dye Hoechst 34580 (1:1000). Cells were washed twice in PBS after 20 min and cells were covered in medium before imaging at a Leica SP5 AOBS with a 63x objective.

4.2.4. Biochemical Assays:

Cytokine detection

Cytokine release after stimulation of cells was quantified using either enzyme-linked imunnosorbent assay (ELISA) or homogenous time-resolved fluorescence assay (HTRF).

Supernatant was either used immediately after the experiment or stored at -20 °C. If necessary, supernatants were diluted in the respective medium.

ELISAs were performed according to the manufacturer's recommendation, except for the fact that all volumes were reduced by 50 %. TMB substrate color change was measured at 450 nm and 570 nm at the SpectraMax i3 plate reader.

HTRFs for mouse cytokines were performed using 12 µL of supernatant and 1.5 µL each of the donor and acceptor antibody. HTRFs for human cytokines were performed using 5 µL of supernatant and 2.5 µL of each antibody. Assays were either incubated for 3 h at RT or over night at 4 °C. Fluorescence of donor and acceptor were measured at 620 and 668 nm, respectively, at the SpectraMax i3 plate reader with a measurement delay of 50 ms.

ELISpot assays were performed according to the manufacturer's recommendations. To assure enough distance between single-cells and to allow for single spot discrimination, 300 hMDMs were seeded per 96 well. ELISpots were measured at CTL Europe (Bonn).

Cell viability assays

Cell viability after inflammasome activation was either assessed via CellTiterBlue (CTB) or lactate dehydrogenase (LDH) release assay. The CTB assay measures cellular viability via the metabolic activity of the cell, whereas the LDH assay

indicates loss of cellular membrane integrity, causing the release of strictly cytosolic LDH into cell supernatants.

After supernatants for cytokine detection had been harvested, 50 µL medium containing 10% CTB reagent were added per 96-well and incubated for 30 min to 2 h. Fluorescence was measured using a SpectraMax i3 fluorescence plate reader using an excitation wavelength of 530-570 nm and detecting emission at a wavelength of 580-620 nm.

If LDH assays were performed, inflammasome activation was performed under serum-free conditions to minimize background. Supernatants were used fresh or after one freeze/thaw cycle. 12 µL of cell supernatants were mixed with 12 µL of assay reagent in a 384 well plate. The colorimetric assay was measured using SpectraMax i3 plate reader at 490 nm und 680 nm.

Generation of lysates/ precipitates from supernatants

$2*10^6$ iMos were seeded per 6-well in complete DMEM. Cells were stimulated after overnight incubation in serum-free medium. Supernatants were harvested and proteins were precipitated by addition of an equal volume of methanol and 0.25 volumes of chloroform. The upper phase was discarded after centrifugation for 3 min at 20 000 x g, the same volume methanol was added and the centrifugation was repeated. The pellet was air-dried and resuspended in LDS-buffer. Cells were washed with PBS and lysed in NP-40 buffer supplemented with cOmplete protease inhibitor and PMSF (0.2 mM). Cells were incubated on ice for 10 min, scrape-harvested, transferred into microreaction tubes and incubated for another 10 min on ice before nuclei were pelleted at 1000 x g for 10 min at 4 °C. A BCA assay was performed according to the manufacturer's recommendations and samples were adjusted to same protein content. Lysates and precipitates were denatured by addition of LDS and reducing reagent and subsequent heating to 85 °C for 10 min. Samples were either stored at -20 °C or used immediately.

(Co-)Immunprecipitation (IP)

1 to 3 confluent 6-wells were lysed in IP-buffer supplemented with cOmplete, PMSF (0.2 mM) and phosStop. Samples were kept on ice for a total of 20 min and carefully vortexed every 5 min. Nuclei were removed as above and protein content was adjusted after BCA. mCitrine IPs were performed in GFP-trap plates, all other IPs using protein G Dynabeads coupled to the respective antibodies. IPs were performed

with agitation at 4 °C for 2 to 4 h. Samples were eluted using LDS buffer and reducing agent.

Isolation of ASC specks

$2*10^6$ cells were seeded per condition, primed as usual and activated with 5 mM ATP for 3 h. Supernatants of pyroptotic cells were harvested and passed through a 5 µm strainer to exclude cells and specks were pelleted at 20,000 x g for 10 min. The pellet was resuspended in LDS buffer and separated by SDS-PAGE.

SDS-PAGE and Westernblotting

Samples were heated up to 85 °C for 10 min with agitation before loading on a 4-12% or 10% NuPage Bis-Tris gel. Samples and 3 µL PAGE Ruler Plus protein marker were separated by gel electrophoresis with MES or MOPS buffer until sufficient separation was achieved. Proteins were transferred at 30-32V for 60 to 90 min in an XCell II blotting system on an Immobilon-FL PVDF membrane. Membranes were blocked with 3% BSA in TBS. Primary antibody staining was performed at 4 °C ON in 3% BSA/TBS-T. Blots were washed 3 times, secondary antibody was incubated for 1 h at RT, Blots were washed another 3 times and imaged with a LICOR near-infrared detection system.

4.2.5. In silico analysis

Sequence motive dependent alternative splice prediction

Spliceport (http://spliceport.cbcb.umd.edu/) was used to analyze the strength of the splice donor and acceptor sites of human NLRP3 [180]. The number of exonic splice enhancer sites within the LRR exons of human NLRP3 was assessed with RescueESE (http://genes.mit.edu/burgelab/rescue-ese/) [181].

Physico-chemical protein characteristics for the (artificial) splice variants were calculated using the ProtParam online tool (http://web.expasy.org/protparam/).

Structural analysis of LRRs

Structural models of the NLRP3 LRR were generated by R. Brinkschulte and M. Geyer using SwissModel. The crystal structure of human ribonuclease inhibitor (PDB accession: 2q4g) was used as a template.

Most structural alignments of LRRs were based on previous work by M. Geyer. RI- and T-Type consensus sequences were published before[182].

NLRP3 LRR sequence logo was generated using Geneious software.

LRR exon structure analysis

LRR exon database extractions were performed by F. R. Ringeling (Gene Center, Ludwig-Maximilians-Universität München), based on my ideas. Data was provided in form of text files listing all LRR exons and the respective genomic locations. Phylogenetic analysis of the identified 'peak-genes' was performed by F. R. Ringeling.

LRR annotations for human proteins were performed using the ensmbldb Bioconductor Package [183]. All known canonical transcripts as defined by UCSC (GRCh38) were queried for LRR domains annotated by the SMART database, namely: SM00369, SM00370, SM00364, SM00367, SM00368 and SM00365.

All exons spanning LRR domains were extracted for further analysis: exons were divided into frame-preserving (dividible by 3) or frame-shifting, and plotted for their length distribution. Genes contributing to the major peaks within the exon length distribution plot (69-75, 81-87, 141-147, 168-174 bp) were identified and used to create a phylogenetic tree. Amino-acid sequences were aligned using MUSCLE [184] and the dist.ml function from the phangorn Bioconductor package [185] was used with default settings to create a distance matrix that was then used to estimate an un-rooted phylogenetic tree using the Neighbor Joining clustering method.

4.2.6. Statistics

Data are typically represented as mean ± standard error of the mean (SEM) for pooled data of a minimum of 3 independent experiments or pooled date from a minimum of 3 individuals. Otherwise, data were represented as mean ± standard deviation (SD). Statistical analysis was performed using Microsoft Excel and GraphPad Prism. Statistical differences were calculated using two-way ANOVA with Tukey post-test for multiple comparisons.

4.2.7. Ethics

Human primary cells were extracted from blood concentrates provided by the blood donation service of the University Clinics Bonn (ERC Ethikantrag Lfd. Nr. 184/16 “Activation and regulation of Inflammasomes (InflammAct)”
Mouse bone marrow was isolated in accordance with local regulations.

5. Results

5.1. The LRR domain of NLRs exhibits a highly conserved exon organization

LRRs are widely used structural elements and the innate immune receptor families of NLRs and TLRs rely on them. While in TLRs most of the LRR is encoded by a single long exon, the NLR LRR is encoded by multiple short exons (Figure 5-1 A).
The repetitive architecture of LRR exons suggests a potential gain of receptor diversity through AS, which might be conserved across further LRR-encoding genes. A database analysis of exons from all human proteins within annotated LRR regions was performed in cooperation with F. R. Ringeling (Figure 5-1 B). The majority of all detected exons contains less than 200 bp (Figure 5-1 C), similar to the exons in NLR LRRs.

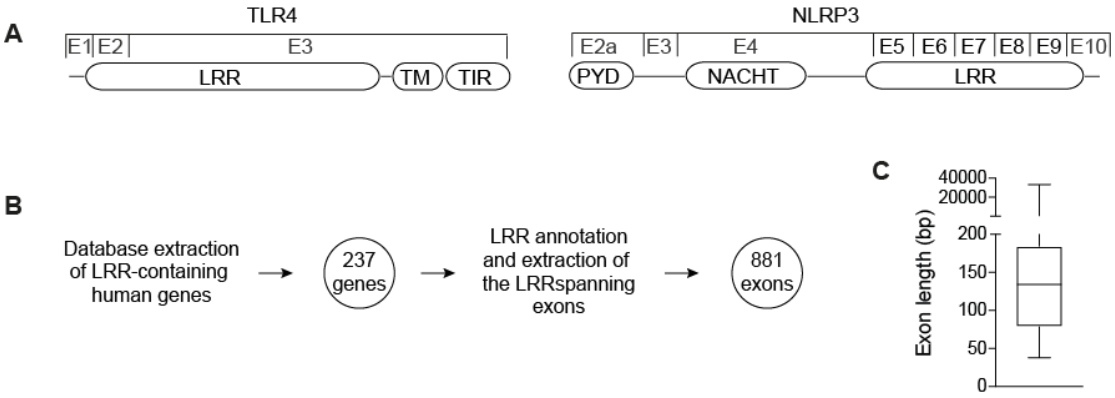

Figure 5-1 LRR domains often consist of multiple short exons
A Schematic of domain and exon distribution in TLR4 and NLRP3. **B** Workflow of the database extraction of LRR exons from the human proteome. Database extraction was performed by F. R. Ringeling according to my design. **C** Length distribution of exons extracted in **B**. E: Exon, TM: trans membrane domain, TIR: Toll/IL-1 receptor homology domain.

Depending on their exact length, exons can be frame-shifting, which results in the disruption of an open-reading frame in case of AS. To further characterize the aforementioned *in silico* extracted exons, they were divided into frame-shifting and frame-preserving exons and plotted for their length distribution (Figure 5-2 A). Although in a random distribution of splice sites, two thirds of exons should be frame-shifting, the huge majority of the LRR exons is frame-preserving, indicating an evolutionary pressure to preserve protein translation after AS. Moreover, the exons

cluster in 4 distinct peaks corresponding to the typical size of one or two LRRs (69-87 bp or 23 to 29 aa per LRR), indicated by grey boxes. Next, the genes contributing to the different peaks were identified and plotted in size according to their contribution to each peak (Figure 5-2 B). To analyze the relationship of the identified genes, a phylogenetic tree was created by F. R. Ringeling (Figure 5-2 C). An enrichment of several gene families, which cluster for the number of encoded LRRs per exon and the LRR type, can be observed. While all LRRs share the characteristic secondary protein structure and a core consensus sequence, several subtypes can be defined [182]. The here extracted LRRs belong either to the ribonuclease inhibitor (RI) or bacterial/typical (S/T) type of LRRs.

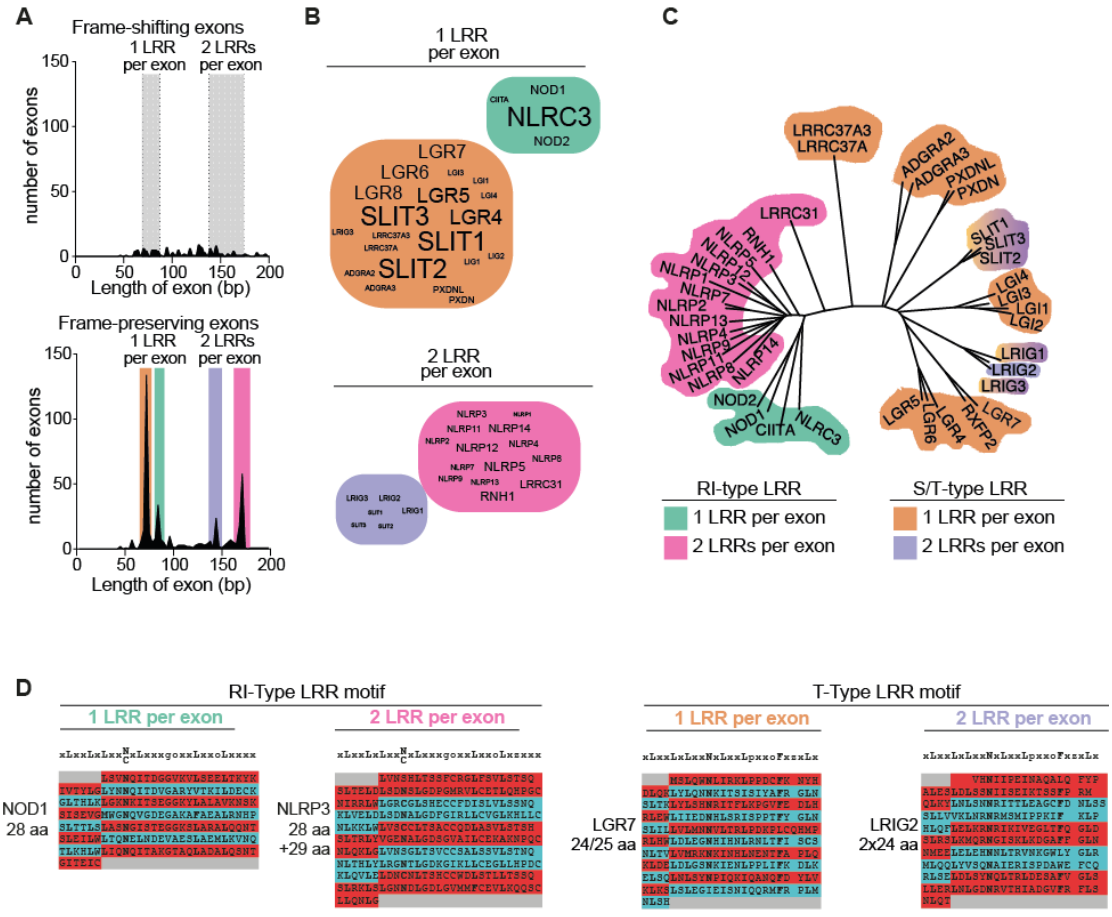

Figure 5-2 LRR domains have a conserved multi-exon organization
A All LRR exons extracted in Figure 1 of up to 200 bp in length were plotted for their frequency distribution. Exons were divided in frame-shifting or frame-preserving. The typical length of LRRs (23 to 29 aa) is indicated by grey boxes in the upper panel. Colored boxes in the lower panel are included to allow for the assignment of groups in the following subfigures. **B** Genes in word clouds represent genes whose exons contribute to the respective peaks in **A**. Word size corresponds to the number of contributing exons. **C** Phylogenetic analysis of all genes contributing to the 4 major peaks in **A**. Phylogenetic tree was created by F. R. Ringeling. **D** LRR consensus sequences [182] and structural alignments for the 4 groups identified in A to C. Each line represents on repeat, colors mark different exons. In the consensus sequence, 'x' is any residue, 'o' is a non-polar residue, 'z' is a frequent deletion. Structural RI-type LRR alignments are based on previous analysis by M. Geyer. aa: amino acid RI: ribonuclease inhibitor, S/T bacterial/ typical.

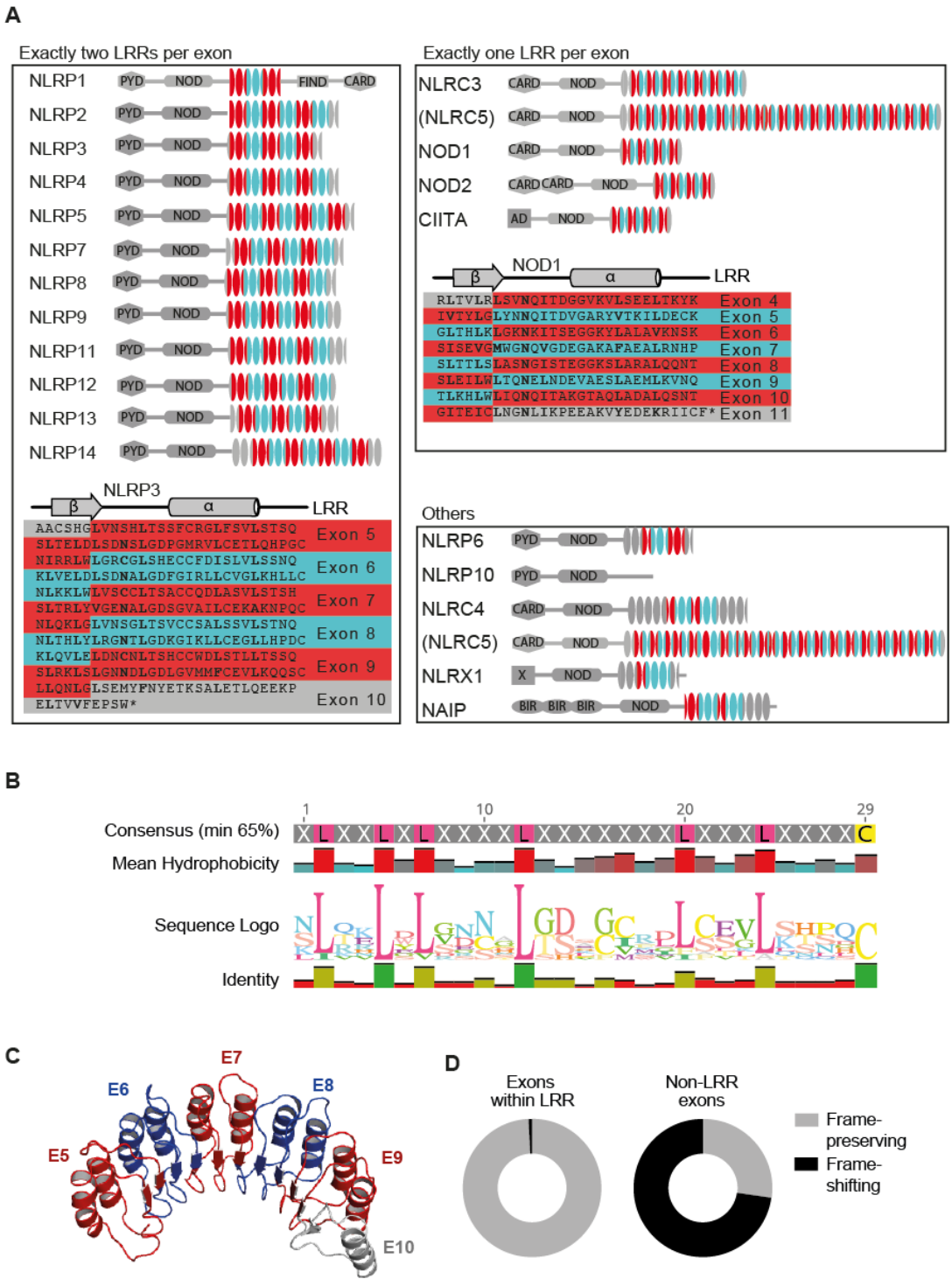

Figure 5-3 NLR LRRs are highly conserved and qualify for alternative splicing
Structural alignments of NLR LRRs were created based on previous work by M. Geyer (for all alignments, see appendix Figure 12-1). **A** Most NLRs can be grouped according to their exon LRR structure: ones encoding two LRRs per exon and ones encoding a single LRR per exon. Structural alignments of NLRP3 and NOD1 LRR are given as examples. Secondary structure elements are indicated on top. Blue and red indicate repetitive LRR exons. Conserved residues defining the LRR fold are highlighted in bold. **B** Sequence logo of the NLRP3 LRR (exon 5 to 9), indicating the high degree of conservation of leucine residues. Size of letters indicates conservation and aminoacids with a minimum of 65 % conservation are shown in the consensus sequence. Mean hydrophobicity and identity of each position of the LRR are plotted as well. **C** Model of the NLRP3 LRR based on the human ribonuclease inhibitor LRR crystal structure. The different exons are indicated in different colors. R. Brinkschulte created the model. **D** Quantification of frame-shifting vs frame-preserving exons of all LLR exons vs. non-LRR exons of all NLRs.

A structural alignment for the RI-type and T-type LRRs encoding one or two LRRs per exon was generated according to the respective consensus sequences [182] (Figure 5-2 D). Each line indicates one LRR encoding for a β-sheet and a α-helix and colors indicate exons. Intriguingly, in all four LRR subtypes, the exon-exon boundary is conserved within the same position of the repeat, suggesting a conservation of the exon-LRR organization to maintain the compatibility for AS in multiple gene families.
The further analysis was focused on LRRs in genes associated with the IS. Structural alignments for all NLR LRRs were generated based on previous work by M. Geyer (for all alignments, see appendix Figure 12-1). Interestingly, most NLRs cluster into two groups based on their exon size. NLRP exons encode two alternating repeats of 28 and 29 aa, while NOD/NLRC exons encode a single LRR of 28 aa. Yet, the exon-exon boundary is conserved in the same position at the end of the β-sheet (Figure 5-3 A). NLRC5 constitutes an exception, as the first part of the unusually long LRR domain (> 40 repeats) does not show a conserved exon-LRR relationship, while the second part correlates with the other NLRCs/NODs. This repetitive exon architecture is a necessary precondition for the generation of functional isoforms by AS. The removal of one or several exons will produce a shorter LRR domain, likely without interfering with the overall protein fold, as the hydrophobic residues forming the core of the LRR scaffold are conserved (Figure 5-3 B). The overall shortening of the LRR without interfering with the secondary structure, is also supported by a model of the NLRP3 LRR structure, based on the RI crystal structure (Figure 5-3 C). Moreover, close to two thirds of the non-LRR exons of all NLRs are frame-shifting as stochastically expected, but nearly all LRR-exons are frame-preserving (Figure 5-3 D), allowing for AS without introducing nonsense mutations.
In conclusion, the small LRR exons of NLRs and some other protein families show a conserved exon organization allowing for AS without frame-shifts and without destroying the secondary structure and support a modular-splicable structure of the LRR.

5.2. The splicing landscape of human NLRP3

In order to analyze AS of NLRs, deep RNASeq was performed from LPS-primed GM-CSF-derived human monocyte derived macrophages (hMDMs) of 5 healthy donors, and bioinformatics analysis was done in cooperation with S. Canzar and F. R. Ringeling (for mapping summary, see appendix Table 12-1). From all previously identified RI-type LRR-expressing genes (Figure 5-2 C), only 8 were expressed

(Figure 5-4 A): RNH1, the prototype LRR ribonuclease inhibitor, as well as NLRP3, NLRP1, NOD2, CIITA, NLRP2, NOD1 and NLRP12. For all of these genes, MISO was used to analyze AS and to generate sashimi plots (Figure 5-4 B and appendix Figure 12-2). Sashimi plots show the mapping of reads to a genomic location and highlight exon-spanning reads as arcs connecting exonic locations. Of all analyzed NLRs, NLRP3 shows the most prominent AS events. In order to quantify the AS events, exon inclusion levels (ψ) and confidence intervals were calculated for exon 5 and 7 (Figure 5-4 C, D). The narrow confidence intervals of the ψ histograms indicate a high level of certainty for the inclusion frequency of the respective exon according to the read distribution. It is obvious that exon 5 is consistently the most skipped exon (33 %) followed by exon 7 (2.6 %). Although this pattern was consistent, minor splicing differences were observed between donors.

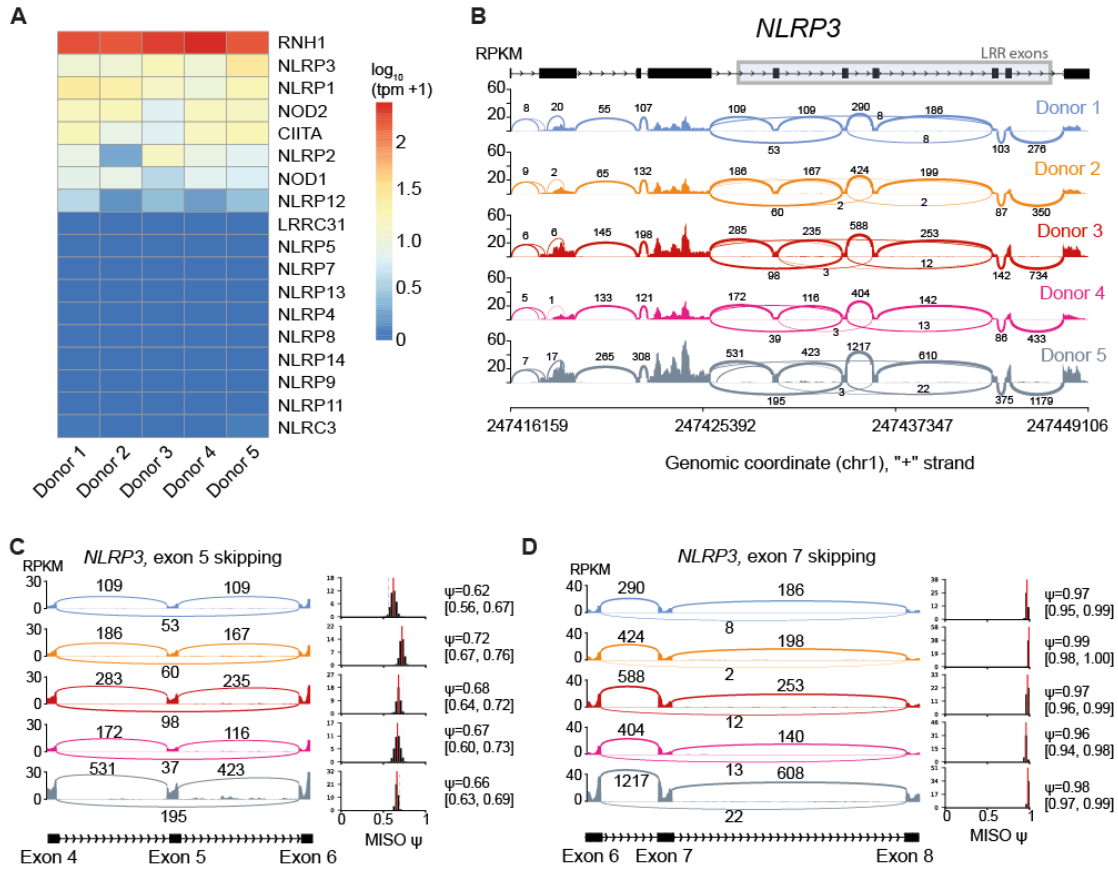

Figure 5-4 The splicing landscape of human NLRP3
Deep RNASeq was performed on LPS-primed human monocyte-derived macrophages (hMDMs) from 5 healthy donors. **A** Gene expression as transcripts per million (tpm) of all previously identified RI-type LRR encoding genes (Figure 5-2 D to F). **B** Sashimi plot of NLRP3 created with MISO. Read frequency within exons is plotted as reads per kilobase million (RPKM) and exon-spanning reads are labeled with the number of mapped reads. The NLRP3 gene structure is plotted above. Boxes indicate exonic regions and arrows within intronic stretches indicate the reading directions. Short repetitive LRR exons are highlighted with a grey box. The genomic location is depicted below. **C** and **D** Sashimi plots as in **B**, focused on exons 4-5-6 and 6-7-8, respectively. MISO ψ values (red bars in histogram) indicate the calculated frequency of exon inclusion. Confidence intervals (CI) are indicated as grey bars in the histogram. Ψ and CI values are also listed numerically.

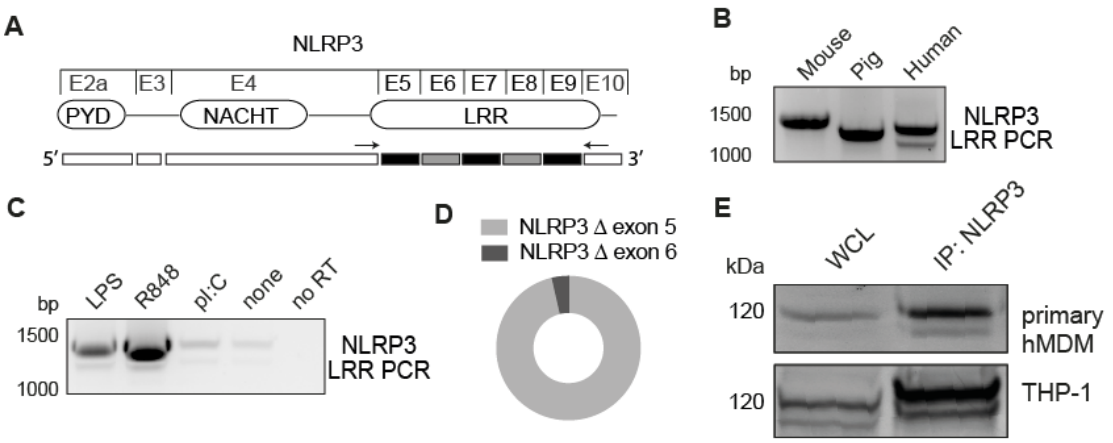

Figure 5-5 The LRR domain of human NLRP3 is subject to alternative splicing
A Illustration of the NLRP3 exons (E) and domains. Arrows indicate primers used in B, C and Figure 5-6) **B** PCR of the NLRP3 LRR on cDNA isolated from LPS-primed mouse BMDMs, pig and human PBMCs, respectively. Data are representative of at least 3 (mouse, human) or 2 (pig) individuals. **C** Human PBMCs primed with TLR agonists or left untreated were analyzed as in B noRT: no reverse transcription. **D** The lower band of PCR reactions (as in B) after LPS priming was isolated and 28 clones from different donors were sequenced to determine which exon is mostly alternatively spliced. **E** Immunoblot of human NLRP3 from primary human monocyte-derived macrophages (hMDM) or THP-1 cells. Whole cell lysates (WCL) or NLRP3 immunoprecipitation (IP) with a monoclonal antibody (mAb) targeted against the NACHT domain of NLRP3, were detected with an mAb targeted against the PYD to ensure NLRP3 specificity. Immunoblots are representative of two experiments.

To validate the bioinformatics analysis, PCRs across the whole canonical LRR region of NLRP3 were performed using primers binding in exon 4 and 10 (Figure 5-5 A). BMDMs or PBMCs from mouse, pig and human were tested for AS. Slightly different primer binding sites in different species cause a different size of the major band representing the full-length versions. Surprisingly, an additional shorter band, corresponding to the exclusion of one exon, could only be detected in human samples (Figure 5-5 B). Next, human PBMCs primed with different TLR agonists were tested to determine whether the alternative splice variant expression would be changed by stimulation (Figure 5-5 C). While overall NLRP3 expression was increased by TLR agonists, the smaller splice variant was neither drastically up- or down-regulated relative to the full-length variant. Since the LRR PCR could not reveal which of the 5 exons of the exact same length was alternatively spliced, the lower band PCR product was isolated, cloned and sequenced. In the large majority of sequenced clones, exon 5 was missing and only in one clone, another exon was missing (Figure 5-5 D). Since transcription does not necessarily correlate with productive translation and a stable protein product, the presence of an alternative NLRP3 splice form was confirmed by immunoblot in primary hMDM and in the human myeloid cell line THP-1 (Figure 5-5 E). To ensure high specificity of both detected bands, the immunoblot was combined with an immunoprecipitation (IP).

Different monoclonal antibodies (mAbs) targeted against the NACHT domain and the PYD were used.

AS is reported to be much more prevalent in human than in mice [149]. Still, an LPS stimulation time-course was performed on mouse BMDMs to exclude a potential up-regulation of AS at later timepoints after prolonged priming. However, AS of the mouse NLRP3 LRR could neither be detected on transcript level by PCR (Figure 5-6 A) nor by a combined IP-immunoblot approach (Figure 5-6 B).

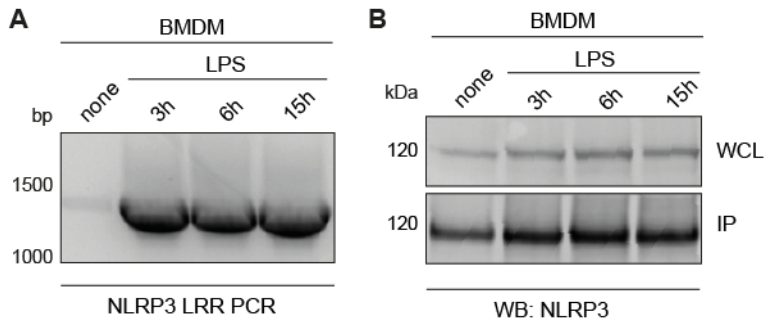

Figure 5-6 Alternative splicing of the NLRP3 LRR cannot be detected in BMDMs
A PCR of NLRP3 LRR on cDNA from mouse bone marrow derived macrophages (BMDMs) after different timepoints of LPS priming. Image is representative of 3 mice. **B** Immunoblot of mouse NLRP3 from BMDMs after different timepoints of LPS priming. Whole cell lysates (WCL) or NLRP3 immunoprecipitation (IP) using mAb against the NLRP3 NACHT domain were detected with an mAb against the PYD to ensure NLRP3 specificity. Immunoblots are representative of 3 mice.

PCRs across the whole LRR are a valuable approach as long as it is not known which exons can be alternatively spliced. However, bioinformatics analysis of the RNASeq data revealed only exon 5 and 7 to be significantly alternatively spliced. A qPCR splice panel was developed to specifically detect the prevalence for 4 NLRP3 isoforms: full-length, Δ exon 5, Δ exon 7, Δ exon 5/7 (Figure 5-7 A). Normalization against a housekeeping gene such as hypoxanthine-guanine phosphoribosyltransferase (HPRT) (Figure 5-7 B) is suitable to detect the differences in expression levels between individuals or after treatments. However, extremely different expression levels make it difficult to visualize changes in splice form abundance that way. Therefore, the relative abundance of NLRP3 splice forms was calculated as a fraction of the overall NLRP3 per sample. As seen before, the most strongly expressed alternative splice form is by far Δ exon 5. Both other targeted isoforms can be detected as well, but at expression levels several orders of magnitude lower (Figure 5-7 C). Since the regulation of the most prominent and likely most biologically important AS events was of highest interest, all results were plotted in a linear scale to focus on the most highly expressed variants (Figure 5-7 D to M). Multiple different primary myeloid cell types and cell lines treated with various pro-

and anti-inflammatory stimuli were tested. Although minor differences could be observed between different donors, the splice ratio was always kept stable within one donor and no major changes could be detected in the ratio of isoforms across all tested samples. Even in a clonal cell line (Figure 5-7 M, BLaER1), the isoform ratio was maintained, suggesting no inherited splicing pattern of subpopulations, but rather a spontaneous de novo adjustment.

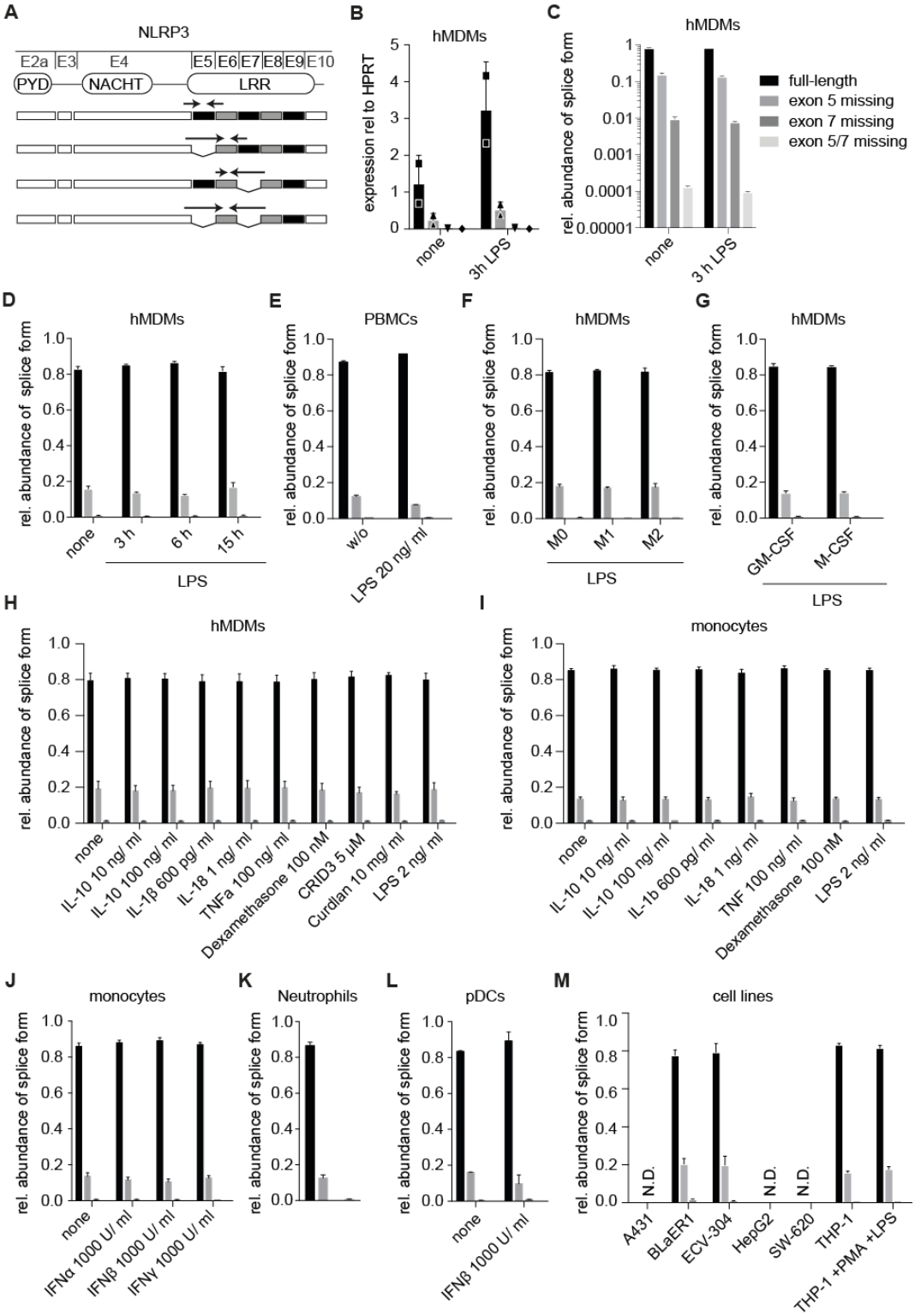

Figure 5-7 NLRP3 isoforms show a non-variable expression ratio
A Illustartion of NLRP3 isoform-specific exon-spanning qPCR primers used to detect NLRP3 full-length, Δ exon 5, Δ exon 7 and Δ exon 5/7. **B** Expression of NLRP3 isoforms relative to the housekeeping gene hypoxanthine-guanine phosphoribosyltransferase (HPRT). **C** Exemplary depiction of one data set with a logarithmic scale to demonstrate the much lower expression of NLRP3 Δ exon 7 and Δ exon 5/7. **C** to **M** Relative expression of NLRP3 isoforms depicted in A. Expression is calculated as fraction of the sum of all NLRP3 isoforms from different human primary cell types and cell lines after different treatments. If not differently indicated, LPS treatment was performed for 3 h with 2 ng/ mL. **H, I, J and L** were stimulated for 15 h as indicated. Figure B, C and D are different presentations of the same dataset. B, C, D, E, F, L Mean and SD of 2 donors, G, J Mean and SEM of 4 donors, H, I, K Mean and SEM of 3 donors, M Mean and SD of 2 independent experiments. cDNAs for J and K were provided by L. Labzin.

The structural features of the NLRP3 LRR described above would allow every LRR exon to be spliced out equally well. However, our RNAseq and PCR analysis revealed a strong tendency for AS of exon 5. Little is known about the complex integration of positive and negative splice factors on each splice site to regulate splicing. Yet, certain sequence elements can be associated with the strength of a splice acceptor or donor side. SplicePort is a tool to analyze pre-mRNA sequences and reports scores for splice acceptor or donor sites respectively [180]. SplicePort was used to analyze the strength of splice donor and acceptor sites in human NLRP3 pre-mRNA and identified the exon 5 acceptor, followed by the exon 7 acceptor, to be the least likely of all NLRP3 LRR splice acceptors to be used (Figure 5-8 A). Exonic splice enhancer (ESE) sites assist in exon recognition and are crucial to direct the spliceosome towards exon integration. In line with the other findings, the fewest ESE sites of the LRR stretch were detected in exon 5 of human NLRP3 using ESEfinder [186] (Figure 5-8 B).

Taken together, these findings reveal that alternative splicing of NLR LRR-exons takes place, that especially NLRP3 exon 5 is alternatively spliced and that the ratios of NLRP3 AS variants are kept stable in all tested conditions and cell types.

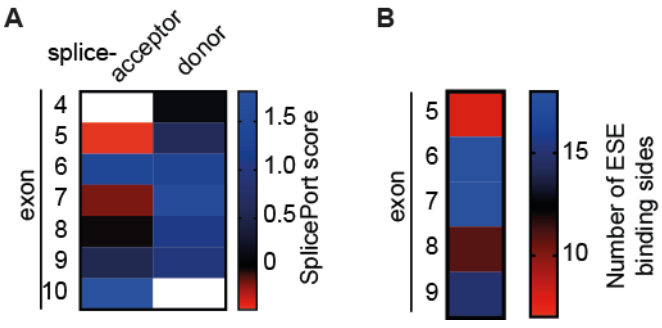

Figure 5-8 NLRP3 exon 5 shows the highest predisposition for alternative splicing
A Scores for the probability to function as splice acceptor and donor sites were calculated for all human NLRP3 LRR exon boundaries using SplicePort. High scores indicate a high probability to be recognized by the spliceosome **B** Number of exonic splice enhancer (ESE) sites within the exons of the LRR as predicted by RESCUE-ESE.

5.3. NLRP3 Δ exon 5 is inactive

The relatively high expression level of NLRP3 Δ exon 5 suggests a deliberate isoform rather than splicing noise. To elucidate a potential function of this splice variant, different model systems and NLRP3 inflammasome activation assays were used, which require some considerations: Assays should be performed in cells not expressing endogenous NLRP3 to not superimpose the observed effects of a given isoform. However, the cells need to express all other inflammasome components or a reporter for inflammasome activation. Moreover, transient transfections of NLRP3 isoforms in cells expressing a functional AIM2 inflammasome result in ASC speck formation, caspase-1 maturation and IL-1β secretion via detection of the plasmid DNA by AIM2, making the NLRP3 isoform analysis impossible. Finally, NLRP3 over-expression can cause NLRP3 activation without any further trigger.

5.3.1. NLRP3 Δ exon 5 is not able to induce ASC speck formation in Flp-In 293 reporter cells

To circumvent the above-mentioned obstacles, 293 T-REx reporter cell lines were created using the Flp-In technology. 293 T-REx cells do not endogenously express inflammasome components and the Flp-In technology enables exactly one integration at a pre-determined site within the genome, reducing the risk of different basal expression levels. The Flp-In constructs used here encode inducible NLRP3-tagRFP behind a tet-repressor, ASC-mTurquoise (mTurq) and a hygromycin selection cassette. NLRP3 integration and transcription was assessed by PCR across the exon 5 area (Figure 5-9 A), and NLRP3 and ASC protein expression were verified by immunoblot (Figure 5-9 B). In order to test the inducible upregulation of NLRP3 expression, cells were treated with increasing amounts of doxycycline to switch off the tet-repressor. TagRFP fluorescence was monitored by flow cytometry as a measure for NLRP3 expression in the different cell lines (Figure 5-9 C and D). Of note, a low background expression of both NLRP3 isoforms was observed even without doxycycline induction.

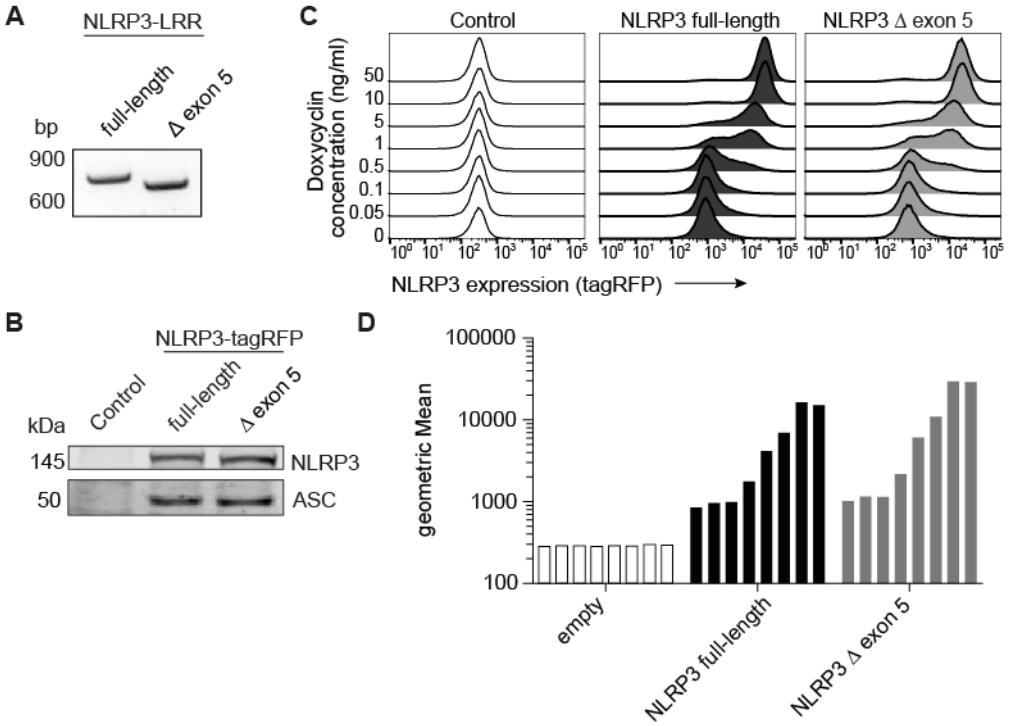

Figure 5-9 Generation of isoform-specific inducible NLRP3 reporter cells
Characterization of Flp-In T-REx 293 cells expressing either tetracycline-inducible NLRP3 full-length or Δ exon 5, both fused C-terminally to tagRFP. Both Flp-In vectors also encode ASC-mTurquoise. **A** PCR on cDNA created from the stable Flp-In cell lines. Primers targeted against exon 4 and the exon 7/8 boundary were used to amplify the LRR exon 5 area to verify isoform specificity of the cell lines. **B** Immunoblot expression control of NLRP3-tagRFP and ASC-mTurquoise from Flp-In T-REx 293 cells. Control: non-transfected Flp-In T-REx 293 cells. **C** NLRP3-tagRFP expression was induced in Flp-In T-REx 293 cells with the respective concentrations of doxycycline. Expression levels were measured by flow cytometry. **D** Quantification of **C**. Shown are the tag-RFP fluorescence levels as geometric means.

Upon inflammasome activation, all molecules of the adapter ASC are recruited into a single multi-protein complex termed ASC speck or pyroptosome. By using fluorescently labeled versions of ASC, ASC speck assembly can be used as readout for inflammasome activation (Figure 5-10 A). The activity of NLRP3 full-length and NLRP3 Δ exon 5 were assessed by fluorescence microscopy after doxycycline-induced overexpression (Figure 5-10 B, C) and in the absence of doxycycline after activation with the NLRP3 activator nigericin (Figure 5-10 D). Nuclei were counterstained and the proportion of cells with an ASC speck was calculated. While NLRP3 full-length induced a dose-dependent ASC speck formation for both triggers, NLRP3 Δ exon 5 remained completely inactive.

To further confirm that NLRP3 Δ exon 5 expressing cells do not assemble inflammasomes with ASC, the interaction between NLRP3 and ASC was investigated by co-IP. NLRP3 was immunoprecipitated with an mAb against its fluorescent label tagRFP. While both cell lines expressed similar amounts of NLRP3 and ASC, an interaction between ASC and NLRP3 could only be detected for NLRP3

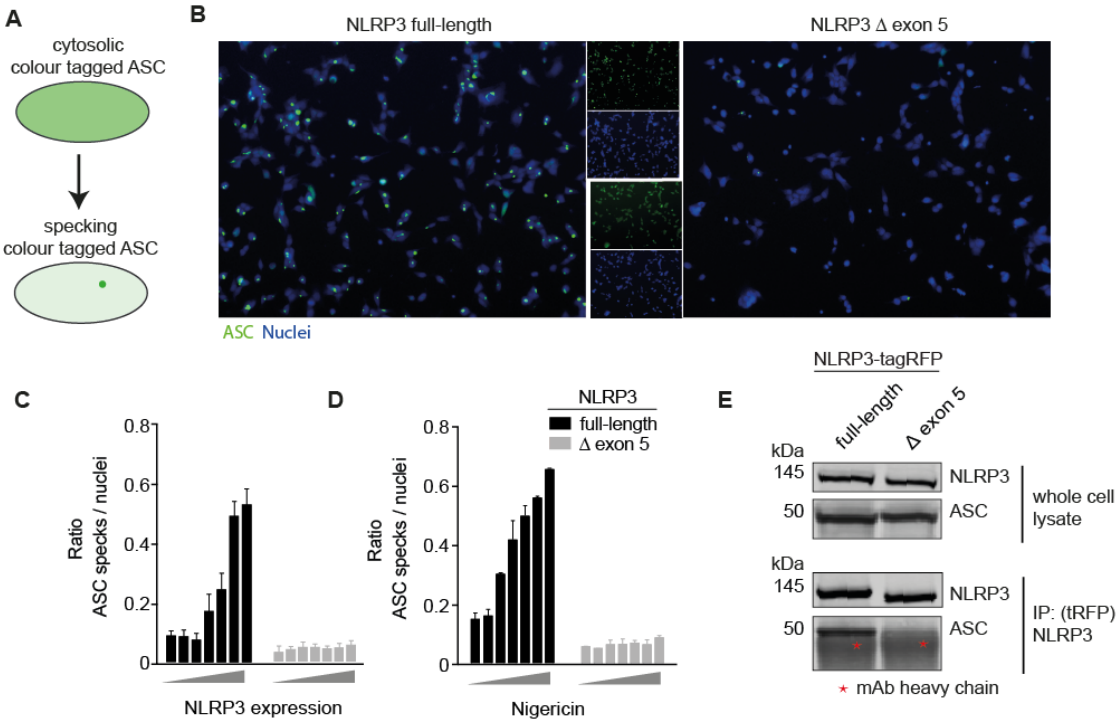

Figure 5-10 10 NLRP3 Δ exon 5 is not able to induce ASC speck formation in Flp-In 293 cells

A Schematic of an inflammasome ASC speck assay. The inflammasome adapter ASC is equally distributed across the cytosol in non-activated cells. Upon inflammasome activation all ASC molecules oligomerize into one speck. **B** Flp-In T-REx 293 cells expressing inducible NLRP3-tagRFP and ASC-mTurquoise (green) were analyzed for ASC speck formation by fluorescence microscopy. Cell nuclei were counterstained with DRAQ5 (blue). **C** Quantification of ASC speck formation after doxycycline-induced NLRP3 overexpression (0 – 10 ng/ mL doxycyclin). Mean and SD of 9 frames per condition N=1. **D** Quantification of ASC speck formation after 2.5 h stimulation with nigericin (0 - 10 µM). Mean and SD of technical duplicates, 9 frames per well, representative of 3 independent experiments. **E** Co-immunoprecipitation (IP) of ASC with NLRP3-tagRFP from Flp-In T-REx 293 cells. NLRP3 was immunoprecipitated using anti-tagRFP mAb. Asterisk indicates heavy chain of mAb used for IP. Blots are representative of 2 independent experiments.

full-length, but not for NLRP3 Δ exon 5 (Figure 5-10 E). While the presence of the heavy chain of the IP mAb (indicated with a red asterisks) at a similar apparent molecular weight complicated the analysis, the differential ASC interaction was nevertheless obvious.

To further investigate NLRP3 activation, an assay to detect inflammasome formation by flow cytometry based on ASC specks was developed during this study. While most flow cytometric assays concentrate on the overall fluorescence (area of the signal pulse) or the maximum peak fluorescence (height of the signal pulse), the width of the signal pulse provides information about the size of the fluorescent object. While the width of a signal, generated by fluorescently marked, randomly distributed proteins correlates with the cell size, a dramatic decrease in the width of the signal can be observed when all fluorescent molecules cluster in one defined aggregate per cell (Figure 5-11 A). Since ASC gets recruited into one spot per cell upon

inflammasome activation, the width of the fluorescent signal can be used to discriminate cells containing an ASC speck from non-activated cells.

As seen before by microscopy, NLRP3 full-length expressing cells form ASC specks upon nigericin stimulation, while NLRP3 Δ exon 5 expressing cells stay inactive. A respective second population/ peak in the ASC-mTurq width channel can be observed for specking cells, confirming the microscopy results (Figure 5-11 B and C). The validity and usefulness of this flow cytometry-based approach was confirmed by Sester et al., who published similar findings[187].

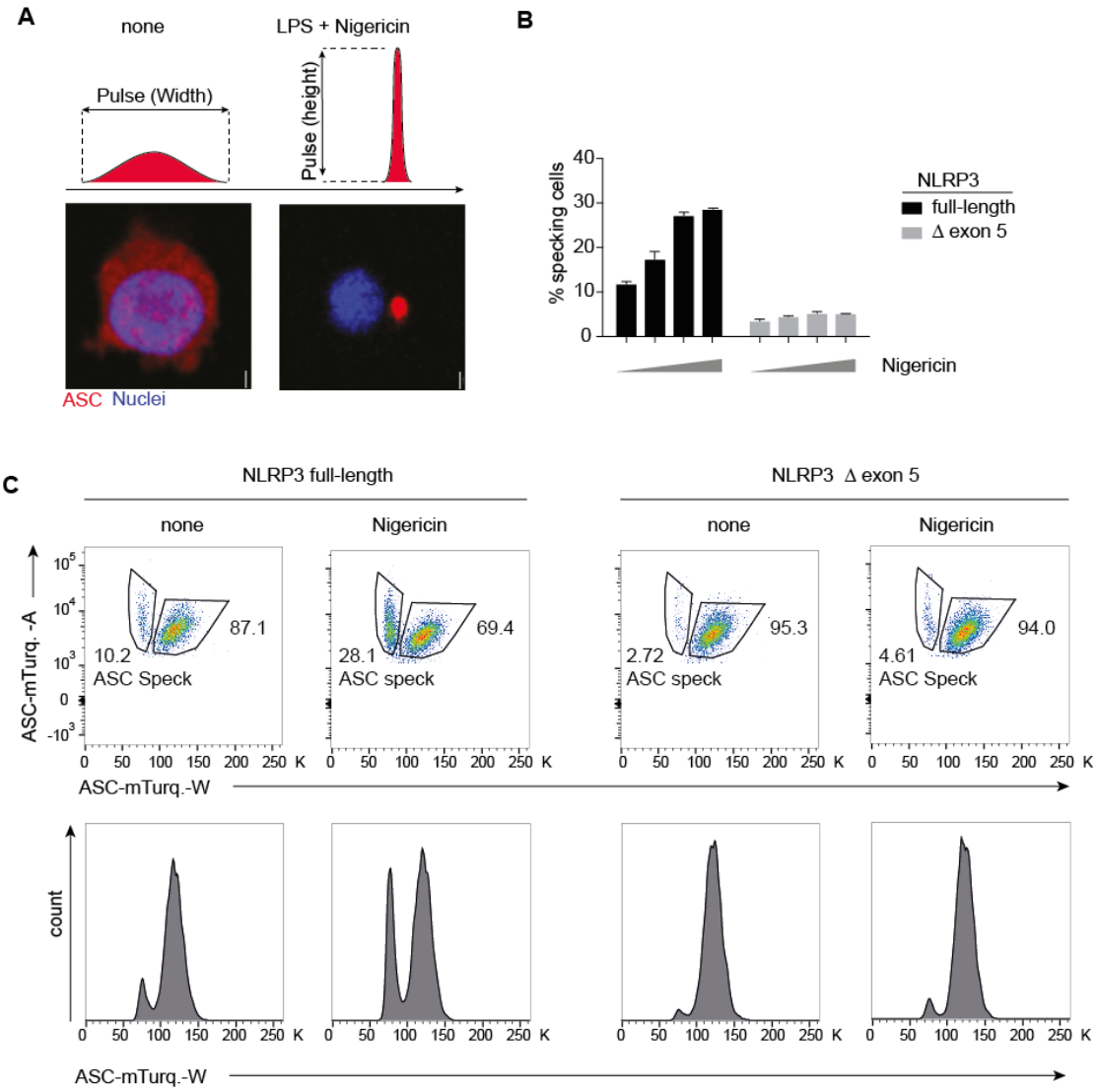

Figure 5-11 ASC speck formation can be detected by flow cytometry

A Principle of the detection of ASC speck formation by flow cytometry. The clustering of all fluorescent ASC molecules results in a reduced width of the signal. Scale bar in micrograph 2.5 µm. Modified from Hoss *et al.* 2018 [188]. **B** Quantification of nigericin (0 - 7.5 µM) -induced ASC speck formation in Flp-In T-REx 293 cells cells, analyzed by flow cytometry. **C** Flow cytometry graphs of B (7.5 µM nigericin). Top panel shows ASC speck formation as a dotplot of ASC-mTurquoise area signal versus width signal A – area, W – width. Bottom panel shows ASC speck formation as an additional smaller peak in the histogram of the ASC-mTurquoise width signal.

In summary, it was shown, that NLRP3 Δ exon 5 is not capable to interact with ASC and to induce ASC speck formation.

5.3.2. NLRP3 Δ exon 5 does not induce caspase-1 maturation and IL-1β secretion in macrophages

Although Flp-In 293 T-REx cells represent a valuable tool, it is critical to analyze the activity of the NLRP3 isoforms also in the context of naturally inflammasome-competent cells. Therefore, NLRP3-deficient immortalized mouse macrophages (iMos) were retroviral reconstituted with the different NLRP3 isoforms fused to a C-terminal mCitrine fluorescence tag. After generation of stable cell lines, they were FACS-sorted to a comparable and low expression level to reduce the risk of overexpression-induced activation (Figure 5-12 A). Of note, constantly expressed functional NLRP3 results in reduced fitness of the cell and down-regulation after a few passages. This might explain the minimally lower expression of NLRP3 full-length.

NLRP3 deficient and reconstituted cells were primed with LPS to induce the up-regulation of pro-IL-1β, and subsequently activated with nigericin or ATP for NLRP3 inflammasome activation or with *B. anthracis* lethal toxin (LT) for NLRP1B inflammasome activation (Figure 5-12 B). While NLRP3 activation of the full-length cell line resulted in mature caspase-1 and IL-1β in lysates and supernatants, NLRP3 knock-out and Δ exon 5 expressing cells generated no detectable levels of mature caspase-1 and IL-1β. However, both cell lines were fully active after NLRP1B stimulation, providing evidence for the functionality of all inflammasome components besides NLRP3 in these cells. The apparently reduced expression of β-actin and

Figure 5-12 NLRP3 Δ exon 5 does not induce caspase-1 maturation and IL-1β secretion in macrophages
NLRP3-deficient immortalized macrophages (iMos) were retrovirally reconstituted with either NLRP3 full-length or NLRP3 Δ exon 5, both with a C-terminal mCitrine tag. Stable cell lines were FACS-sorted on a low equivalent NLRP3 expression level. **A** Flow cytometry analysis of NLRP3-mCitrine showing the expression levels of NLRP3 isoforms in the respective cell lines. **B** Immunoblots of iMos after activation of the NLRP3 inflammasome (ATP, nigericin) or the NLRP1B inflammasome (lethal toxin, LT). Blots are representative of two independent experiments. **C** IL-1β secretion after activation of the NLRP3, NLRP1B or AIM2 inflammasomes. **D** TNF secretion after LPS treatment. C and D Mean and SD of technical triplicates, representative of 3 independent experiments. **E** IL-1β secretion after Pam3CSK4 priming and non-canonical inflammasome activation. Mean and SD of technical duplicates representative of 2 independent experiments. **F** and **G** IL-1β secretion after potassium-independent NLRP3 inflammasome activation via R837 and PGN. F Mean and SD of 2 independent experiments G Mean and SD of technical triplicates. N=1. **H** Confocal micrograph of LPS-primed and nigericin-pulsed iMos. Nuclei and Membranes were stained with Hoechst 34580 and wheat germ agglutinin (WGA) AF-633, respectively. Arrowheads indicate NLRP3 specks. Representative of 2 independent experiments.

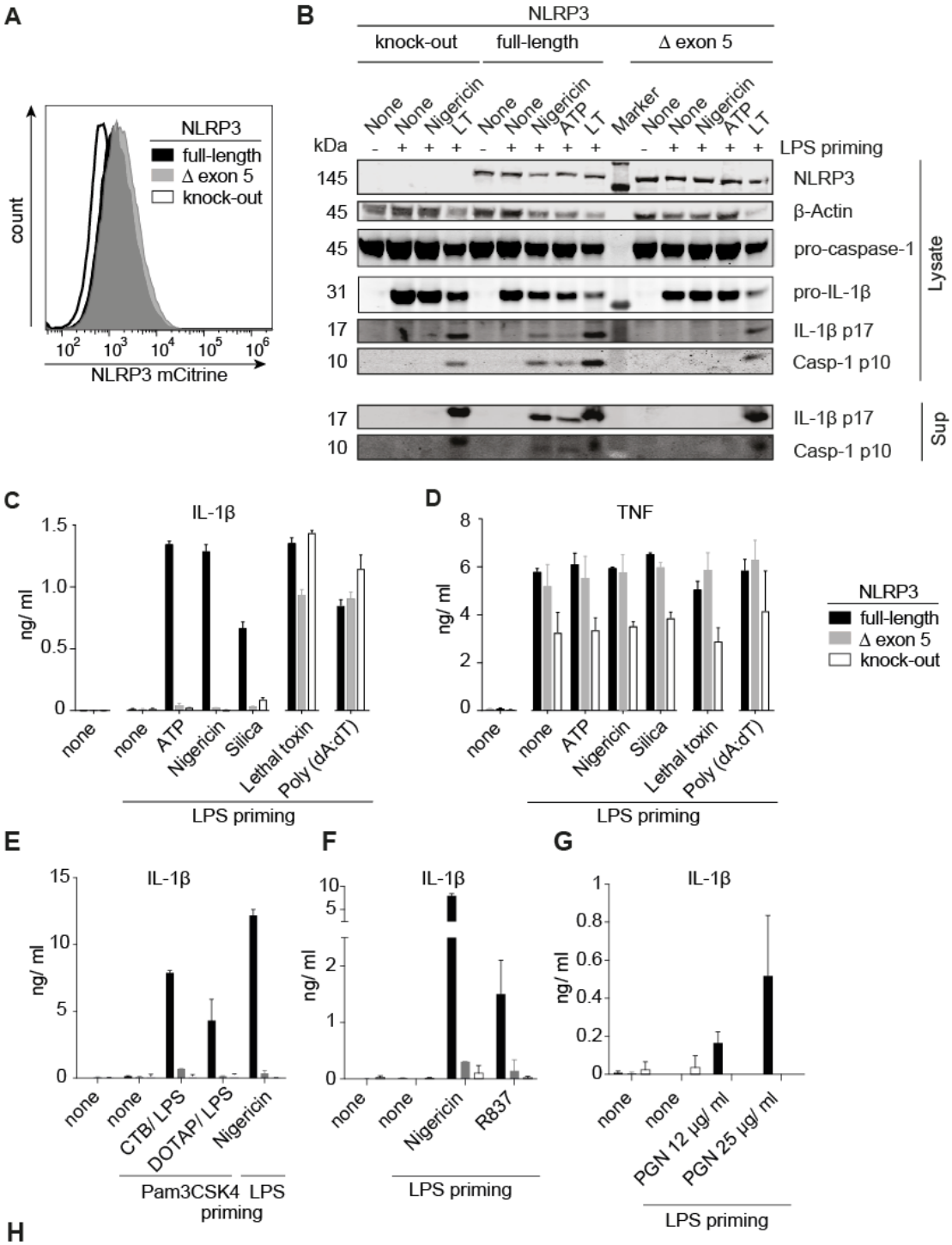
A
count
NLRP3
full-length
Δ exon 5
knock-out
NLRP3 mCitrine
B
NLRP3
knock-out
full-length
Δ exon 5
None None Nigericin LT None None Nigericin ATP LT Marker None None Nigericin ATP LT
kDa
LPS priming
145 NLRP3
45 β-Actin
45 pro-caspase-1
31 pro-IL-1β
17 IL-1β p17
10 Casp-1 p10
Lysate
17 IL-1β p17
10 Casp-1 p10
Sup
C
IL-1β
ng/ ml
none none ATP Nigericin Silica Lethal toxin Poly (dA:dT)
LPS priming
D
TNF
ng/ ml
none none ATP Nigericin Silica Lethal toxin Poly (dA:dT)
LPS priming
NLRP3
full-length
Δ exon 5
knock-out
E
IL-1β
ng/ ml
none none CTB/ LPS DOTAP/ LPS Nigericin
Pam3CSK4 priming
LPS priming
F
IL-1β
ng/ ml
none none Nigericin R837
LPS priming
G
IL-1β
ng/ ml
none none PGN 12 µg/ ml PGN 25 µg/ ml
LPS priming
H
NLRP3 full-length
Nucleus
Membrane
NLRP3
NLRP3 Δ exon 5

NLRP3 after inflammasome activation is caused by a pyroptotic burst of inflammasome-activated cells and loss of protein content.

Further inflammasome activators were tested and released IL-1β levels were analyzed by ELISA. The NLRP3 activators nigericin, ATP, and silica induced IL-1β secretion exclusively in NLRP3 full-length expressing cells, while all cell lines secreted IL-1β upon activation of the AIM2 (poly dA:dT) or the NLRP1B (LT) inflammasome. LPS-induced TNF secretion (as a control for priming and therefore the expression of pro-IL-1β) was also comparable between the cell lines (Figure 5-12 D).

After ruling out a role for NLRP3 Δ exon 5 in canonical inflammasome activation, the activation of the non-canonical inflammasome was tested. The non-canonical inflammasome is activated upon detection of cytosolic LPS [101]. As LPS already serves as the activation signal, cells were primed with the TLR2 agonist Pam3CSK4. LPS was delivered to the cytosol either using cholera toxin B (CTB) induced endocytosis or via transfection with DOTAP. Again, only the NLRP3 full-length cell line secreted IL-1β in response to cytosolic LPS (Figure 5-12 E). The same was observed when NLRP3 was activated via the non-potassium dependent activators R837 and PGN (Figure 5-12 F, G).

Since inflammasome activation downstream of NLRP3 (recruitment of ASC, polymerization of ASC, maturation of caspase-1, and secretion of IL-1β) was not triggered, the question was addressed whether NLRP3 Δ exon 5 is still capable to form a seed for ASC recruitment. While some NLRP3 aggregates could be observed by confocal microscopy after inflammasome activation in the full-length expressing cells, this was not as obvious for NLRP3 Δ exon 5 (Figure 5-12 H).

In summary, NLRP3 Δ exon 5 was shown to be not activatable in reconstituted iMos, while NLRP3 full-length acted as expected.

5.3.3. Morpholinos can be used to alter splice patterns in primary human monocyte-derived macrophages

While the inactive phenotype of NLRP3 Δ exon 5 was highly reproducible in model systems, confirmation of these findings in primary cells was missing. However, it remained a challenge to analyze this splice form in primary cells because they always expressed both major splice variants and none of the tested stimuli was shown to regulate NLRP3 splicing.

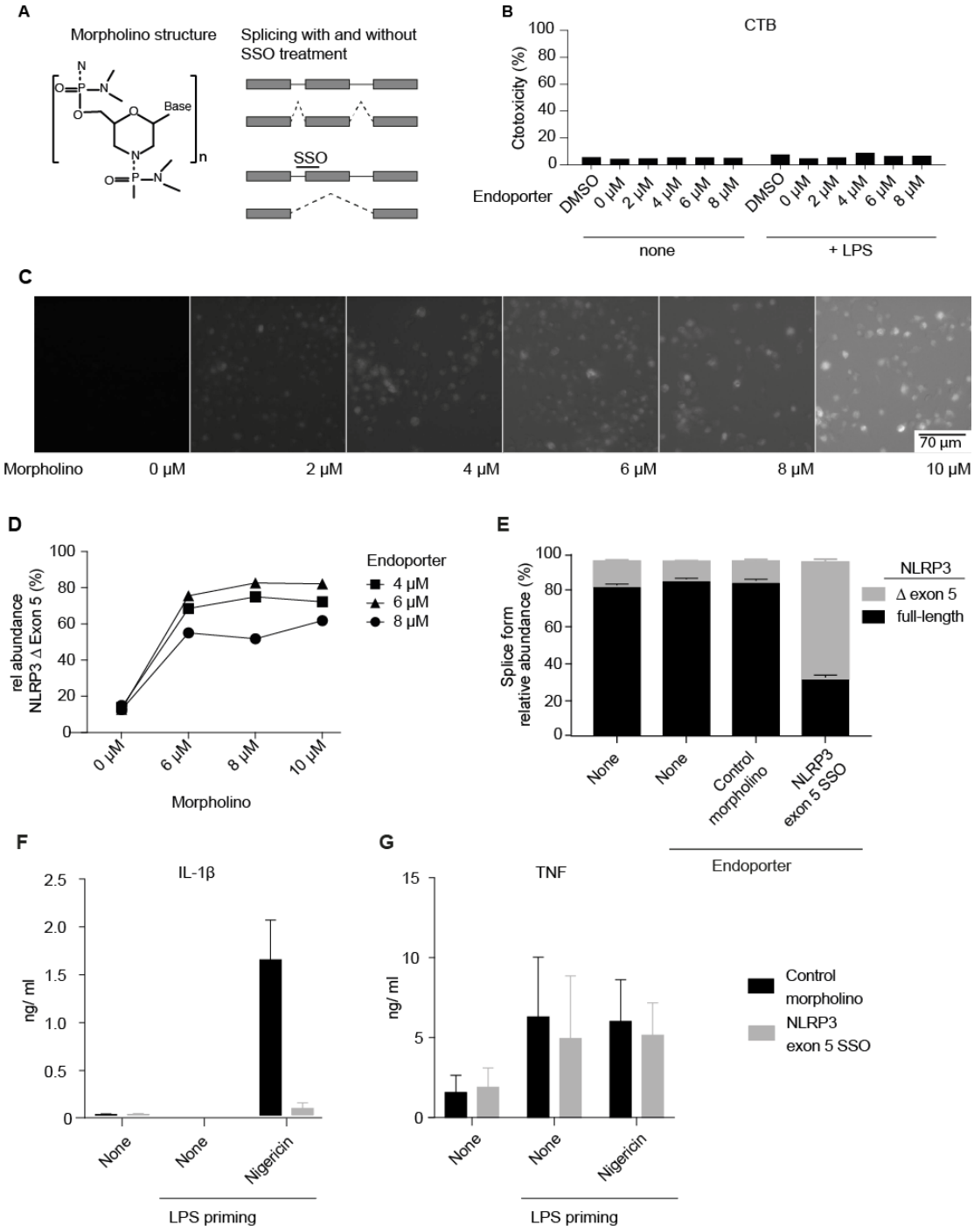

Figure 5-13 Morpholinos can be used to alter splice patterns in primary human monocyte-derived macrophages

A Left panel: Chemical structure of morpholino oligomers. Right panel: schematic of the principle of splice-switching oligonucleotide (SSOs). **B** Endoporter titration to assess cytotoxicity. DMSO only corresponds to the highest used DMSO concentration (10 µM Endoporter, 1% DMSO). Cells were incubated for 48 h after Endoporter treatment. LPS was added for the last 24 h. **C** Titration of a fluorescein-tagged morpholino transfected with 6 µM Endoporter. **D** Cross-titration of Endoporter concentration and the concentration of a SSO morpholoino targeted against the NLRP3 exon 5. Graph shows qPCR analysis of the relative abundance of the NLRP3 Δ exon 5 after splice induction N=1. **E** Changes in the NLPR3 alternative splicing pattern of hMDMs were induced with an exon 5 SSO. NLRP3 isoform expression analysis by qPCR. Mean and SEM of 3 (or 2, untreated ctr.) donors. **F** IL-1β secretion of morpholino-treated cells after nigericin-induced activation of the NLRP3 inflammasome (IL-1β). **G** TNF secretion after LPS treatment. F and G mean and SEM of 3 donors (2 donors, LPS-only ctr.).

Morpholinos are a class of DNA analogues with a non-charged backbone, which are highly protected against degradation. I made use of morpholinos as so-called splice-switching oligonucleotides (SSOs), which can direct alternative splicing towards the exclusion of an exon by complementary binding and blocking the spliceosomal access to the intron-exon boundary (Figure 5-13 A). The intracellular delivery of these uncharged oligonucleotides can be achieved by Endoporter, which induces phagocytosis and release into the cytosol. First, it was confirmed that Endoporter treatment of primary hMDMs had no cytotoxic effects (Figure 5-13 B). Next, the cytosolic delivery of morpholinos was controlled using a fluorescein-tagged oligonucleotide (Figure 5-13 C). An increased background fluorescent was detected with increasing oligonucleotide concentration, probably due to binding to the plastic dish. Yet, an intracellular enrichment can be observed with increasing concentrations. To analyze the splice-switching effect, different concentrations of a NLRP3 intron 4/ exon 5 targeted SSO were applied to hMDMs of one donor (Figure 5-13 D). The relative abundance of NLRP3 Δ exon 5 was analyzed by qPCR, demonstrating 6 µM Endoporter to be the most effective concentration. Since no dramatic difference could be observed between the tested concentrations of SSO, the lowest concentration (6 µM) was chosen for all following experiments.

While Endoporter treatment alone or a control Morpholino did not induce any changes in the NLRP3 splice pattern, the specific NLRP3 exon 5 SSO strongly induced alternative splicing of NLRP3 Δ exon 5 across hMDMs of multiple donors (Figure 5-13 E). SSO treatment before NLRP3 activation resulted in a nearly complete inhibition of the IL-1β secretion, while TNF levels remained unaffected (Figure 5-13 F). Of note, some degree of inter-donor differences can be observed, as well as a slight background activation for TNF in the non-primed cells, possibly due to Endoporter-induced increased phagocytosis.

Taken together, these results provide evidence for the inactivity of NLRP3 Δ exon 5 in primary human cells.

5.3.4. NLRP3 Δ exon 5 has no inhibitory function on the NLRP3 full-length variant

After establishing evidence for the inactivity of NLRP3 Δ exon 5, the role of this transcript variant remained elusive. A possible role for NLRP3 Δ exon 5 might be the inhibition of full-length NLRP3 when co-expressed. To investigate whether this was the case, the NLRP3 full-length expressing iMo cell line was retrovirally transduced

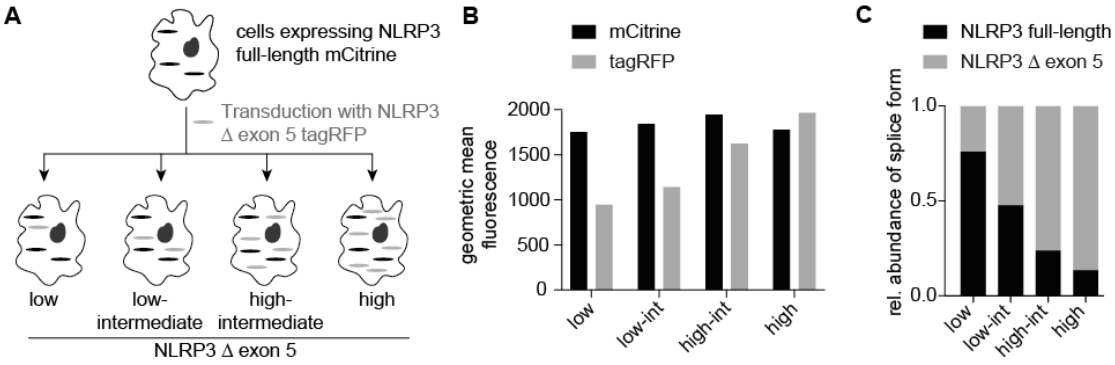

Figure 5-14 Generation of iMos co-expressing NLRP3 full-length and Δ exon 5 in different ratios

A iMos expressing NLRP3 full-length with a fluorescent mCitrine tag were retrovirally transduced with NLRP3 Δ exon 5 with a fluorescent tagRFP tag. The resulting stable cell line was FACS-sorted into 4 different NLRP3 Δ exon 5 expression bins (low, low-intermediate, high-intermediate, high), while keeping the NLRP3 full-length expression stable. **B** Flow cytometry analysis of mCitrine (NLRP3 full-length) and tagRFP (NLRP3 Δ exon 5) expression levels shown as geometric means of the respective fluorescence. **C** qPCR analysis of the expression of both transduced NLRP3 isoforms. Shown are the expression levels as relative abundance of the overall NLRP3.

with NLRP3 Δ exon 5-tagRFP. The cells were FACS-sorted for 4 different NLRP3 Δ exon 5 expression levels, while keeping NLRP3 full-length expression constant (Figure 5-14 A). The desired expression levels of NLRP3 full-length-mCitrine and NLRP3 Δ exon 5-tagRFP expression in the stable cell lines were confirmed by flow cytometry (Figure 5-14 B). While a linear increase in tagRFP was detectable across the four cell lines, mCitrine levels remained comparable. Since fluorescence intensities acquired in different channels are not comparable, NLRP3 transcription was analyzed by qPCR (Figure 5-14 C). As intended, the NLRP3 isoform ratio ranged from mostly full-length to mostly Δ exon 5 expression across the 4 cell lines.

The co-expressing cell lines were primed with LPS and activated for NLRP3 or the NLRP1B inflammasome as above. No significant difference in IL-1β secretion could be observed with increasing levels of NLRP3 Δ exon 5 expression (Figure 5-15 A). The non-significant increase in IL-1β from low NLRP3 Δ exon 5 to high-intermediate NLRP3 Δ exon 5 correlates with minimally higher NLRP3 full-length expression (Figure 5-14 B) and with a minor, non-significant increase in priming as testified by increased TNF levels (Figure 5-15 B). LDH release as a measure for pyroptosis could be detected after inflammasome activation, however without any significant differences between different expression levels of NLRP3 Δ exon 5 (Figure 5-15 C).

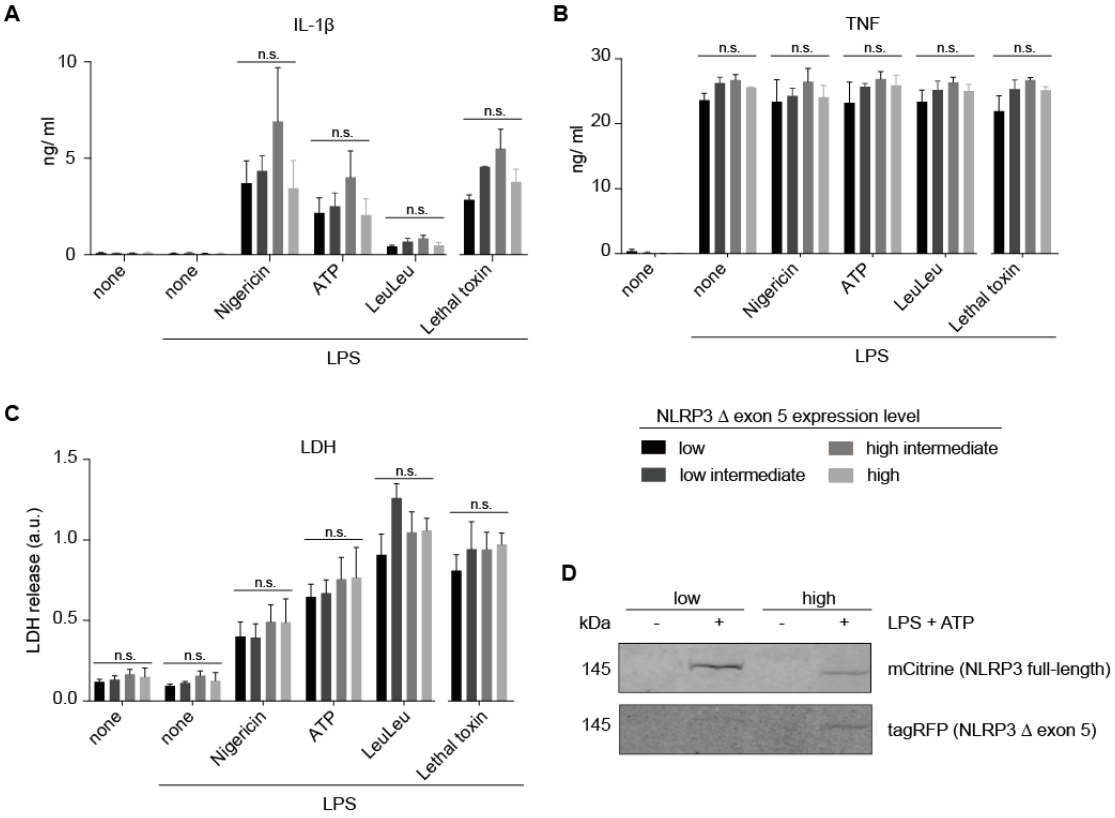

Figure 5-15 NLRP3 Δ exon 5 has no inhibitory function on the NLRP3 full-length variant.
A IL-1β secretion after activation of the NLRP3 or NLRP1B inflammasome. **B** TNF priming control after LPS treatment. A and B mean and SEM of 3 independent experiments. **C** Cell death was measured by LDH release as surrogate marker for loss of membrane integrity of cells after inflammasome activation. Mean and SEM of 3 independent experiments. **D** Cells expressing low or high levels of NLRP3 Δ exon 5 were primed with LPS and stimulated for 2.5 h with ATP in order to induce pyroptosis and speck formation. ASC specks were purified from the supernatant and immunoblotted for the presence of NLRP3 full-length and NLRP3 Δ exon 5. Representative of 3 independent experiments. LeuLeu: l-Leucyl l-leucine methyl ester, ns: non-significant, two-way ANOVA with Tukey multiple comparison correction.

The same dual expressing cells were used to check whether NLRP3 Δ exon 5 is actively excluded from the inflammasome complex. After prolonged NLRP3 inflammasome activation with ATP to induce strong ASC speck formation and pyroptosis, ASC specks were isolated from the supernatant of NLRP3 Δ exon 5 low and high expressing cells. Purified ASC specks were analyzed by immunoblot to detect whether both NLRP3 variants could be detected within NLRP3 specks. Although NLRP3 full-length seemed to be predominantly incorporated, NLRP3 Δ exon 5 could be detected as well (Figure 5-15 D).

In conclusion, NLRP3 Δ exon 5 seems not to act as dominant negative form to inhibit NLRP3 full-length activation. Instead, if highly expressed, it can be incorporated into ASC specks.

5.4. NLRP3 splicing is regulated on a single-cell level

After demonstrating that NLRP3 Δ exon 5 does not act as a regulator of full-length NLRP3 when co-expressed, the question of its function remained open. A conceivable hypothesis would be that NLRP3 alternative splicing is regulated on a single-cell level. This would result in different 'populations' with different NLRP3 activities.

To analyze NLRP3 isoform expression on single-cell level, LPS-primed, viable hMDMs were FACS-sorted into separate wells of 96-well PCR plates. Nearly 200 cells of each of 3 donors were lysed, cDNA was reverse-transcribed and NLRP3 isoforms and the housekeeping gene HPRT were pre-amplified in a nested PCR set-up. Then, expression of NLRP3 isoforms, HPRT and 18S rRNA was analyzed by TaqMan PCR (Figure 5-16 A and B). In each of the 3 donors, 4 different NLRP3 expressing populations were observed: Cells expressing both isoforms, cells expressing only one or the other, and cells with no detectable NLRP3 expression. In some cells, it was not even possible to detect HPRT expression. This is because the transcription process is subject to a burst kinetic. Once a gene locus is activated and transcribed, the mRNA level increases in a transcriptional burst and slowly declines after the gene locus is inactivated. While the protein product is as well affected by theses fluctuations, it is more stable (Figure 5-16 C) [189,190]. When analyzing gene expression on a pool of cells, the mRNA level of a gene of interest is expressed at a stable mean over all cells, as they are not synchronized in their transcriptional burst of a given gene. Moreover, the expression of different genes is not necessarily synchronized on single-cell level, making it unreasonable to normalize RNA

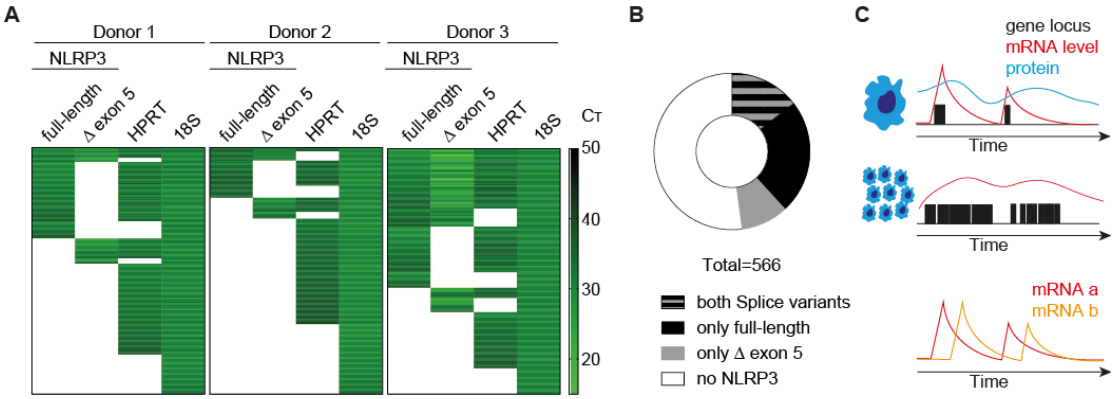

Figure 5-16 NLRP3 splicing is regulated on a single-cell level.
A Dead cells were discriminated by PI stain. Single, PI-negative hMDMs were FACS-sorted into individual wells and lysed. RNA was reverse-transcribed and NLRP3 full-length, NLRP3 Δ exon 5 and HPRT encoding mRNAs were pre-amplified. Transcripts were detected with nested TaqMan assays. 187 to 192 individual cells per donor were analyzed, each line represents the CT-values of a single-cell. **B** Quantification of the single-cell NLRP3 splice pattern. Shown as the mean of 3 donors from A. **C** Schematic of the burst-kinetic of gene-expressions on single-cell level, resulting in oscillations of produced mRNA levels per gene over time.

expression. 18S rRNA is an exception and can be used to control for technical dropouts. It is expressed several orders of magnitude higher than most other RNAs and even more importantly, the RNA itself and not a protein product is the active moiety which needs to be stably present in a cell.

After providing evidence for the stochastic expression of NLRP3 isoforms, the next question to be addressed was whether this expression pattern correlates with NLRP3 activity of single human primary cells. To investigate NLRP3 activity on a single-cell level, NLRP3 was activated with increasing amounts of nigericin or NLRC4 with PrgI in primary hMDMs and the percentage of cells with ASC specks was determined. Surprisingly, only a small fraction of cells responded to NLRP3 stimulation, while 100% of the cells formed ASC specks upon NLRC4 activation (Figure 5-17 A, B). To control for a typical NLRP3 activation, the secreted IL-1β was measured by HTRF. For better visualization, cells were treated with the caspase inhibitor VX-765 to

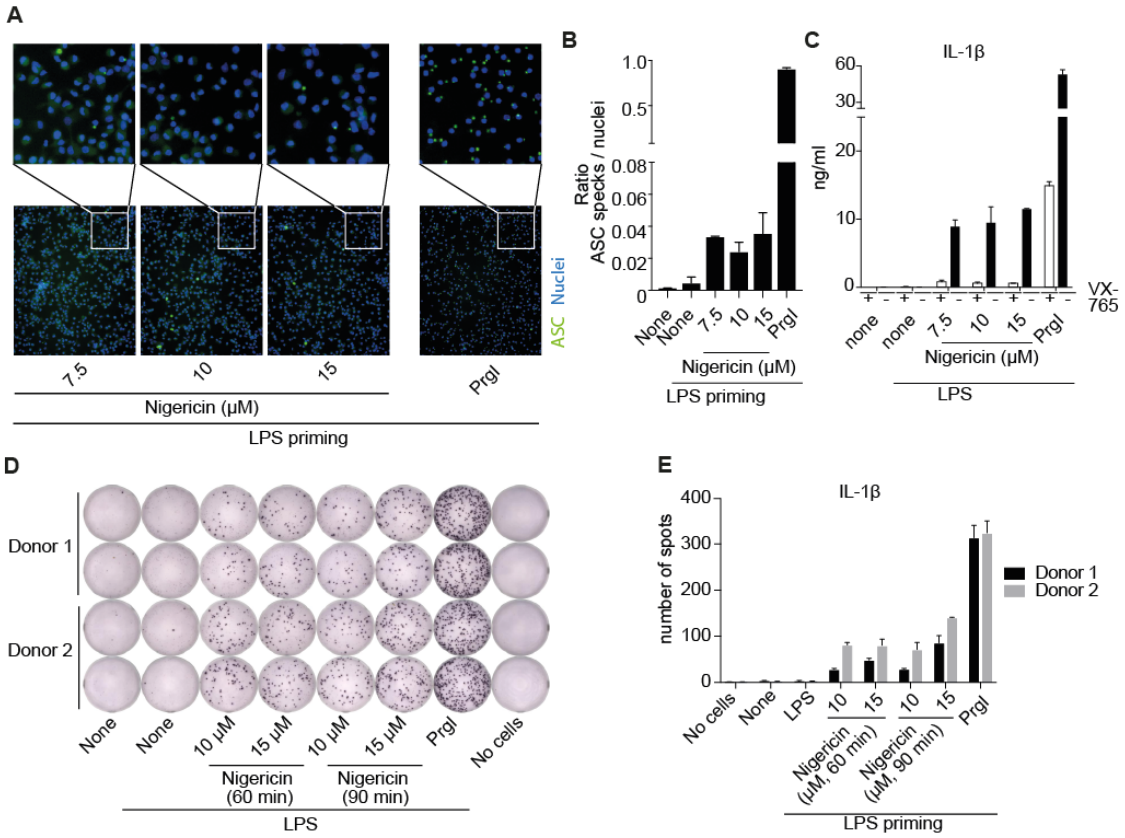

Figure 5-17 Only a fraction of primary hMDMs can activate the NLRP3 inflammasome
A and **B** ASC speck analysis of hMDMs after NLRP3 activation with nigericin and NLRC4 activation with bacterial product PrgI. 5 images per well were captured, plotted are means and SD of two replicate wells, representative of 4 individual experiments. **C** Secretion of IL-1β measured in parallel to A/B with and without caspase inhibitor VX-765 treatment (ASC speck analysis samples were treated with VX-765 to prevent pyroptosis) **D** and **E** IL-1β ELISpot assay of hMDMs after NLRP3 or NLRC4 inflammasome activation. Shown are results from two donors. Assays were performed in technical duplicates. Mean and SD of technical duplicates.

prevent pyroptosis during ASC speck assays. Since VX-765 would inhibit the release of IL-1β, cells for IL-1β detection were treated with and without VX-765 in parallel to the ASC speck assay. An IL-1β response in the expected range could be observed (Figure 5-17 C). Of note, NLRC4 activation resulted also in a higher IL-1β response compared to NLRP3 activation, which was not completely inhibited at the used VX-765 concentration. While hMDMs were capable of secreting IL-1β, only a minor fraction of the cells formed ASC specks. The question remained how many cells contribute to the secreted IL-1β. To address this, ELISPOT assays were performed. ELISPOT assays capture and visualize a cytokine at the site of secretion, resulting in discriminate spots for each activated cell. While again, all cells secreted IL-1β upon NLRC4 activation, the number of responsive cells was much lower for NLRP3 activation, even at later time points and with increased nigericin concentrations (Figure 5-17 D, E). Together these findings suggest that NLRP3 as a danger sensor is highly regulated in primary human cells, correlating to the observed single-cell AS pattern, while NLRC4 as a sensor for microbial infections induces an unbridled response.

5.5. NLRP3 Δ exon 5 does not interact with NEK7

While the stochastic single-cell NLPR3 isoform expression and NLRP3 activity provide a physiological relevance for NLRP3 splicing, the molecular mechanistic reason for the NLRP3 Δ exon 5 inactivity remained to be determined. NEK7 binding was demonstrated as a pre-requisite for NLRP3 activation [97–99]. To test whether NLRP3 Δ exon 5 was inactive due to the loss of the NEK7 interaction, NLRP3-NEK7 Co-IPs were performed from iMos using the mCitrine tag to pull down either NLRP3 full-length or NLRP3 Δ exon 5. While NLRP3 full-length co-precipitated NEK7, NEK7 could not be detected in the Co-IP of NLRP3 Δ exon 5 (Figure 5-18 A). In the literature, NEK7 is postulated to bind NLRP3 progressively upon activation [99]. However, here the interaction could be observed independent of NLRP3 activation. Yet the same assay was also performed after NLRP3 activation with nigericin. As a further control, treatment with the NLRP3 inhibitor CRID3 was included (Figure 5-18 B). Regardless of the activation status NLRP3-NEK7 interaction could be demonstrated, but only for the NLRP3 full-length variant.

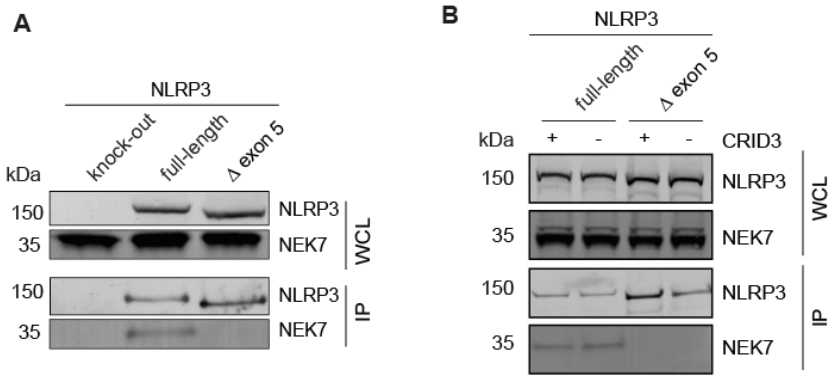

Figure 5-18 NLRP3 full-length, but not NLRP3 Δ exon 5 interacts with NEK7
A Co-immunoprecipitation (IP) from iMos stably expressing the respective NLRP3-mCitrine variants. IP was performed in GFP-trap plates. **B** as A, but from LPS-primed and nigericin-activated iMos with and without treatment with the NLRP3 inhibitor CRID3. WCL – whole cell lysate.

Two hypotheses why NLRP3 Δ exon 5 is inactive and why it does not interact with NEK7 are conceivable: Either, due to the overall shortened LRR, or because exon 5 is critical for the NEK7 interaction. To distinguish between these two hypotheses, a NLRP3 variant containing no exon 5 but a doubled exon 6 was created (Figure 5-19 A). This was possible due to the high degree of conservation of the LRR exons. As before, stable iMo cell lines were created and IL-1β secretion was analyzed after NLRP3, AIM2 and NLRC4 activation (Figure 5-19 B). While all cell lines secreted IL-1β upon AIM2 or NLRC4 activation, NLRP3 Δ exon 5 and 2x exon 6 could both not be activated with NLRP3 stimuli. All cell lines responded to priming with LPS as assessed by TNF secretion (Figure 5-19 C). These results suggest that not the shortened overall length of NLRP3 Δ exon 5 LRR but rather the specific absence of exon 5 caused the NLRP3 inactivity.

Assuming that exon 5 acts as the interaction surface for NEK7 binding, is can be assumed that the surface exposed amino acids are especially important. Therefore, a NLRP3 hybrid variant of NLRP3 full-length and 2x exon 6 was generated. All amino acids defining the NLRP3 exon 5 surface according to the structural model were mutated to their respective analogues from exon 6 (Figure 5-20 A). IL-1β secretion after inflammasome activation was measured, demonstrating the inactivity of NLRP3 lacking the exon 5 surface, while all cells were capable of IL-1β secretion after AIM2 or NLRC4 activation (Figure 5-20 B). The TNF response as a surrogate for priming was similar for all cell lines under all conditions (Figure 5-20 C).

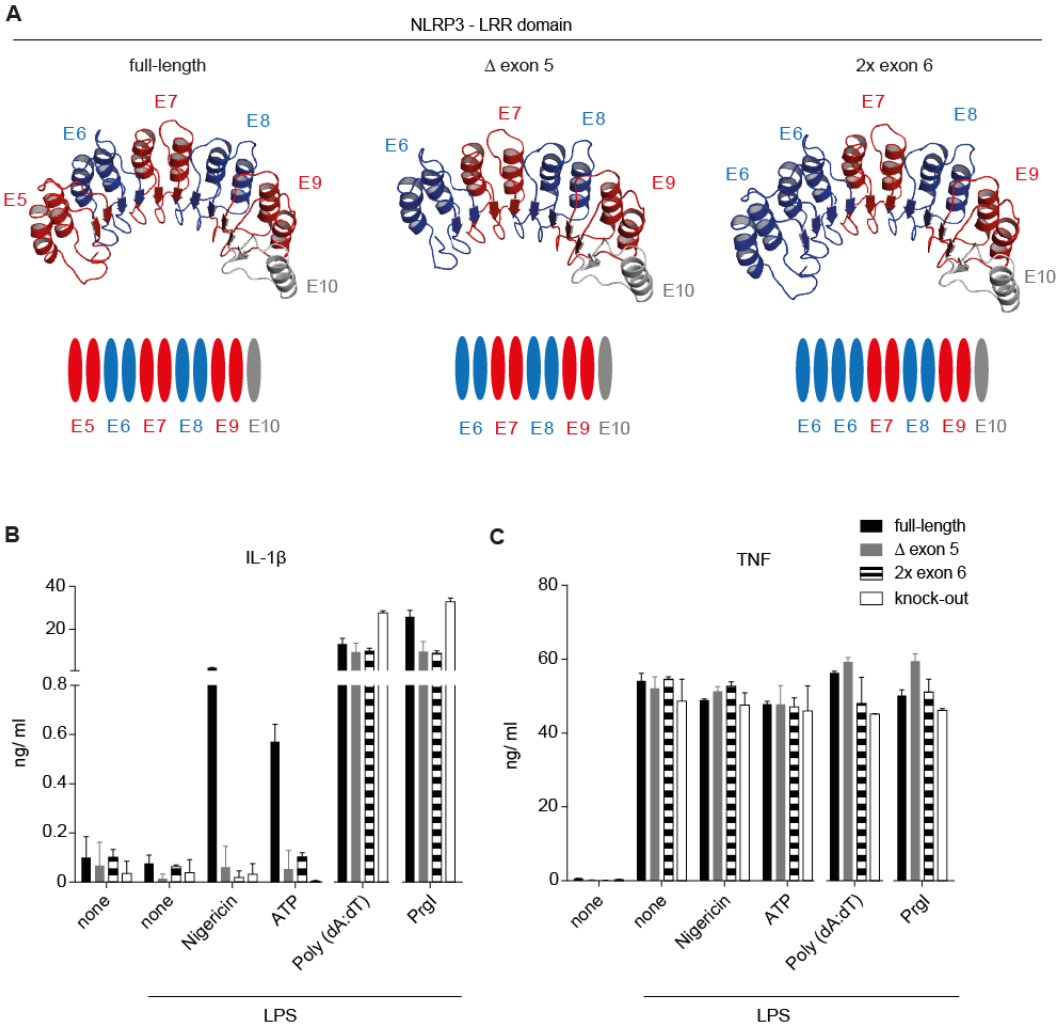

Figure 5-19 NLRP3 Δ exon 5 is not inactive due to its shortened LRR
A Models of the NLRP3 LRRs based on the crystal structure of human ribonuclease inhibitor. Shown are the LRR model structures and schematics of NLRP3 full-length and NLRP3 Δ exon 5, as well as an artificially created LRR: NLRP3 LRR lacking exon 5 but carrying a duplicate exon 6. R. Brinkschulte generated the ribbon models. **B** Stable iMo cell lines expressing the respective NLRP3 variants were created as described above. IL-1β secretion was analyzed after activation of the NLRP3, AIM2 or NLRC4 inflammasome. **C** TNF secretion after LPS treatment. B and C mean and SD of technical triplicates N=1.

Introducing as many mutations, even in a highly conserved repeat unit, may cause an unspecific loss of functionality, caused by mis-folding of the protein. Therefore, a rescue mutation strategy was chosen: Based on the inactive 2x exon 6 NLRP3 variant, a surface rescue for the residues of exon 5 was generated (Figure 5-21 A). Due to the high level of conservation of the LRR exons, the overall physico-chemical characteristics of the hybrid isoforms are similar to the wildtype (wt) isoforms (see appendix, Table 12-2). Stable iMo cell lines were primed and activated as before. As expected, all cell lines secreted IL-1β after AIM2 and NLRC4 activation, but only the NLRP3 full-length and NLRP3 2x exon 6 surface rescue variant were responsive to

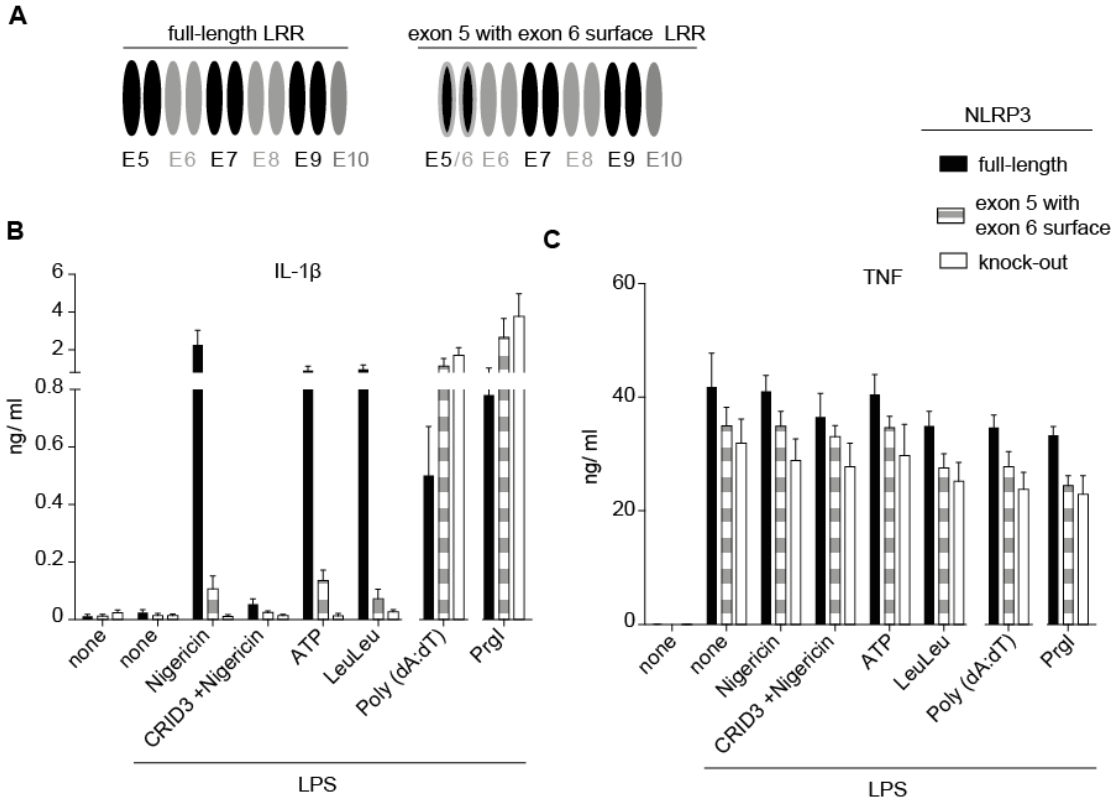

Figure 5-20 The NLRP3 exon 5 surface is relevant for the activity
An exon 5 hybrid variant, in which all surface amino acids of the structural model were mutated to their analogue from exon 6, was created and a stable cell line expressing this NLRP3 variant was generated. **A** IL-1β secretion was analyzed after activation of the NLRP3, AIM2 or NLRC4 inflammasome. **B** TNF secretion after LPS treatment. A and B mean and SEM of 5 independent experiments.

NLRP3 activators (Figure 5-21 B), while all of them were equally primed (Figure 5-21 C).

Taken together, these experiments provide evidence that the surface of exon 5 is needed for the activation of NLRP3.

Given that NLRP3 Δ exon 5 was not capable of interacting with NEK7 and that the specific surface of NLRP3 exon 5 is needed for activation, the exon 5 replacement mutants from above were used to investigate the NEK7 interaction. NLRP3 Co-IPs for the interaction with NEK7 were performed from iMo lysates using the mCitrine tag to pull down NLRP3 (Figure 5-21 D). Although the interaction between NLRP3 2x exon 6 surface rescue and NEK7 was weaker than between NLRP3 full-length and NEK7, a clear increase in interaction was detectable compared to the Δ exon 5 and 2x exon 6 NLRP3 variants. It has to be taken into account that in these cell lines human NLRP3 interacts with mouse NEK7, which may be sufficient to allow for NLRP3 activation, but may be more sensitive to minor structural differences at the interaction side than a human-human interaction pair. Therefore, the experiments were repeated in 293T cells, which were transiently transfected to express the

different NLRP3 isoforms before mCitrine pull-downs were performed. Under these conditions, a solid interaction between NLRP3 2x exon 6 surface rescue and NEK7 could be detected, while Δ exon 5 and 2x exon 6 NLRP3 variants did not interact with NEK7 (Figure 5-21 E).

Taken together, these experiments map the interaction site of NEK7 to exon 5 of NLRP3 and thereby explain why NLRP3 Δ exon 5 is inactive.

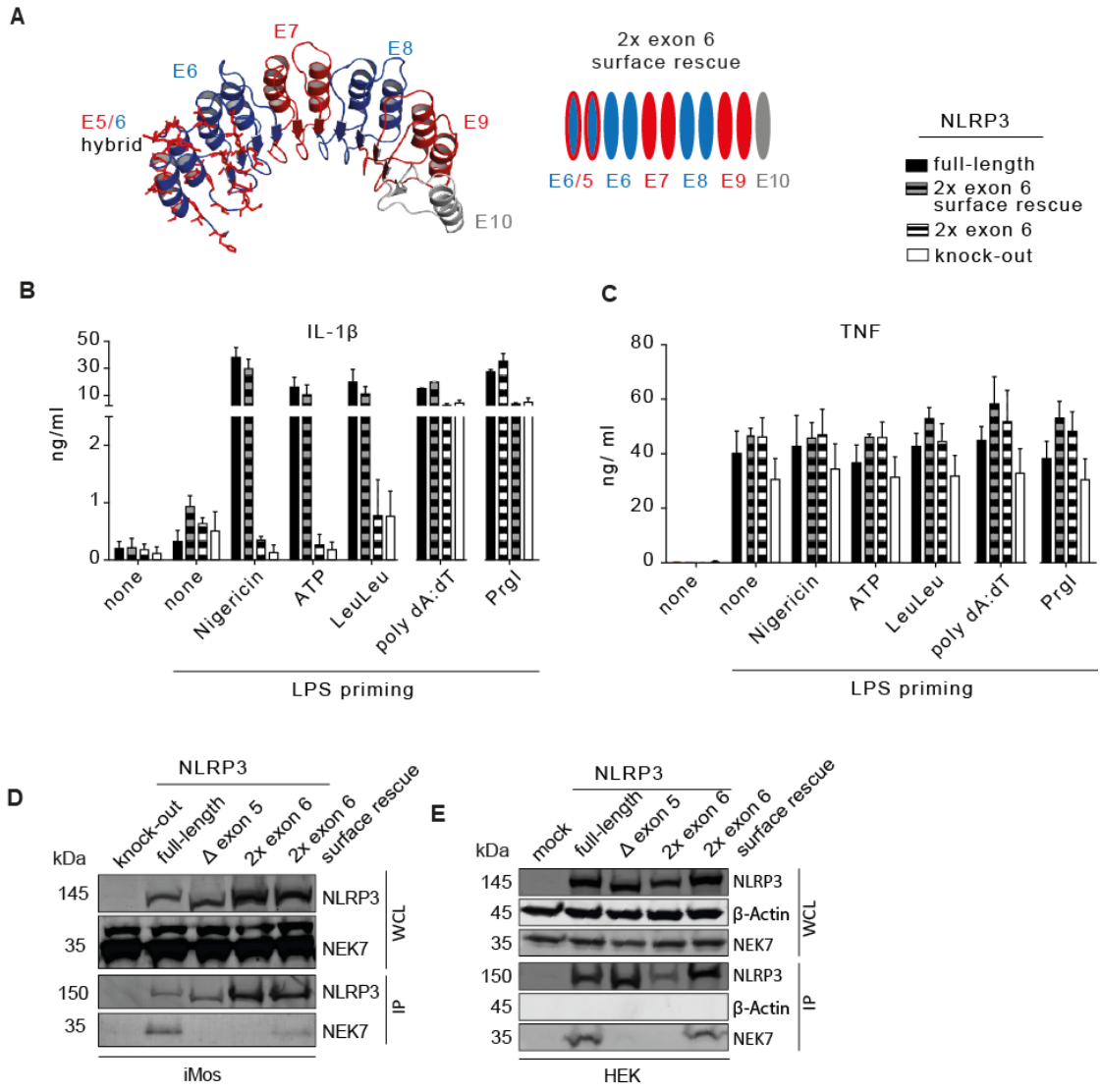

Figure 5-21 The NLRP3 exon 5 surface is essential for the interaction with NEK7

A Schematic and ribbon model of an artificial NLRP3 hybrid LRR based on the crystal structure of human ribonuclease inhibitor. Surface residues of exon 5 are shown in red. The model was generated by R. Brinkschulte. The LRR lacks exon 5 but carries a duplicate exon 6 in which all surface amino acids of exon 5 were rescued. NLRP3-deficient iMos were reconstituted with full-length or the hybrid NLRP3-mCitrine variants as before. **B** IL-1β secretion was analyzed after activation of the NLRP3, AIM2 or NLRC4 inflammasome. **C** TNF secretion after LPS treatment. B and C mean and SEM of 5 independent experiments. **D** Co-immunoprecipitation (IP) from iMos stably expressing the respective NLRP3-mCitrine variants. IP was performed in GFP-trap plates. Representative of 2 independent experiments. **E** As D, but from HEK 293T cells transiently transfected to express the respective NLRP3-mCitrine variants. Representative of 3 independent experiments.

5.6. NLRP3 Δ exon 5 regains activity after prolonged priming

BLaER1 cells are derived from a human B cell line, and can be transdifferentiated into macrophage-like cells [191]. In these cells, an LPS-dependent NLRP3 inflammasome activation was demonstrated independently of the non-canonical inflammasome, the so-called alternative inflammasome [105]. To rule out non-canonical inflammasome activation, these cells were generated in a caspase-4 (the human homologue of mouse caspase-11) deficient background. Similar to the NLRP3 Δ exon 5 variant, the alternative inflammasome was described to only exist in human, but not in mouse cells [105]. To control for an involvement of NLRP3 Δ exon 5 in the alternative inflammasome, NLRP3/caspase-4 double deficient cells were retrovirally reconstituted with NLRP3 full-length or NLRP3 Δ exon 5, both with a C-terminal tagRFP (Figure 5-22 A). An isoform-specific qPCR was performed to ensure that both cell lines only express the indicated NLRP3 splice variant (Figure 5-22 B). Next, the cells were primed for 3 h or for 14 h with LPS before nigericin activation. As expected, only NLRP3 full-length cells secreted IL-1β after short priming and nigericin activation. The alternative inflammasome activation following 14 h of LPS as a sole stimulus was also NLRP3 full-length dependent. Unexpectedly, after prolonged priming for 14 h followed by nigericin activation, NLRP3 Δ exon 5 became fully active (Figure 5-22 C). The overall higher levels of IL-1β after 14 h of LPS treatment can be explained by prolonged priming as evinced by the higher TNF levels after 14 h LPS treatment (Figure 5-22 D). As observed before, LPS treatment induced increased metabolic activity, resulting in 'viability' values above 100% compared to an untreated control (especially after 14 h of LPS). However, after inflammasome stimulation and IL-1β secretion, a reduction in viability relative to the respective control was observed in the activated cells (Figure 5-22 E). To ensure that the secreted IL-1β by NLRP3 Δ exon 5 cells is not only non-specifically released pro-IL-1β, but bioactive, cleaved IL-1b, immunoblots were performed (Figure 5-22 F). Although pro-IL-1β was detected as well, NLRP3 Δ exon 5 induced similar levels of mature IL-1β secretion after 14 h LPS and nigericin as NLRP3 full-length. Finally, it could be shown that the long priming effect is not LPS-specific but could also be achieved with the TLR agonist R848 (Figure 5-22 G). Taken together, these findings suggest an unexpected role for NLRP3 Δ exon 5 as an inflammasome sensor allowing a delayed response. How the NLRP3 Δ exon 5 splice variant overcomes the NEK7 dependency remains to be addressed by further studies.

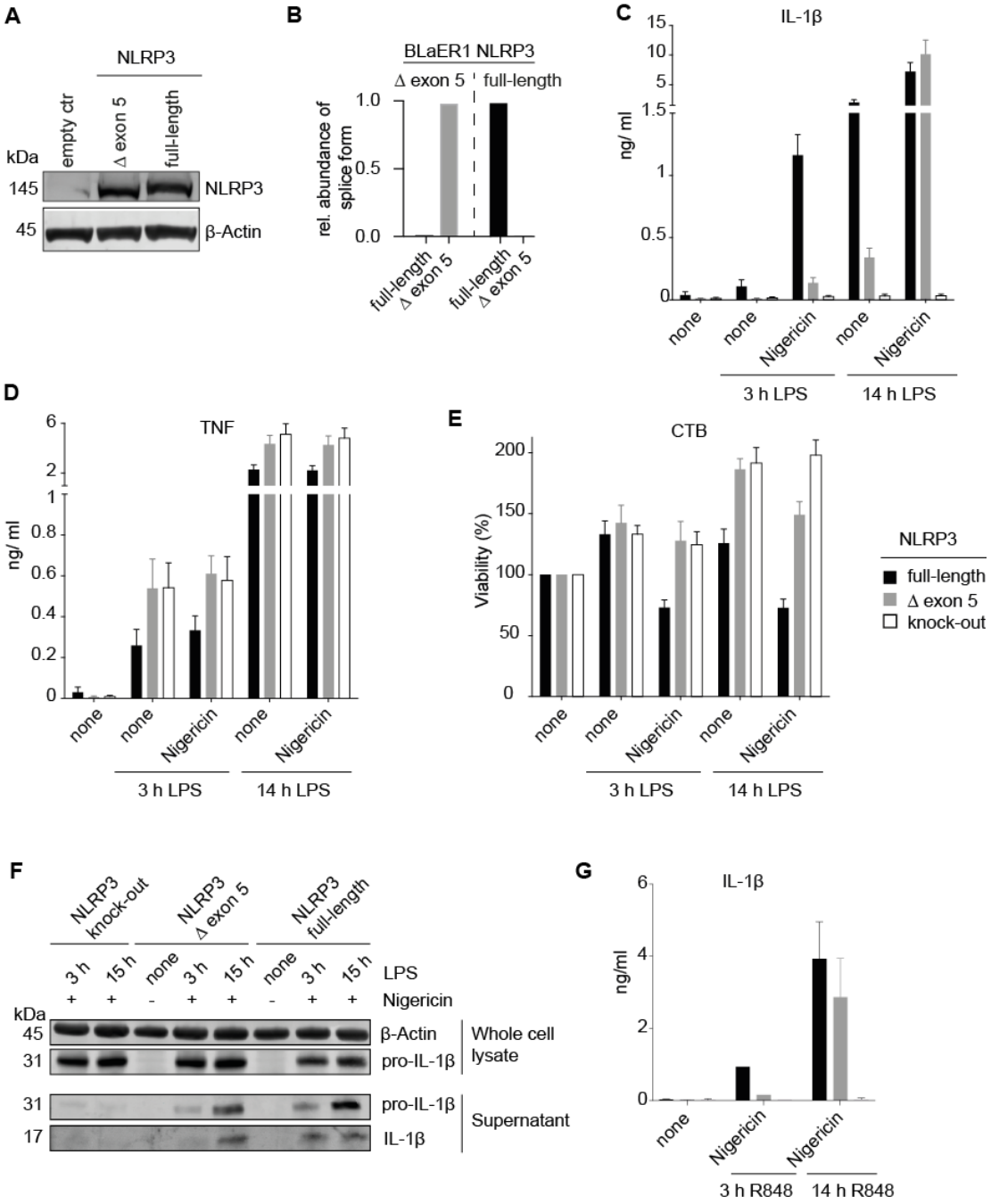

Figure 5-22 NLRP3 Δ exon 5 regains activity after prolonged priming
Human BLaER1 caspase-4/ NLRP3 double-deficient cells (a kind gift from M. Gaidt, V. Hornung) were virally transduced to express either NLRP3 full-length or NLRP3 Δ exon 5, both with a C-terminal tagRFP. Stable cell lines were FACS-sorted for equal NLRP3 expression. **A** Immunoblot of NLRP3 to verify comparable expression levels of both isoforms. **B** Isoform-specific qPCR to verify the exclusive expression of only the respective NLRP3 isoform in both cell lines. **C** to **E** BlaER1 cells were transdifferentiated into macrophages and primed either for 3 or 14 h with LPS before stimulation with nigericin. **C** IL-1β secretion after nigericin stimulation. Mean and SEM of 7 independent experiments **D** TNF secretion after LPS priming. Mean and SEM of 6 independent experiments. **E** CTB assay to determine the viability after inflammasome activation. Mean and SEM of 5 independent experiments. **F** Immunoblot of mature and pro-IL-1β from lysates and supernatants after indicated activations. Representative of 2 independent experiments. **G** IL-1β secretion after short and long priming with R848 followed by nigericin activation. Mean and SEM of 3 independent experiments (3 h: 1 experiment).

6. Discussion

Alternative splicing is a key mechanism driving diversity of the proteome, especially but not exclusively in higher eukaryotes. Since proteins are key molecules that contribute to the cell structure, act as molecular machines to generate lipids, nucleic acids and metabolites and coordinate nearly all cellular functions, AS can dramatically influence cell identity and cell specific functions. Alternatively spliced proteins can vary in their domain composition and sub-cellular localization. Different isoforms of the same gene can even act like unrelated proteins and are frequently characterized by significantly different interaction profiles [161]. These transcriptional alterations provide additional functional diversity from a limited genome allowing for a much faster diversification, specialization and adaptation than classical mutagenesis driven evolution.

The work described here shows the conservation of a spliceable LRR motif across multiple gene families and how AS influences the innate IS. Surprisingly, alternative splicing of NLRP3 could only be detected in human, but not in mouse or pig cells. The most prevalent alternative splice variant of NLRP3 lacks exon 5 and is not activatable by commonly used NLRP3 activation protocols. It is only after a prolonged priming phase of more than 10 h that NLRP3 Δ exon 5 suddenly gains full activity. Furthermore, it was shown that NLRP3 exon 5 is an integral component of the NLRP3-NEK7 interaction interface and loss of NEK7 binding was accompanied by loss of NLRP3 activity. NLRP3 isoform expression was shown to be stochastic at single-cell level, most likely contributing to the low number of NLRP3 responsive human primary cells. Together with the gain of activity after prolonged priming, this suggests that NLRP3 Δ exon 5 expressing cells act as a backup population, which does not immediately succumbs pyroptosis, but rather allows for a sustained inflammatory response.

Although many new insights have been gained over the last decade in the field of inflammasome research, most work is performed in mouse models. We have only started to decipher the functional and regulatory differences between the mouse and human inflammasome [105,106,192]. The species differences between mouse and human NLRP3 reported here indicate the importance of NLRP3 studies performed in (primary) human cells to discover all regulatory levels of human NLRP3 activation.

6.1. LRR domains of the NLR family have a conserved multi-exon organization suitable for AS

Although TLRs and NLRs both contain LRRs, they belong to different subfamilies and are more closely related to other non-immune genes than to each other [76]. While the other functional domains of NLRs are usually encoded by single exons, most of the LRR domain is encoded by a repetitive exon pattern [193]. The LRR region of NLRPs is characterized by alternating 28 and 29 amino acid stretching LRRs with one exon encoding two repeats, while in NODs one exon encodes one repeat of 28 residues. This repetitive exon structure is not present in TLRs, in which the LRR is encoded by a single exon [76]. This is in line with the exon-LRR relationship, which was observed in the structural alignments presented here (Figure 5-2, Figure 5-3, appendix Figure 12-1). The LRR pattern in NLRP3 is very suitable as a target for AS, since the exon length of 171 nucleotides prevents AS-induced frame shifts. Moreover, the exon-exon boundary is always located within the same position of the β-strand of the LRR, making it unlikely to destroy the three-dimensional structure. The here detected exons, which mostly encode for either 24 or 28/29 aa LRRs, represent LRR modules which were identified as ideal self-compatible building blocks to create well-folded protein structures when repeatedly stacked [194]. Together, these two findings suggest that spliceability of NLR LRR-exons comprises an evolutionary benefit and that AS of LRR modules could create diverse protein functions or could regulate the activity of human NLR family members. Furthermore, the exon-LRR structure relationship, resembles the jawless vertebrate VLR system, which is based on the recombination of LRRs [148]. The parallels between the jawless vertebrate adaptive immune system and the exonic organization of the NLR LRRs may suggest a convergent evolution of different classes of immune receptors.

The *in silico* approach employed here to detect multiple spliceable LRR encoding gene-families is a database approach, and therefore dependent on available annotation data (Figure 5-2). LRR motifs are not always automatically detected and annotated, especially if the consensus sequence is interrupted or degenerated. Therefore, many LRRs are only partially or not at all annotated and consequently not picked up in this analysis. For example, the NLRP6 and NLRC5 LRRs are at least partially encoded by repetitive canonical exons (see structural alignments, appendix Figure 12-1), yet they were not identified as LRR-exons in the databases approach. However, the primary aim of this analysis was not to discover all LRR exons, but to assess whether spliceable, short, repetitive exons represent a conserved feature.

Domain boundaries and exon junctions show a consistently strong correlation, which further increases from invertebrates to higher vertebrates [195]. On the one hand, this correlation allows for genomic exon re-shuffling [196], and on the other hand, it facilitates the recombination or deletion of functional units by AS.

Interestingly, some of the non-NLR LRR-proteins, which were discovered *in silico* as containing small modular LRR exonic structures are indeed reported to encode multiple isoforms. As an example, LRRC37 was restricted to the testis in earlier evolution, but its expression pattern rapidly evolved in the hominid lineage with an increasing diversity of alternative splice forms and higher levels of expression in the cerebellum and thymus [197]. Similarly, LRR-containing Slit proteins act as synaptic adhesion molecules and are involved in axon guidance. A large heterogeneity of Slit mRNA could be identified, and multiple Slit protein isoforms are suggested to exist with a varying number of LRR units that may regulate their binding properties [198,199]. Even some NLRs were reported to be alternatively spliced, although to my knowledge, AS of the LRR region was never systematically analyzed. Similar to my findings for NLRP3, multiple isoforms of NOD2, mostly differing in their LRR, were described. The alternative isoforms are inactive for MDP stimulation, but do not antagonize the full-length MDP response [200]. Similarly, 4 different AS variants of the NLRP12 LRR are reported, although the respective data is not shown in the original publication [201]. Even the original study describing the role of NLRP3 in CAPS mentions multiple AS variants within the LRR region, but again, without showing any data [202]. The importance of AS in context of inflammasomes is further emphasized by the existence of up to 4 different ASC isoforms, of which two are LPS inducible and act as negative inflammasome regulators[72]. Moreover, AS has been reported in the context of plant R-proteins as a key feature in defense against pathogens and in stress situations. R-proteins in plants are structural and functional homologous of vertebrate NLRs [171,172]. Analogous to the AS mediated removal of the NKE7 binding site described in this study, human NLRP3 mRNA can be alternatively polyadenylated in order to remove regulatory sites. Consequently, the resulting shortened 3'UTR lacks the binding site for the negative regulators miRNA-223 and tristetraprolin [173].

From the data presented in this thesis and related publications, AS of the LRR region appears to be a conserved feature to create functional diversity not only in the immune system. However, it is surprising that multiple spliceable LRR exons per gene exist, although only a fraction can be detected as alternatively spliced. One potential explanation is that AS of other LRR exons happens in a tissue- or

environment-specific manner correlating with different functionality, as it is described for many genes [203,204]. Consequently, potential isoforms and AS of other exons might be missed in the approach used here. Likewise, the exon structure, as seen in human NLRP3, is conserved in mouse and pig NLRP3, yet AS of the LRR could not be detected in mouse BMDMs and pig PBMCs.

SplicePort and RESCUE-ESE analysis of the NLRP3 LRR support a static, sequence-dependent preference for AS of the NLRP3 exon 5 (Figure 5-8). It might be possible that the conserved LRR exons are derived from genomic duplication events or are conserved to allow for exon shuffling during evolution [195,196] and the respective highly repetitive exons were only harnessed later in evolution by AS processes. Existing exons can gain AS patterns due to a lower conservation of the consensus splice-sites and increased numbers of regulatory splice factors in higher-order organisms [149]. Overall, the species differences in AS underline the importance of studies performed in human *in vitro* systems instead of relying solely on mouse model systems. To decipher the evolutionary conservation of AS in NLRs, it would be of further interest to also analyze RNA samples of species closer related to humans, like monkeys or apes.

6.2. Detection of AS by NGS

Although databases as *Ensemble* or *NCBIgene* list a large number of isoforms for many genes, it can not be assumed that all of them are expressed in every tissue or cell type at a certain time. For some annotated isoforms, it is even questionable whether they play any physiological role.

As the focus of this thesis is not the detection of alternative splicing events using bioinformatics approaches, I decided, together with our bioinformatics collaboration partners, to stick to a conservative approach, which rather focuses on exon skipping than transcript calling. The sashimi plots[205] presented in Figure 5-4 (and appendix, Figure 12-2) show the read distribution across a gene of interest and highlight exon-spanning reads as arcs. Arcs joining non-adjacent exons give a good intuitive impression on AS events. Quantification of AS events is possible, but should be treated with caution because it relies on an equal read distribution within a library. As it can be seen in Figure 5-4, read distribution within one long stretching exon, which cannot be affected by AS, can still vary even more than between AS exons. Since these coverage biases are mostly derived during library preparation and depend on the local sequence environment [206,207], the bias between the highly conserved LRR

exons should be smaller than within non-conserved regions. Still, exon-spanning reads of adjacent LRR exons show a variability in counts, which cannot be explained by AS. Although many approaches have been developed to bioinformatically reduce these biases in follow-up quantifications, employing and evaluating these approaches would be beyond the scope of this thesis and outside the field of my research. Therefore, I decided to rather use the RNAseq-derived results as qualitative indicators for AS events than for transcript quantification.

A promising approach for further analysis of AS would be the use of third generation long-read sequencing technologies as PacBio or Oxford Nanopore. Although they overcome transcript assembly issues by covering a whole transcript in one read, they are much more limited in the number of generated reads and suffer from comparably high sequencing error rates [208].

6.3. NLRP3 splice ratios are non-variable

To my knowledge, the regulation of exon skipping in NLRs has not yet been addressed. The coordination of AS is very complex and in addition to the core spliceosome, many additional factors are involved.

When analyzing the relative expression of NLRP3 full-length, Δ exon 5, Δ exon 7 and Δ exon 5/7 by qPCR across multiple cell types in a variety of conditions, no considerable change in the AS ratios could be observed despite diverse pro- or anti-inflammatory treatments (Figure 5-7). However, this was not a technical problem because the experimental design correctly detected induced splice changes, such as the upregulation of Δ exon 5 NLRP3 after SSO treatment (Figure 5-13 E) and the reconstitution of BLaER1 cells with Δ exon 5 NLRP3 (Figure 5-22 B).

Although minor changes of a few percent in the AS ratio can be observed between different cell types, these are rather derived from individual differences between the blood donors than from cell-type or treatment differences. Moreover, minor changes in measured splice ratios, even if statistically significant, are considered biologically non-significant in the splicing field and only a change of at least 10-20% in AS ratios is considered relevant [153].

The binding of the initial spliceosomal factors, defining the splice site, is a probabilistic process determined by the binding energy of a given site. Therefore, the splice site recognition represents a stochastic minimization process aiming for a global (or local) minimum in binding energy [209]. Based on this assumption, a mathematical model for the relative abundance of alternative splice variants was

developed and validated on simulated and measured RNAseq data. The model predicts always one predominant splice variant and mean frequency distributions for all variants[209]. The here measured ratios of the four NLRP3 isoforms fit to the calculated mean frequency distributions. Furthermore, the detected differences in ESE-binding sites and conservation of the scpliceosomal recognition motifs of the splice-donors and acceptors of the NLRP3 LRR exons are most likely shaping the observed AS pattern. Since the model does not include the effect of all splice factors and provides mean frequency distributions, it does not exclude a differential regulation of AS, but explains the surprisingly stable relative expression levels between the major and minor isoforms. Of note, further dynamic regulatory mechanisms in a specific environmental context cannot be excluded, neither by the here analyzed isoform expression levels and sequence-based splice site analysis, nor by the transcriptome wide mathematical model.

6.4. NLRP3 Δ exon 5 remains inactive after standard activation

I could demonstrate the inactivity of NLRP3 Δ exon 5 after standard priming followed by standard activation, non-canonical activation and potassium independent activation with multiple readouts covering all levels of inflammasome assembly and IL-1β secretion (Figure 5-10 to Figure 5-13). Although this is the first analysis on the effect of AS on the NLRP3 inflammasome, two alternative NLRP3 isoforms were used before in functional assays. Shortly after the discovery of the NLRP3 gene (*CIAS1*) and the mention of AS in the NLRP3 LRR [202], the NLRP3 variants Δ exon 5 and Δ exon 5/7 (annotated with a different exon nomenclature as exon 4 and 6) were tested, without any effect, for their NF-κB-inhibitory activity [210], which was the proposed effect of NLRP3 before the inflammasome concept was developed.

Many key experiments in this thesis were performed with NLRP3-deficient mouse iMos, which were heterologously reconstituted to stably express the human NLRP3 splice variants. The same system was used before [78,85] and findings achieved with human NLRP3 in iMos could be recapitulated with mouse NLRP3 reconstitution in iMos. Since the investigated NLRP3 splice variant could not be detected in murine samples, I decided to only work with human NLRP3 instead of generating artificial mouse NLRP3 isoforms. The mouse iMos were used as a model system, but the

obtained findings were corroborated by experiments with HEK cells, BLaER1 cells and primary hMDMs.

MRP is an AS variant of the innate signaling adaptor STING and suppresses STING-mediated interferon signaling. A mouse model of HBV suggests that both STING and MRP coordinate the innate and adaptive immune response in concert [170]. Similarly, splice variants of ASC can suppress Inflammasome formation [72]. As NLRP3 Δ exon 5 remained inactive for all tested stimuli, an inhibitory function similar to MRP or ASC-c was conceivable. However, the mixed reconstituted cell lines expressing both NLRP3 splice variants in different ratios did not provide any indication for a suppressive function of the NLRP3 Δ exon 5 variant (Figure 5-15). Although non-significant differences in IL-1β secretion could be detected between the four NLRP3 co-expressing cell lines, they correlate perfectly with slightly different expression levels of full-length NLRP3 (Figure 5-14 B) and with minimal differences in priming efficiency (Figure 5-15 B). Therefore, it is very unlikely that the observed differences in IL-1β levels refer to a modulating capacity of NLRP3 Δ exon 5.

While NLRP3 Δ exon 5 was neither activatable after normal priming nor acted as an NLRP3 full-length inhibitor, it could be detected in ASC-specks of activated cells expressing both splice variants (Figure 5-15 D). Whether this is by PYD-PYD interaction after activated full-length NLRP3 molecules form a seed for homo-interactions, or whether NLRP3 Δ exon 5 just binds non-specifically to the ASC protein aggregate needs further investigation.

Together, the findings show that NLRP3 Δ exon 5 has no inhibitory capabilities over full-length NLRP3.

6.5. NLRP3 exon 5 is critical for the interaction with NEK7

Three independent studies identified NEK7 as an interaction partner of NLRP3, which is necessary for NLRP3 inflammasome activation [97–99] The interaction surface could be localized to the NLRP3 LRR and the catalytic domain of NEK7, although its catalytic activity is dispensable [99].

In the experiments presented here, I could show that NEK7 binding to NLRP3 specifically requires the surface of NLRP3 exon 5, and that the NEK7-NLRP3 interaction correlated with NLRP3 activatability (Figure 5-18 to Figure 5-21). I could detect a stable interaction between NLRP3 and NEK7 already in non-activated cells.

In my hands, the NLRP3-NEK7 interaction was not highly strengthened in activated cells and pretreatment with the NLRP3 inhibitor CRID3 did not affect the NLRP3-NEK7 interaction. This places the NLRP3-NEK7 interaction upstream of NLRP3 activation and inflammasome formation and indicates that the mechanism of NLRP3 inhibition by CRID3 is independent of NEK7.

According to the literature a weak NLRP3-NEK7 interaction can be observed under steady-state conditions and an enhanced interaction after NLRP3 activation in mouse macrophages [99]. The authors claim that K^+ efflux in primed cells initiates the interaction between NLRP3 and NEK7, nominating NEK7 as the missing integrator of the highly diverse NLRP3 activators [99]. This is partially in contrast to the here observed NLRP3-NEK7 interactions independent of NLRP3 activation. However, several reported findings also support the NLRP3-NEK7 interaction upstream of NLRP3 activation. First, the increase in interaction was only observed when NLRP3 was immunoprecipitated, and not when NEK7 was immunoprecipitated [99]. Second, experiments with mouse NLRP3 R258W (corresponding to the human CAPS mutation R260W) demonstrated a NEK7 requirement for activation, but no K^+ efflux [99]. Third, overexpressed NLRP3 mutants bound NEK7 solely dependent on their intrinsic activity [97]. Forth, all cell lysates and IPs were generated under K^+-free condition in the publication suggesting NEK7 as the activator downstream of K^+ efflux [99]. However, if the interaction between NLRP3 and NEK7 were solely dependent on the drop in K^+ levels, one could also expect an interaction in the non-activated conditions. Together, the above-mentioned and my results suggest that NEK7 binding is a necessary prerequisite for NLRP3 activation which occurs upstream of the activation process.

One limitation of this study is that some results are based on human NLRP3 expressed in mouse iMos. Human NLRP3 and endogenous murine NEK7 might not be ideal interaction partners. Yet, all active NLRP3 variants demonstrated interaction with NEK7, while all inactive variants did not. Although NLRP3-NEK7 interaction strength was reduced in the NLRP3 2x exon 6 surface rescue variant in iMos, a comparable level of interaction could be shown between NLRP3 full-length and 2x exon 6 surface rescue in HEKs (Figure 5-21 D and E). A possible explanation is that the interaction surface between human NLRP3 and human NEK7 is evolutionarily better fitted than between human NLRP3 and mouse NEK7 and therefore tolerates minimal structural changes, which might occur in the artificial NLRP3 2x exon 6 surface rescue variant.

I cannot prove that the generated artificial NLRP3 variants (Figure 5-19 to Figure 5-21) fold perfectly into the natural NLRP3 secondary structure. However, based on

the perfect building block architecture of the human NLRP3 exons [194], the high degree of exon conservation (Figure 5-3), the stable expression in generated cell lines (Figure 5-21 D), the similar physico-chemical properties (appendix, Table 12-2), the fit to the LRR model (Figure 5-19 A and Figure 5-21 A) and the activity rescue of the 2x exon 6 surface rescue variant (Figure 5-21), it is very likely that the NLRP3 secondary structure is not affected by the introduced mutations.
In summary, the structure-guided surface mapping approach for the NLRP3-NEK7 interaction provides a molecular mechanism explaining why NLRP3 Δ exon 5 is not responsive to standard NLRP3 activation.

6.6. Single-cell gene expression of NLRP3 splice variants

Single-cell gene expression analysis of NLRP3 full-length and Δ exon 5 revealed a stochastic expression of both splice variants. Of note, it was shown before that 30-100 single cells provide a reliable and robust measure for the transcriptome of bulk cells [211]. In this study, I analyzed nearly 200 cells per donor of three donors, suggesting that the observed expression pattern reflects the overall expression of that donor (Figure 5-16). Four different populations in terms of NLRP3 isoform expression were identified in all 3 donors: Only NLFP3 full-length, only NLRP3 Δ exon 5, both NLRP3 isoforms, or neither NLRP3 isoform expressing cells. Yet, the number of NLRP3 expressing cells varied between donors. Individual levels of LPS response between different donors can explain inter-donor differences in the percentage of NLRP3 expressing cells. This is a common phenomenon of primary cells from different donors which was observed before in our lab (e.g. Figure 5-7 B), but also by others [212]. It is not clear how the stochastic expression is regulated. Since gene expression on a single-cell level is subject to a burst kinetic [213], one might argue that such bursts also cause the observed differences in NLRP3 isoform expression. However, both transcript variants are expressed as the same pre-mRNA from the same gene locus and are therefore not independent. Thus, a stochastic regulation of AS is more likely than an experimental bias caused by the single-cell burst kinetics. A monoallelic expression was shown for several genes including many cytokines [214,215], but an allele-specific expression is not known to correlate with specific isoforms. If NLRP3 splice variants were allele-specifically expressed, a single-cell expression analysis could be affected by the burst kinetics. However, the

allele-specific expression would already imply a stochastic allele regulation as a pre-requisite. Therefore, in either case one can assume a stochastic element in the expression of NLRP3 splice variants at single-cell level.

In general, little is known about splice regulation on single-cell level. Expression and splicing differences on single-cell level are reported [211] and a few years ago, a large study on single-cell transcriptomics in BMDCs showed a bimodal expression and splicing pattern in immune cells after LPS challenge [216]. However, it was later shown that the studied cell population of GM-CSF-derived BMDCs actually consisted of DCs and macrophages and that the bimodal response rather reflected the different cell types [217,218]. Theoretically, the hMDMs used in this study could represent as well a mixed population. hMDMs were not generated from a heterogenic population such as bone marrow, but from CD14+ selected monocytes, which are much more limited in their differentiation capabilities than stem cells. Yet, in vitro generated hMDMs were also shown to be phenotypically heterogeneous [219]. Nevertheless, it is unlikely that different subpopulations contribute to the different splicing patterns on single-cell level in this study, as I observed the expression of NLRP3 isoforms in the same fixed ratios on multiple cell-lines and other primary cell types (Figure 5-7). Together, a stochastic 'de novo' AS decision in each cell is more likely than a lineage-dependent isoform expression.

6.7. Stochastic distribution of NLRP3 activity in human macrophages

The single-cell gene expression analysis demonstrated that NLRP3 splicing is not deterministic, because both NLRP3 full-length and NLRP3 Δ exon 5 expressing cells were detected at the same time. Stochasticity in gene transcription influences the variability of cell responses because single cells can behave differently depending on the expression of any given gene. To assess whether the stochastic expression of NLRP3 might contribute to an adjustable response of cells to danger signals, I evaluated whether AS of NLRP3 correlates to the number of cells responsive to NLRP3 triggers. I made use of two independent assays to analyze the activation status of single cells after inflammasome activation in primary human macrophages. While nearly all human macrophages responded to an NLRC4 trigger, surprisingly, only a minor fraction of human macrophages responded to NLRP3 stimuli (Figure 5-17). It is tempting to speculate that AS of NLRP3 contributes to the stochastic

nature of NLRP3 responses. The stochastic distribution of NLRP3 inflammasome activation causes stimulated cells to exhibit large variability in their response to danger signals. Since the NLRP3 inflammasome is highly regulated by many feed-forward as well as negative feed-back loops, stochastic distribution in the inflammasome response would allow for fine-tuning of a graded, adjusted response. At the same time, different activation thresholds of NLRP3 could be important to prevent a coordinated pyroptotic cell death of macrophages in the presence of danger signals, which could subject the host to increased susceptibility for infections. In contrast, detection of cytosolic bacterial components (e.g. PrgI by NLRC4) most likely reflects an infection of the macrophage itself. In this scenario, limiting bacterial proliferation within the macrophage by pyroptotic self-removal is favorable and an immediate full response is necessary to prevent further spreading of an infection.
Of course, many factors as NLRP3 expression [78], PTMs [85], NEK7 regulation via the cell cycle [97] and others were shown to influence NLRP3 activity, but AS of NLRP3 defines a new level of NLRP3 regulation.

6.8. Delayed inflammasome assembly by NLRP3 Δ exon 5

Unexpectedly, it was found that NLRP3 Δ exon 5 could gain full activity after prolonged priming. This is independent of the alternative inflammasome, because LPS treatment for 14 h alone did not induce IL-1β secretion, but only the combination of 14 h of priming followed by canonical inflammasome activation (Figure 5-22). Moreover, this effect was not LPS-specific, but could also be achieved with another TLR agonist (R848). Although immature pro-IL-1β was also secreted from all cell lines after activation, cleaved IL-1β could be detected from NLRP3 full-length and to the same degree from NLRP3 Δ exon 5 expressing cells. To exclude a potential cross-contamination of NLRP3 full-length causing the increased activity after prolonged priming, I checked the cell lines for their 'purity' by NLRP3 isoform-specific qPCR. A marginal level of NLRP3 full-length can be detected by qPCR in the BLaER1 NLRP3 Δ exon 5 cell line (Figure 5-22 B). Since the NLRP3 deficiency of the parental cell line was achieved by CRISPR/Cas9-mediated genomic modification, a functional endogenous NLRP3 expression is prevented by introducing a nonsense mutation. This mutation does not prevent the production of endogenous NLRP3 encoding mRNA. The detected minimal level of NLRP3 full-length mRNA

corresponds to the level of NLRP3 full-length mRNA in the parental NLRP3-deficient cell line (data not shown) and does not contribute to functional NLRP3 protein, as shown by the lack of response to nigericin.

How NLRP3 Δ exon 5 gains activity after prolonged priming, and the physiological consequences of this activity need further investigation. If the NLRP3 LRR acts as a self-inhibiting domain, as shown for NLRC4[40], NEK7 might stabilize an activatable state instead of directly causing inflammasome activation. Indeed, a nonsense mutation in NLRP3 exon 4 (R554X) results in the complete loss of the LRR and the patient presents an inflammatory FMF/FCAS-like phenotype [220], suggesting that self-inhibition of NLRP3 is lost. It would be conceivable that beside NEK7 other factors might get activated or up-regulated after prolonged priming and are capable of taking over the role of NEK7, but act independently of exon 5. One possibility to address this question would be a differential mass spectrometry interaction screen.

The physiological role of the delayed inflammasome assembly of NLRP3 Δ exon 5 remains to be determined.

Possibly, cells which are not immediately responsive for NLRP3 activators act as a backup population, which is spared of pyroptosis in the first round of NLRP3 inflammasome activation. Thereby, NLRP3 Δ exon 5 contributes to a long-lasting IL-1β response. In response to danger signals, cells expressing full-length NLRP3 quickly activate inflammasome signaling and produce a first wave of IL-1β, to recruit and activate other immune cells. In contrast, cells expressing NLRP3 Δ exon 5 can respond at a later time point if the danger signals are still present and a second wave of IL-1β is required. Through these two waves of response to danger signals, the innate immune response can be maintained over a longer period of time and non-pyroptotic macrophages are still capable of recruiting an adaptive immune response.

6.9. Further implications of NLRP3 splicing

Beside gene expression and AS, post-translational modifications comprise another important layer to modulate the function of proteins. Although the integration of all three regulatory layers is not far to seek, little is known about their interplay on a global level. Interestingly, for some GPCRs it was shown that AS can influence GPCR activity or localization by removing exons which bear crucial PTM sites [221]. Similarly, AS-mediated removal of PTM sites within NFAT transcription factors was shown [221].

Of note, mass spectrometry of NLRP3 identified three phosphorylation sites, one of which is located in exon 5. However, when mutating the exon 5 phosphorylation site to a phospho-mimetic residue (S to D) or to a non-phosphorylatable residue (S to A), no changes in NLRP3 activity could be observed [85]. Another group reported a NLRP3 phosphorylation in exon 7 as a negative regulator of NLRP3 [86]. It is tempting to speculate about a functional connection between these two alternatively spliced exons and the detected phosphorylated residues. However, a role for the phosphorylation in exon 5 could not be established and due to the low expression levels of NLRP3 Δ exon 7, I did not functionally characterize this isoform. When examining a potential relationship between annotated PTM sites (https://www.phosphosite.org [222], accessed may 2018) with spliceable NLR-LRR exons, no enrichment could be found (data not shown). The overall interplay between AS and PTMs is still to be defined and requires further investigation.

In this thesis, the use of SSOs to induce an inactive NLRP3 variant was demonstrated (Figure 5-13). SSOs cannot only be used as research tools, but also as therapeutics. For example, they can be used to correct the reading frame by inducing AS of certain genes after exon duplications or deletions. Tow SSO drugs have been recently approved to treat Duchenne muscular dystrophy and spinal muscular atrophy [223,224]. Using SSOs to induce the skipping of NLRP3 exon 5 in NLRP3-driven diseases might also hold therapeutic potential as an NLRP3-specific anti-inflammatory approach.

6.10. Conclusion

AS is known to significantly contribute to protein diversity and flexibility of the transcriptome. In this thesis, I could show that NLRs, but also other LRR domain-containing protein families, are characterized by an evolutionarily conserved modularity of exons encoding for short LRR segments. The exonic organization of LRR modules allows for multiple AS events, while keeping the overall domain architecture unaffected. Indeed, RNAseq revealed AS of the LRR domain in several NLR proteins in human macrophages, most prominently in NLRP3. I focused the further analysis on NLRP3 and identified exon 5 as the most prominent alternatively spliced exon. Of note, alternative splicing of the NLRP3 LRR seems to be a unique feature of humans, which could not be detected in mouse or pig cells, stressing the value of studies using human primary cells.

I characterized the Δ exon 5 isoform as a loss of function version of NLRP3 and surface mapping analysis determined exon 5 to be critical for NEK7 binding and thus for NLRP3 activity. NLRP3 isoform expression was shown to be stochastic at a single-cell level and contributes to an adjustable NLRP3 inflammasome response. Moreover, NLRP3 Δ exon 5 was found to gain activity after prolonged priming, allowing for the activation of those cells, which were kept in standby in an immediate first wave responds.

The findings presented in this study describe a novel, human specific mechanism involved in the regulation of innate immunity by shaping the NLRP3 inflammasome response.

7. List of abbreviations

aa	amino acid
AIM2	absent in melanoma 2
AS	alternative splicing
ASC	apoptosis associated speck-like protein containing a CARD
ATP	Adenosine triphosphate
BMDM	bone marrow derived macrophage
bp	basepair
CAPS	cryopyrin-associated periodic syndrome
CARD	caspase activation and recruitment domain
cGAMP	cyclic GMP-AMP
cGAS	cGAMP synthase
CI	confidence interval
CIITA	class II MHC transactivator
CLR	C-type lectin receptors
COP	CARD-only proteins
CTD	C-terminal heptad repeat domain
DAMP	damage associated molecular pattern
DNA	Deoxyribonucleic acid
dsRNA	double strand RNA
ELISA	enzyme-linked immunosorbent assay
ERK1	extracellular signal-regulated kinase 1
ESE	Exonic splice enhancer
FMF	familial Mediterranean fever
GSDMD	gasdermin D
HAMP	homeostasis altering molecular processe
hMDM	human monocyte derived macrophage
hnRNP	heterogeneous nuclear ribonucleoproteins
HPRT	hypoxanthine-guanine phosphoribosyltransferase
HTRF	homogenous time-resolved fluorescent assay
IFI-16	interferon gamma inducible protein 16
IFN	interferon

IL	interleukin
IL-1R	interleukin-1 receptor
IL-1Ra	IL-1 receptor antagonist
iMo	immortalized mouse macrophage
IP	Immunoprecipitation
IRAK4	IL-1R-associated kinase 4
IS	immune system
LPS	lipopolysaccharide
LRR	leucine-rich repeat
LT	anthrax lethal toxin
mAb	monoclonal antibody
MAPK	mitogen-activated protein kinase
MHC	major histocompatibility complex
mtDNA	mitochondrial DNA
mTurq	mTurquoise
MyD88	myeloid differentiation primary-response protein 88
NACHT	NAIP, CIITA, HET-E and TP1
NAIP	NLR family apoptosis inhibitor protein
NEK7	never in mitosis gene a related Kinase 7
NF-$_k$B	nuclear factor kappa-light-chain-enhancer of activated B cells
NLR	NOD-like receptor
NLRC	NLR family CARD containing
NLRP	NLR family PYD containing
NOD	nucleotide oligomerization domain
noRT	no reverse transcription
PAMP	pathogen associated molecular pattern
pol II	(RNA) polymerase II
POP	pyrin-only proteins
PRR	pattern recognition receptors
PTM	post-translational modification
PYD	pyridine domain
PYHIN	N-terminal PYD and C-terminal DNA binding HIN domain containing
RI	ribonuclease inhibitor

RIG-I	retinoic acid inducible gene 1
RLR	RIG-I-like receptor
RNA	ribonucleic acid
RNA pol II	RNA polymerase II
ROS	reactive oxygen species
RPKM	reads per kilobase million
SD	standard deviation
SEM	standard error of the mean
snRNA	small nuclear RNA
SR	serine-arginine repeat factor
SSO	splice switching oligonucleotide
STAT	signal transducer and activator of transcription
STING	stimulator of interferon genes
T2B	type 2 diabetes
TLR	Toll-like receptor
TNF	tumor necrosis factor
tpm	transcripts per million
TRAF	TNF receptor associated factor
TRIF	Toll-/ IL-1R homologous domain containing adapter inducing interferon-β
WCL	whole cell lysate
wt	wildtype

8. List of figures

9. List of Tables

10. Bibliography

1. Murphy K, Travers P, Walport M. *Janeway's Immunobiology*. 7th Editio. New York NY: Garland Science, Taylor & Francis Group; 2008.
2. Medzhitov R. Origin and physiological roles of inflammation. *Nature* 2008;454(7203):428-35. doi:10.1038/nature07201.
3. Matzinger P. Tolerance, danger, and the extended family. *Annu. Rev. Immunol.* 1994;12:991-1045. doi:10.1146/annurev.iy.12.040194.005015.
4. Medzhitov R. Recognition of microorganisms and activation of the immune response. *Nature* 2007;449(7164):819-26. doi:10.1038/nature06246.
5. Ali RA, Wuescher LM, Worth RG. Platelets: essential components of the immune system. *Curr. Trends Immunol.* 2015;16:65-78.
6. Esmon CT. The interactions between inflammation and coagulation. *Br. J. Haematol.* 2005;131(4):417-430. doi:10.1111/j.1365-2141.2005.05753.x.
7. Kawai T, Akira S. The role of pattern-recognition receptors in innate immunity: update on Toll-like receptors. *Nat. Immunol.* 2010;11(5):373-84. doi:10.1038/ni.1863.
8. Chen GY, Nuñez G. Sterile inflammation: sensing and reacting to damage. *Nat. Rev. Immunol.* 2010;10(12):826-37. doi:10.1038/nri2873.
9. Tang D, Kang R, Coyne CB, Zeh HJ, Lotze MT. PAMPs and DAMPs: signal 0s that spur autophagy and immunity. *Immunol. Rev.* 2012;249(1):158-75. doi:10.1111/j.1600-065X.2012.01146.x.
10. Liston A, Masters SL. Homeostasis-altering molecular processes as mechanisms of inflammasome activation. *Nat. Rev. Immunol.* 2017;17(3):208-214. doi:10.1038/nri.2016.151.
11. Akira S, Uematsu S, Takeuchi O. Pathogen Recognition and Innate Imunity. *Cell* 2006;124(4):783-801. doi:10.1016/j.cell.2006.02.015.
12. Blasius AL, Beutler B. Intracellular toll-like receptors. *Immunity* 2010;32(3):305-15. doi:10.1016/j.immuni.2010.03.012.
13. Kato H, Takahasi K, Fujita T. RIG-I-like receptors: cytoplasmic sensors for non-self RNA. *Immunol. Rev.* 2011;243(1):91-8. doi:10.1111/j.1600-065X.2011.01052.x.
14. Hornung V, Ellegast J, Kim S, et al. 5'-Triphosphate RNA is the ligand for RIG-I. *Science* 2006;314(5801):994-7. doi:10.1126/science.1132505.
15. Hoving JC, Wilson GJ, Brown GD. Signalling C-type lectin receptors, microbial recognition and immunity. *Cell. Microbiol.* 2014;16(2):185-94.

doi:10.1111/cmi.12249.

16. Chen G, Shaw MH, Kim Y-G, Nuñez G. NOD-like receptors: role in innate immunity and inflammatory disease. *Annu. Rev. Pathol.* 2009;4:365-98. doi:10.1146/annurev.pathol.4.110807.092239.
17. Devaiah BN, Singer DS. CIITA and Its Dual Roles in MHC Gene Transcription. *Front. Immunol.* 2013;4:476. doi:10.3389/fimmu.2013.00476.
18. Jin T, Perry A, Jiang J, et al. Structures of the HIN domain:DNA complexes reveal ligand binding and activation mechanisms of the AIM2 inflammasome and IFI16 receptor. *Immunity* 2012;36(4):561-71. doi:10.1016/j.immuni.2012.02.014.
19. Sun L, Wu J, Du F, Chen X, Chen ZJ. Cyclic GMP-AMP Synthase Is a Cytosolic DNA Sensor That Activates the Type I Interferon Pathway. *Science* 2012;(December):1-10. doi:10.1126/science.1232458.
20. Latz E, Xiao TS, Stutz A. Activation and regulation of the inflammasomes. *Nat. Rev. Immunol.* 2013;13(6):397-411. doi:10.1038/nri3452.
21. Martinon F, Burns K, Tschopp J. The Inflammasome: A Molecular Platform Triggering Activation of Inflammatory Caspases and Processing of proIL-β. *Mol. Cell* 2002;10(2):417-426. doi:10.1016/S1097-2765(02)00599-3.
22. de Vasconcelos NM, van Opdenbosch N, Lamkanfi M. Inflammasomes as polyvalent cell death platforms. *Cell. Mol. Life Sci.* 2016:1-13. doi:10.1007/s00018-016-2204-3.
23. Man SM, Karki R, Kanneganti T-D. Molecular mechanisms and functions of pyroptosis, inflammatory caspases and inflammasomes in infectious diseases. *Immunol. Rev.* 2017;277(1):61-75. doi:10.1111/imr.12534.
24. Broz P, Dixit VM. Inflammasomes: mechanism of assembly, regulation and signalling. *Nat. Rev. Immunol.* 2016. doi:10.1038/nri.2016.58.
25. Broderick L, DeNardo D, Franklin BS, Hoffman HM, Latz E. The Inflammasomes and Autoinflammatory Syndromes. *Annu. Rev. Pathol. Mech. Dis.* 2015;10:395-424. doi:10.1146/annurev-pathol-012414-040431.
26. Guo H, Callaway JB, Ting JP. Inflammasomes: mechanism of action, role in disease, and therapeutics. *Nat. Med.* 2015;21(7):677-687. doi:10.1038/nm.3893.
27. Kayagaki N, Stowe IB, Lee BL, et al. Caspase-11 cleaves gasdermin D for non-canonical inflammasome signaling. *Nature* 2015. doi:10.1038/nature15541.
28. Shi J, Zhao Y, Wang K, et al. Cleavage of GSDMD by inflammatory caspases determines pyroptotic cell death. *Nature* 2015. doi:10.1038/nature15514.

29. Hoss F, Rodriguez-alcazar JF, Latz E. Assembly and regulation of ASC specks. *Cell. Mol. Life Sci.* 2016. doi:10.1007/s00018-016-2396-6.
30. Wang L, Manji GA, Grenier JM, et al. PYPAF7, a Novel PYRIN-containing Apaf1-like Protein That Regulates Activation of NF-κ B and Caspase-1-dependent Cytokine Processing *. *J. Biol. Chem.* 2002;277(33):29874-29880. doi:10.1074/jbc.M203915200.
31. Dick MS, Sborgi L, Ru S, Hiller S, Broz P. ASC filament formation serves as a signal amplification mechanism for inflammasome. *Nat. Commun.* 2016;(May). doi:10.1038/ncomms11929.
32. Park HH, Lo Y-C, Lin S-C, Wang L, Yang JK, Wu H. The death domain superfamily in intracellular signaling of apoptosis and inflammation. *Annu. Rev. Immunol.* 2007;25:561-586. doi:10.1146/annurev.immunol.25.022106.141656.
33. Liepinsh E, Barbals R, Dahl E, Sharipo A, Staub E, Otting G. The death-domain fold of the ASC PYRIN domain, presenting a basis for PYRIN/PYRIN recognition. *J. Mol. Biol.* 2003;332(5):1155-1163. doi:10.1016/j.jmb.2003.07.007.
34. Bae JY, Park HH. Crystal structure of NALP3 protein pyrin domain (PYD) and its implications in inflammasome assembly. *J. Biol. Chem.* 2011;286(45):39528-36. doi:10.1074/jbc.M111.278812.
35. Jin T, Perry A, Smith P, Jiang J, Xiao TS. Structure of the absent in melanoma 2 (AIM2) pyrin domain provides insights into the mechanisms of AIM2 autoinhibition and inflammasome assembly. *J. Biol. Chem.* 2013;288(19):13225-35. doi:10.1074/jbc.M113.468033.
36. Pinheiro AS, Proell M, Eibl C, Page R, Schwarzenbacher R, Peti W. Three-dimensional structure of the NLRP7 pyrin domain: insight into pyrin-pyrin-mediated effector domain signaling in innate immunity. *J. Biol. Chem.* 2010;285(35):27402-10. doi:10.1074/jbc.M110.113191.
37. Pinheiro AS, Eibl C, Ekman-Vural Z, Schwarzenbacher R, Peti W. The NLRP12 pyrin domain: structure, dynamics, and functional insights. *J. Mol. Biol.* 2011;413(4):790-803. doi:10.1016/j.jmb.2011.09.024.
38. Hiller S, Kohl A, Fiorito F, et al. NMR structure of the apoptosis- and inflammation-related NALP1 pyrin domain. *Structure* 2003;11(10):1199-205. doi:10.1016/j.str.2003.08.009.
39. Eibl C, Grigoriu S, Hessenberger M, et al. Structural and functional analysis of the NLRP4 pyrin domain. *Biochemistry* 2012;51(37):7330-41. doi:10.1021/bi3007059.

40. Hu Z, Yan C, Liu P, et al. Crystal Structure of NLRC4 Reveals Its Autoinhibition Mechanism. *Science (80-.).* 2013;341(6142):172-175. doi:10.1126/science.1236381.
41. Lu A, Magupalli VG, Ruan J, et al. Unified Polymerization Mechanism for the Assembly of ASC-Dependent Inflammasomes. *Cell* 2014;156(6):1193-206. doi:10.1016/j.cell.2014.02.008.
42. Cai X, Chen J, Xu H, et al. Prion-like Polymerization Underlies Signal Transduction in Antiviral Immune Defense and Inflammasome Activation. *Cell* 2014;156(6):1207-22. doi:10.1016/j.cell.2014.01.063.
43. Sborgi L, Ravotti F, Dandey VP, et al. Structure and assembly of the mouse ASC inflammasome by combined NMR spectroscopy and cryo-electron microscopy. *Proc. Natl. Acad. Sci. U. S. A.* 2015. doi:10.1073/pnas.1507579112.
44. de Alba E. Structure and interdomain dynamics of apoptosis-associated speck-like protein containing a CARD (ASC). *J. Biol. Chem.* 2009;284(47):32932-32941. doi:10.1074/jbc.M109.024273.
45. Fernandes-Alnemri T, Wu J, Yu J-W, et al. The pyroptosome: a supramolecular assembly of ASC dimers mediating inflammatory cell death via caspase-1 activation. *Cell Death Differ.* 2007;14(9):1590-1604. doi:10.1038/sj.cdd.4402194.
46. Richards N, Schaner P, Diaz A, et al. Interaction between Pyrin and the Apoptotic Speck Protein (ASC) Modulates ASC-induced Apoptosis. *J. Biol. Chem.* 2001;276(42):39320-39329. doi:10.1074/jbc.M104730200.
47. Sahillioglu AC, Sumbul F, Ozoren N, Haliloglu T. Structural and dynamics aspects of ASC speck assembly. *Structure* 2014;22(12):1722-1734. doi:10.1016/j.str.2014.09.011.
48. Schmidt FI, Lu A, Chen JW, et al. A single domain antibody fragment that recognizes the adaptor ASC defines the role of ASC domains in inflammasome assembly. *J. Exp. Med.* 2016. doi:10.1084/jem.20151790.
49. Zhang L, Chen S, Ruan J, et al. Cryo-EM structure of the activated NAIP2-NLRC4 inflammasome reveals nucleated polymerization. *Sci. express* 2015;4(October):12-14.
50. Thornberry NA, Bull HG, Calaycay JR, et al. A novel heterodimeric cysteine protease is required for interleukin-1 beta processing in monocytes. *Nature* 1992;356(6372):768-74. doi:10.1038/356768a0.
51. Lu A, Wu H. Structural mechanisms of inflammasome assembly. *FEBS J.* 2015;5:435-444. doi:10.1111/febs.13133.

52. Wilson KP, Black J-AF, Thomson JA, et al. Structure and mechanism of interleukin-lβ converting enzyme. *Nature* 1994;370(6487):270-275. doi:10.1038/370270a0.
53. Walker NP, Talanian R V, Brady KD, et al. Crystal structure of the cysteine protease interleukin-1 beta-converting enzyme: a (p20/p10)2 homodimer. *Cell* 1994;78(2):343-52.
54. Boucher D, Monteleone M, Coll RC, et al. Caspase-1 self-cleavage is an intrinsic mechanism to terminate inflammasome activity. *J. Exp. Med.* 2018:1-14.
55. Fantuzzi G, Dinarello CA. Interleukin-18 and Interleukin-lβ: Two Cytokine Substrates for ICE (Caspase-1). *J. Clin. Immunol.* 1999;19(I):1-11. doi:10.1023/A:1020506300324.
56. Howard AD, Kostura MJ, Thornberry N, et al. IL-1-converting enzyme requires aspartic acid residues for processing of the IL-1 beta precursor at two distinct sites and does not cleave 31-kDa IL-1 alpha . IL-1-CONVERTING ENZYME REQUIRES ASPARTIC ACID RESIDUES FOR PROCESSING OF THE IL-1 / 3 PRECURSOR. *J. Immunol.* 1991;147(November):2964-2969.
57. Ghayur T, Banerjee S, Hugunin M, et al. Caspase-1 processes IFN-γ-inducing factor and regulates LPS-induced IFN- γ production. *Nature* 1997;386(6625):619-623. doi:10.1038/386619a0.
58. Ding J, Wang K, Liu W, et al. Pore-forming activity and structural autoinhibition of the gasdermin family. *Nature* 2016;535(7610):111-116. doi:10.1038/nature18590.
59. Aglietti RA, Estevez A, Gupta A, et al. GsdmD p30 elicited by caspase-11 during pyroptosis forms pores in membranes. *Proc. Natl. Acad. Sci. U. S. A.* 2016;113(28):7858-7863. doi:10.1073/pnas.1607769113.
60. Liu X, Zhang Z, Ruan J, et al. Inflammasome-activated gasdermin D causes pyroptosis by forming membrane pores. *Nature* 2016;535(7610):153-158. doi:10.1038/nature18629.
61. Agard NJ, Maltby D, Wells JA. Inflammatory stimuli regulate caspase substrate profiles. *Mol. Cell. Proteomics* 2010;9(5):880-93. doi:10.1074/mcp.M900528-MCP200.
62. Walsh JG, Logue SE, Lüthi AU, Martin SJ. Caspase-1 promiscuity is counterbalanced by rapid inactivation of processed enzyme. *J. Biol. Chem.* 2011;286(37):32513-24. doi:10.1074/jbc.M111.225862.
63. Hoffman HM, Broderick L. The role of the inflammasome in patients with autoinflammatory diseases. *J. Allergy Clin. Immunol.* 2016;138(1):3-14.

doi:10.1016/j.jaci.2016.05.001.

64. Dorfleutner A, Chu L, Stehlik C. Inhibiting the inflammasome : one domain at a time. *Immunol. Rev.* 2015;265:205-216.
65. Le HT, Harton JA. Pyrin- and CARD-only Proteins as Regulators of NLR Functions. *Front. Immunol.* 2013;4:1-10. doi:10.3389/fimmu.2013.00275.
66. Porter KA, Duffy EB, Nyland P, Atianand MK, Sharifi H, Harton JA. The CLRX.1/NOD24 (NLRP2P) pseudogene codes a functional negative regulator of NF-κB, pyrin-only protein 4. *Genes Immun.* 2014;15(6):392-403. doi:10.1038/gene.2014.30.
67. Bedoya F, Sandler LL, Harton JA. Pyrin-Only Protein 2 Modulates NF-kB and Disrupts ASC:CLR Interactions. *J. Immunol.* 2007;178(6):3837-3845. doi:10.4049/jimmunol.178.6.3837.
68. Srimathi T, Robbins SL, Dubas RL, et al. Mapping of POP1-binding site on pyrin domain of ASC. *J. Biol. Chem.* 2008;283(22):15390-8. doi:10.1074/jbc.M801589200.
69. Khare S, Ratsimandresey R a, de Almeida L, et al. The PYRIN domain-only protein POP3 inhibits ALR inflammasomes and regulates responses to infection with DNA viruses. *Nat. Immunol.* 2014;15(4):343-353. doi:10.1038/ni.2829.
70. Atianand MK, Harton JA. Uncoupling of Pyrin-only protein 2 (POP2)-mediated dual regulation of NF-κB and the inflammasome. *J. Biol. Chem.* 2011;286(47):40536-40547. doi:10.1074/jbc.M111.274290.
71. Stehlik C, Krajewska M, Welsh K, Krajewski S, Godzik A, Reed JC. The PAAD/PYRIN-only protein POP1/ASC2 is a modulator of ASC-mediated nuclear-factor-kappa B and pro-caspase-1 regulation. *Biochem. J.* 2003;373(Pt 1):101-13. doi:10.1042/BJ20030304.
72. Bryan NB, Dorfleutner A, Kramer SJ, Yun C, Rojanasakul Y, Stehlik C. Differential splicing of the apoptosis-associated speck like protein containing a caspase recruitment domain (ASC) regulates inflammasomes. *J. Inflamm. (Lond).* 2010;7:23. doi:10.1186/1476-9255-7-23.
73. Lu A, Li Y, Schmidt FI, et al. Molecular basis of caspase-1 polymerization and its inhibition by a new capping mechanism. *Nat. Struct. Mol. Biol.* 2016;23(April):1-12. doi:10.1038/nsmb.3199.
74. Lamkanfi M, Denecker G, Kalai M, et al. INCA, a novel human caspase recruitment domain protein that inhibits interleukin-1β generation. *J. Biol. Chem.* 2004;279(50):51729-51738. doi:10.1074/jbc.M407891200.
75. Garlanda C, Dinarello C a, Mantovani A. The interleukin-1 family: back to the

future. *Immunity* 2013;39(6):1003-18. doi:10.1016/j.immuni.2013.11.010.

76. Istomin AY, Godzik A. Understanding diversity of human innate immunity receptors: analysis of surface features of leucine-rich repeat domains in NLRs and TLRs. *BMC Immunol.* 2009;15(10):48. doi:10.1186/1471-2172-10-48.
77. Hu Z, Zhou Q, Zhang C, et al. Structural and biochemical basis for induced self-propagation of NLRC4. *Sci. express* 2015;4(October):1-11.
78. Bauernfeind FG, Horvath G, Stutz A, et al. Cutting edge: NF-kappaB activating pattern recognition and cytokine receptors license NLRP3 inflammasome activation by regulating NLRP3 expression. *J. Immunol.* 2009;183(2):787-791. doi:10.4049/jimmunol.0901363.
79. Juliana C, Fernandes-Alnemri T, Kang S, Farias A, Qin F, Alnemri ES. Non-transcriptional Priming and Deubiquitination Regulate NLRP3 Inflammasome Activation. *J. Biol. Chem.* 2012;287(43):36617-36622. doi:10.1074/jbc.M112.407130.
80. Py BF, Kim M-S, Vakifahmetoglu-Norberg H, Yuan J. Deubiquitination of NLRP3 by BRCC3 critically regulates inflammasome activity. *Mol. Cell* 2013;49(2):331-8. doi:10.1016/j.molcel.2012.11.009.
81. Ghonime MG, Shamaa OR, Das S, et al. Inflammasome Priming by Lipopolysaccharide Is Dependent upon ERK Signaling and Proteasome Function. *J. Immunol.* 2014. doi:10.4049/jimmunol.1301974.
82. Mao K, Chen S, Chen M, et al. Nitric oxide suppresses NLRP3 inflammasome activation and protects against LPS-induced septic shock. *Cell Res.* 2013;23(2):201-12. doi:10.1038/cr.2013.6.
83. Mishra BB, Rathinam VAK, Martens GW, et al. Nitric oxide controls the immunopathology of tuberculosis by inhibiting NLRP3 inflammasome-dependent processing of IL-1β. *Nat. Immunol.* 2013;14(1):52-60. doi:10.1038/ni.2474.
84. Hernandez-Cuellar E, Tsuchiya K, Hara H, et al. Cutting edge: nitric oxide inhibits the NLRP3 inflammasome. *J. Immunol.* 2012;189(11):5113-7. doi:10.4049/jimmunol.1202479.
85. Stutz A, Kolbe CC, Stahl R, et al. NLRP3 inflammasome assembly is regulated by phosphorylation of the pyrin domain. *J. Exp. Med.* 2017:1-12. doi:10.1084/jem.20160933.
86. Spalinger MR, Kasper S, Gottier C, et al. NLRP3 tyrosine phosphorylation is controlled by protein tyrosine phosphatase PTPN22. *J. Clin. Invest.* 2016;126(5):1783-800. doi:10.1172/JCI83669.
87. Mortimer L, Moreau F, MacDonald JA, Chadee K. NLRP3 inflammasome

inhibition is disrupted in a group of auto-inflammatory disease CAPS mutations. *Nat. Immunol.* 2016;17(10):1176-1186. doi:10.1038/ni.3538.

88. Zhou R, Yazdi AS, Menu P, Tschopp J. A role for mitochondria in NLRP3 inflammasome activation. *Nature* 2011;469(7329):221-225.
89. Shimada K, Crother TR, Karlin J, et al. Oxidized Mitochondrial DNA Activates the NLRP3 Inflammasome during Apoptosis. *Immunity* 2012;36(3):401-414. doi:10.1016/j.immuni.2012.01.009.
90. Iyer SS, He Q, Janczy JR, et al. Mitochondrial cardiolipin is required for Nlrp3 inflammasome activation. *Immunity* 2013;39(2):311-23. doi:10.1016/j.immuni.2013.08.001.
91. Muñoz-Planillo R, Kuffa P, Martínez-Colón G, Smith B, Rajendiran T, Núñez G. K+ Efflux Is the Common Trigger of NLRP3 Inflammasome Activation by Bacterial Toxins and Particulate Matter. *Immunity* 2013;38(6):1142-1153. doi:10.1016/j.immuni.2013.05.016.
92. Próchnicki T, Mangan MS, Latz E. Recent insights into the molecular mechanisms of the NLRP3 inflammasome activation. *F1000Research* 2016;5(0):1-15. doi:10.12688/f1000research.8614.1.
93. Perregaux D, Gabel CA. Interleukin-1β maturation and release in response to ATP and nigericin. *J. Biol. Chem.* 1994;269(21):15195-15203.
94. Kelkar DA, Chattopadhyay A. The gramicidin ion channel: A model membrane protein. *Biochim. Biophys. Acta - Biomembr.* 2007;1768(9):2011-2025. doi:10.1016/j.bbamem.2007.05.011.
95. Pressman BC. Biological Applications of Ionophores. *Annu. Rev. Biochem.* 1976;45(1):501-530. doi:10.1146/annurev.bi.45.070176.002441.
96. Grebe A, Hoss F, Latz E. NLRP3 Inflammasome and the IL-1 Pathway in Atherosclerosis. *Circ. Res.* 2018;122(12):1722-1740. doi:10.1161/CIRCRESAHA.118.311362.
97. Shi H, Wang Y, Li X, et al. NLRP3 activation and mitosis are mutually exclusive events coordinated by NEK7 , a new inflammasome component. *Nat. Immunol.* 2015;(December):1-12. doi:10.1038/ni.3333.
98. Schmid-Burgk JL, Chauhan D, Schmidt T, et al. A Genome-wide CRISPR Screen Identifies NEK7 as an Essential Component of NLRP3 Inflammasome Activation. *J. Biol. Chem.* 2015;1(3). doi:10.1074/jbc.C115.700492.
99. He Y, Zeng MY, Yang D, Motro B, Núñez G. Nek7 is an essential mediator of NLRP3 oligomerization and inflammasome activation downstream of potassium efflux. *Nature* 2016:1-16. doi:10.1038/nature16959.
100. Hagar J a, Powell D a, Aachoui Y, Ernst RK, Miao E a. Cytoplasmic LPS

activates caspase-11: implications in TLR4-independent endotoxic shock. *Science* 2013;341(6151):1250-3. doi:10.1126/science.1240988.

101. Kayagaki N, Wong M, Stowe I. Noncanonical Inflammasome Activation by Intracellular LPS Independent of TLR4. *Science (80-.).* 2013;341(2013):1246-1249. doi:10.5061/dryad.bt51g.
102. Shi J, Zhao Y, Wang Y, et al. Inflammatory caspases are innate immune receptors for intracellular LPS. *Nature* 2014. doi:10.1038/nature13683.
103. Casson CN, Yu J, Reyes VM, et al. Human caspase-4 mediates noncanonical inflammasome activation against gram-negative bacterial pathogens. *Proc. Natl. Acad. Sci. U. S. A.* 2015;112(21):6688-93. doi:10.1073/pnas.1421699112.
104. Yang D, He Y, Muñoz-Planillo R, Liu Q, Núñez G. Caspase-11 Requires the Pannexin-1 Channel and the Purinergic P2X7 Pore to Mediate Pyroptosis and Endotoxic Shock. *Immunity* 2015;43(5):923-932. doi:10.1016/j.immuni.2015.10.009.
105. Gaidt MM, Ebert TS, Chauhan D, et al. Human Monocytes Engage an Alternative Inflammasome Pathway. *Immunity* 2016;44(4):833-846. doi:10.1016/j.immuni.2016.01.012.
106. Gaidt MM, Ebert TS, Chauhan D, et al. The DNA Inflammasome in Human Myeloid Cells Is Initiated by a STING-Cell Death Program Upstream of NLRP3. *Cell* 2017:1-15. doi:10.1016/j.cell.2017.09.039.
107. Wolf AJ, Reyes CN, Liang W, et al. Hexokinase Is an Innate Immune Receptor for the Detection of Bacterial Peptidoglycan. *Cell* 2016;166(3):624-636. doi:10.1016/j.cell.2016.05.076.
108. Moon J-S, Hisata S, Park M-A, et al. mTORC1-Induced HK1-Dependent Glycolysis Regulates NLRP3 Inflammasome Activation. *Cell Rep.* 2015;12(1):102-115. doi:10.1016/j.celrep.2015.05.046.
109. Xie M, Yu Y, Kang R, et al. PKM2-dependent glycolysis promotes NLRP3 and AIM2 inflammasome activation. *Nat. Commun.* 2016;7:13280. doi:10.1038/ncomms13280.
110. Youm Y-H, Nguyen KY, Grant RW, et al. The ketone metabolite β-hydroxybutyrate blocks NLRP3 inflammasome–mediated inflammatory disease. *Nat. Med.* 2015;(October 2014):1-9. doi:10.1038/nm.3804.
111. Yan Y, Jiang W, Spinetti T, et al. Omega-3 Fatty Acids Prevent Inflammation and Metabolic Disorder through Inhibition of NLRP3 Inflammasome Activation. *Immunity* 2013;38(6):1154-1163. doi:10.1016/j.immuni.2013.05.015.
112. Yan Y, Jiang W, Liu L, et al. Dopamine Controls Systemic Inflammation

through Inhibition of NLRP3 Inflammasome. *Cell* 2015;160(1-2):62-73. doi:10.1016/j.cell.2014.11.047.

113. Guarda G, Braun M, Staehli F, et al. Type I Interferon Inhibits Interleukin-1 Production and Inflammasome Activation. *Immunity* 2011;34(2):213-223. doi:10.1016/j.immuni.2011.02.006.
114. Sciacca FL, Canal N, Grimaldi LM. Induction of IL-1 receptor antagonist by interferon beta: implication for the treatment of multiple sclerosis. *J. Neurovirol.* 2000;6 Suppl 2:S33-7.
115. Man SM, Karki R, Malireddi RKS, et al. The transcription factor IRF1 and guanylate-binding proteins target AIM2 inflammasome activation by Francisella infection. *Nat. Immunol.* 2015;6(2):356-372. doi:10.1007/s12671-013-0269-8.Moving.
116. Meunier E, Wallet P, Dreier RF, et al. Guanylate-binding proteins promote activation of the AIM2 inflammasome during infection with Francisella novicida. *Nat. Immunol.* 2015;16(5). doi:10.1038/ni.3119.
117. Man SM, Karki R, Sasai M, et al. IRGB10 liberates bacterial ligands for sensing by the AIM2 and caspase - 11 – NLRP3 inflammasomes. *Cell* 2016;167(2):382–396. doi:10.1016/j.cell.2016.09.012.
118. Arbore G, West EE, Spolski R, et al. T helper 1 immunity requires complement-driven NLRP3 inflammasome activity in CD4 + T cells. *Science* 2016;352(6292):aad1210-1-aad1210-11. doi:10.1126/science.aad1210.
119. Bruchard M, Rebé C, Derangère V, et al. The receptor NLRP3 is a transcriptional regulator of T H 2 differentiation. *Nat. Immunol.* 2015;(June). doi:10.1038/ni.3202.
120. Hwang I, Yang J, Hong S, et al. Non-transcriptional regulation of NLRP3 inflammasome signaling by IL-4. *Immunol. Cell Biol.* 2015. doi:10.1038/icb.2014.125.
121. Romberg N, Al Moussawi K, Nelson-Williams C, et al. Mutation of NLRC4 causes a syndrome of enterocolitis and autoinflammation. *Nat Genet* 2014;46(10):1135-1139.
122. Canna SW, de Jesus AA, Gouni S, et al. An activating NLRC4 inflammasome mutation causes autoinflammation with recurrent macrophage activation syndrome. *Nat Genet* 2014;46(10):1140-1146.
123. Dostert C, Petrilli V, Van Bruggen R, Steele C, Mossman BT, Tschopp J. Innate Immune Activation Through Nalp3 Inflammasome Sensing of Asbestos and Silica. *Science (80-.).* 2008;320(5876):674-677. doi:10.1126/science.1156995.

124. Hornung V, Bauernfeind F, Halle A, et al. Silica crystals and aluminum salts activate the NALP3 inflammasome through phagosomal destabilization. *Nat. Immunol.* 2008;9(8):847-856. doi:10.1038/ni.1631.
125. Cassel SL, Eisenbarth SC, Iyer SS, et al. The Nalp3 inflammasome is essential for the development of silicosis. *Proc. Natl. Acad. Sci.* 2008;105(26):9035-9040. doi:10.1073/pnas.0803933105.
126. Hirota JA, Hirota SA, Warner SM, et al. The airway epithelium nucleotide-binding domain and leucine-rich repeat protein 3 inflammasome is activated by urban particulate matter. *J. Allergy Clin. Immunol.* 2012;129(4):1116-1125.e6. doi:10.1016/j.jaci.2011.11.033.
127. Martinon F, Pétrilli V, Mayor A, Tardivel A, Tschopp J. Gout-associated uric acid crystals activate the NALP3 inflammasome. *Nature* 2006;440(7081):237-241. doi:10.1038/nature04516.
128. Wen H, Gris D, Lei Y, et al. Fatty acid–induced NLRP3-ASC inflammasome activation interferes with insulin signaling. *Nat. Immunol.* 2011;12(5):408-415. doi:10.1038/ni.2022.
129. Spranger J, Kroke A, Möhlig M, et al. Inflammatory cytokines and the risk to develop type 2 diabetes: results of the prospective population-based European Prospective Investigation into Cancer and Nutrition (EPIC)-Potsdam Study. *Diabetes* 2003;52(3):812-7.
130. Masters SL, Dunne A, Subramanian SL, et al. Activation of the NLRP3 inflammasome by islet amyloid polypeptide provides a mechanism for enhanced IL-1β in type 2 diabetes. *Nat. Immunol.* 2010;11(10):897-904. doi:10.1038/ni.1935.
131. Lorenzo A, Razzaboni B, Weir GC, Yankner BA. Pancreatic islet cell toxicity of amylin associated with type-2 diabetes mellitus. *Nature* 1994;368(6473):756-760. doi:10.1038/368756a0.
132. Duewell P, Kono H, Rayner KJ, et al. NLRP3 inflammasomes are required for atherogenesis and activated by cholesterol crystals. *Nature* 2010;464(7293):1357-1361. doi:10.1038/nature08938.
133. Zimmer S, Grebe A, Latz E. Danger Signaling in Atherosclerosis. *Circ. Res.* 2015;116(2):323-340. doi:10.1161/CIRCRESAHA.116.301135.
134. Allen IC, Scull MA, Moore CB, et al. The NLRP3 Inflammasome Mediates In Vivo Innate Immunity to Influenza A Virus through Recognition of Viral RNA. *Immunity* 2009;30(4):556-565. doi:10.1016/j.immuni.2009.02.005.
135. Ichinohe T, Lee HK, Ogura Y, Flavell R, Iwasaki A. Inflammasome recognition of influenza virus is essential for adaptive immune responses. *J. Exp. Med.*

2009;206(1):79-87. doi:10.1084/jem.20081667.

136. Pang IK, Ichinohe T, Iwasaki A. IL-1R signaling in dendritic cells replaces pattern-recognition receptors in promoting CD8(+) T cell responses to influenza A virus. *Nat. Immunol.* 2013;(January):1-9. doi:10.1038/ni.2514.
137. Chakrabarti A, Banerjee S, Franchi L, et al. RNase L Activates the NLRP3 Inflammasome during Viral Infections. *Cell Host Microbe* 2015;17(4):466-477. doi:10.1016/j.chom.2015.02.010.
138. Mitoma H, Hanabuchi S, Kim T, et al. The DHX33 RNA helicase senses cytosolic RNA and activates the NLRP3 inflammasome. *Immunity* 2013;39(1):123-35. doi:10.1016/j.immuni.2013.07.001.
139. Kobe B, Deisenhofer J. Crystal structure of porcine ribonuclease inhibitor, a protein with leucine-rich repeats. *Nature* 1993;366(6457):751-756. doi:10.1038/366751a0.
140. Matsushima N, Miyashita H, Enkhbayar P, Kretsinger RH. Comparative Geometrical Analysis of Leucine-Rich Repeat Structures in the Nod-Like and Toll-Like Receptors in Vertebrate Innate Immunity. *Biomolecules* 2015;5(3):1955-1978. doi:10.3390/biom5031955.
141. Kofoed EM, Vance RE. Innate immune recognition of bacterial ligands by NAIPs determines inflammasome specificity. *Nature* 2011:2-7. doi:10.1038/nature10394.
142. Zhao Y, Yang J, Shi J, et al. The NLRC4 inflammasome receptors for bacterial flagellin and type III secretion apparatus. *Nature* 2011;477(7366):596-600. doi:10.1038/nature10510.
143. Park BS, Song DH, Kim HM, Choi B-S, Lee H, Lee J-O. The structural basis of lipopolysaccharide recognition by the TLR4–MD-2 complex. *Nature* 2009;458(7242):1191-1195. doi:10.1038/nature07830.
144. Ohto U, Shibata T, Tanji H, et al. Structural basis of CpG and inhibitory DNA recognition by Toll-like receptor 9. *Nature* 2015. doi:10.1038/nature14138.
145. Tanji H, Ohto U, Shibata T, Miyake K, Shimizu T. Structural reorganization of the toll-like receptor 8 dimer induced by agonistic ligands. *Science (80-.).* 2013. doi:10.1126/science.1229159.
146. Zhang Z, Ohto U, Shibata T, et al. Structural Analysis Reveals that Toll-like Receptor 7 Is a Dual Receptor for Guanosine and Single-Stranded RNA. *Immunity* 2016;45(4):737-748. doi:10.1016/j.immuni.2016.09.011.
147. Lee H-A, Yeom S-I. Plant NB-LRR proteins: tightly regulated sensors in a complex manner. *Brief. Funct. Genomics* 2015;14(4):233-242. doi:10.1093/bfgp/elv012.

148. Boehm T, McCurley N, Sutoh Y, Schorpp M, Kasahara M, Cooper MD. VLR-based adaptive immunity. *Annu. Rev. Immunol.* 2012;30:203-20. doi:10.1146/annurev-immunol-020711-075038.
149. Lee Y, Rio DC. Mechanisms and Regulation of Alternative Pre-mRNA Splicing. *Annu. Rev. Biochem.* 2015;84(1):291-323. doi:10.1146/annurev-biochem-060614-034316.
150. Alberts B, Johnson A, Lewis J, Raff M, Roberts K, Walter P. *Molecular Biology of the Cell*. 5th Editio. Garland Science, Taylor & Francis Group; 2008.
151. Black DL. Mechanisms of alternative pre-messenger RNA splicing. *Annu. Rev. Biochem.* 2003;72(1):291-336. doi:10.1146/annurev.biochem.72.121801.161720.
152. Will CL, Lührmann R. Spliceosome Structure and Function. *Cold Spring Harb. Perspect. Biol.* 2011;3(7):a003707-a003707. doi:10.1101/cshperspect.a003707.
153. Martinez NM, Lynch KW. Control of alternative splicing in immune responses: many regulators, many predictions, much still to learn. *Immunol. Rev.* 2013;253(1):216-236. doi:10.1111/imr.12047.
154. Hirose Y, Tacke R, Manley JL. Phosphorylated RNA polymerase II stimulates pre-mRNA splicing. *Genes Dev.* 1999;13(10):1234-9.
155. Saldi T, Cortazar MA, Sheridan RM, Bentley DL. Coupling of RNA Polymerase II Transcription Elongation with Pre-mRNA Splicing. *J. Mol. Biol.* 2016;428(12):2623-2635. doi:10.1016/j.jmb.2016.04.017.
156. Wang ET, Sandberg R, Luo S, et al. Alternative isoform regulation in human tissue transcriptomes. *Nature* 2008;456(7221):470-476. doi:10.1038/nature07509.
157. Pan Q, Shai O, Lee LJ, Frey BJ, Blencowe BJ. Deep surveying of alternative splicing complexity in the human transcriptome by high-throughput sequencing. *Nat. Genet.* 2008;40(12):1413-5. doi:10.1038/ng.259.
158. Vuong CK, Black DL, Zheng S. The neurogenetics of alternative splicing. *Nat. Rev. Neurosci.* 2016;17(5):265-81. doi:10.1038/nrn.2016.27.
159. Chang MX, Zhang J. Alternative Pre-mRNA splicing in mammals and teleost fish: A effective strategy for the regulation of immune responses against pathogen infection. *Int. J. Mol. Sci.* 2017;18(7). doi:10.3390/ijms18071530.
160. Faustino NA, Cooper TA. Pre-mRNA splicing and human disease. *Genes Dev.* 2003;17(4):419-437. doi:10.1101/gad.1048803.
161. Yang X, Coulombe-Huntington J, Kang S, et al. Widespread Expansion of Protein Interaction Capabilities by Alternative Splicing. *Cell* 2016;164(4):805-

817. doi:10.1016/j.cell.2016.01.029.

162. Ergun A, Doran G, Costello JC, et al. Differential splicing across immune system lineages. *Proc. Natl. Acad. Sci. U. S. A.* 2013;110(35):14324-9. doi:10.1073/pnas.1311839110.
163. Baralle FE, Giudice J. Alternative splicing as a regulator of development and tissue identity. *Nat. Rev. Mol. Cell Biol.* 2017;18(7):437-451. doi:10.1038/nrm.2017.27.
164. Melamud E, Moult J. Stochastic noise in splicing machinery. *Nucleic Acids Res.* 2009;37(14):4873-86. doi:10.1093/nar/gkp471.
165. Pickrell JK, Pai A a, Gilad Y, Pritchard JK. Noisy splicing drives mRNA isoform diversity in human cells. *PLoS Genet.* 2010;6(12):e1001236. doi:10.1371/journal.pgen.1001236.
166. Tress ML, Abascal F, Valencia A. Alternative Splicing May Not Be the Key to Proteome Complexity. *Trends Biochem. Sci.* 2017;42(2):98-110. doi:10.1016/j.tibs.2016.08.008.
167. Djebali S, Davis CA, Merkel A, et al. Landscape of transcription in human cells. *Nature* 2012;489(7414):101-8. doi:10.1038/nature11233.
168. Xu Z, Weiss A. Negative regulation of CD45 by differential homodimerization of the alternatively spliced isoforms. *Nat. Immunol.* 2002;3(8):764-71. doi:10.1038/ni822.
169. Gray P, Michelsen KS, Sirois CM, et al. Identification of a novel human MD-2 splice variant that negatively regulates LPS-induced Toll-like receptor 4 signaling. *J. Immunol.* 2010;184(11):6359-6366. doi:10.4049/jimmunol.0903543.
170. Liu S, Zhao K, Su X, et al. MITA/STING and Its Alternative Splicing Isoform MRP Restrict Hepatitis B Virus Replication. Guo H, ed. *PLoS One* 2017;12(1):e0169701. doi:10.1371/journal.pone.0169701.
171. Shang X, Cao Y, Ma L. Alternative Splicing in Plant Genes: A Means of Regulating the Environmental Fitness of Plants. *Int. J. Mol. Sci.* 2017;18(2). doi:10.3390/ijms18020432.
172. Yang S, Tang F, Zhu H. Alternative Splicing in Plant Immunity. *Int. J. Mol. Sci.* 2014;15:10424-10445. doi:10.3390/ijms150610424.
173. Haneklaus M, O'Neil JD, Clark AR, Masters SL, O'Neill LAJ. The RNA-binding protein Tristetraprolin (TTP) is a critical negative regulator of the NLRP3 inflammasome. *J. Biol. Chem.* 2017:jbc.M116.772947. doi:10.1074/jbc.M116.772947.
174. Carpenter AE, Jones TR, Lamprecht MR, et al. CellProfiler: image analysis

software for identifying and quantifying cell phenotypes. *Genome Biol.* 2006;7(10):R100. doi:10.1186/gb-2006-7-10-r100.

175. Schindelin J, Arganda-Carreras I, Frise E, et al. Fiji: an open-source platform for biological-image analysis. *Nat Meth* 2012;9(7):676-682.
176. Dobin A, Davis CA, Schlesinger F, et al. STAR: ultrafast universal RNA -seq aligner. *Bioinformatics* 2013. doi:doi: 10.1093/bioinformatics/bts635.
177. Bray NL, Pimentel H, Melsted P, Pachter L. Near-optimal probabilistic RNA-seq quantification. *Nat. Biotechnol.* 2016;34(5):525-527. doi:10.1038/nbt.3519.
178. Soneson C, Love MI, Robinson MD. Differential analyses for RNA-seq: transcript-level estimates improve gene-level inferences. *F1000Research* 2015;4:1521. doi:10.12688/f1000research.7563.2.
179. Katz Y, Wang ET, Airoldi EM, Burge CB. Analysis and design of RNA sequencing experiments for identifying isoform regulation. *Nat. Methods* 2010;7(12):1009-15. doi:10.1038/nmeth.1528.
180. Dogan RI, Getoor L, Wilbur WJ, Mount SM. SplicePort — An interactive splice-site analysis tool. *Nucleic Acids Res.* 2007;35(301):285-291. doi:10.1093/nar/gkm407.
181. Fairbrother WG, Yeh R-F, Sharp PA, Burge CB. Predictive Identification of Exonic Splicing Enhancers in Human Genes. *Science (80-.).* 2002;297(August):1007-1014. doi:10.1126/science.1073774.
182. Ng ACY, Eisenberg JM, Heath RJW, et al. Human leucine-rich repeat proteins: a genome-wide bioinformatic categorization and functional analysis in innate immunity. *Proc. Natl. Acad. Sci.* 2011;108:4631-4638. doi:10.1073/pnas.1000093107.
183. Rainer J. ensembldb: Utilities to create and use Ensembl-based annotation databases. 2018. doi:10.18129/B9.bioc.ensembldb.
184. Edgar RC. MUSCLE: Multiple sequence alignment with high accuracy and high throughput. *Nucleic Acids Res.* 2004. doi:10.1093/nar/gkh340.
185. Schliep KP. phangorn: phylogenetic analysis in R. *Bioinformatics* 2011;27(4):592-3. doi:10.1093/bioinformatics/btq706.
186. Cartegni L, Wang J, Zhu Z, Zhang MQ, Krainer AR. ESEfinder : a web resource to identify exonic splicing enhancers. *Nucleic Acids Res.* 2003;31(13):3568-3571. doi:10.1093/nar/gkg616.
187. Sester DP, Thygesen SJ, Sagulenko V, et al. A Novel Flow Cytometric Method To Assess Inflammasome Formation. *J. Immunol.* 2014. doi:10.4049/jimmunol.1401110.
188. Hoss F, Rolfes V, Davanso MR, Braga TT, Franklin BS. Detection of ASC

Speck Formation by Flow Cytometry and Chemical Cross-linking. In: *Methods in Molecular Biology (Clifton, N.J.)*.Vol 1714.; 2018:149-165. doi:10.1007/978-1-4939-7519-8_10.

189. Raj A, Peskin CS, Tranchina D, Vargas DY, Tyagi S. Stochastic mRNA synthesis in mammalian cells. *PLoS Biol.* 2006;4(10):1707-1719. doi:10.1371/journal.pbio.0040309.
190. Pedraza JM, Paulsson J, Gatfield D, Schneider K, Schibler U, Naef F. Effects of molecular memory and bursting on fluctuations in gene expression. *Science* 2008;319(5861):339-43. doi:10.1126/science.1144331.
191. Rapino F, Robles EF, Richter-larrea JA, Kallin EM, Martinez-Climent JA, Graf T. C/EBPa Induces Highly Efficient Macrophage Transdifferentiation of B Lymphoma and Leukemia Cell Lines and Impairs Their Tumorigenicity. *CellReports* 2013;3(4):1153-1163. doi:10.1016/j.celrep.2013.03.003.
192. Wang H, Mao L, Meng G. The NLRP3 inflammasome activation in human or mouse cells, sensitivity causes puzzle. *Protein Cell* 2013;4(8):565-568. doi:10.1007/s13238-013-3905-0.
193. Martinon F, Tschopp J. Inflammatory caspases and inflammasomes: master switches of inflammation. *Cell Death Differ.* 2007;14(1):10-22. doi:10.1038/sj.cdd.4402038.
194. Park K, Shen BW, Parmeggiani F, Huang PS, Stoddard BL, Baker D. Control of repeat-protein curvature by computational protein design. *Nat. Struct. Mol. Biol.* 2015;22(2):167-174. doi:10.1038/nsmb.2938.
195. Liu M, Grigoriev A. Protein domains correlate strongly with exons in multiple eukaryotic genomes – evidence of exon shuffling? *Trends Genet.* 2004;20(9):399-403. doi:10.1016/J.TIG.2004.06.013.
196. Kolkman JA, Stemmer WPC. Directed evolution of proteins by exon shuffling. *Nat. Biotechnol.* 2001;19(5):423-428. doi:10.1038/88084.
197. Giannuzzi G, Siswara P, Malig M, et al. Evolutionary dynamism of the primate LRRC37 gene family. *Genome Res.* 2013;23(1):46-59. doi:10.1101/gr.138842.112.
198. Little M, Rumballe B, Georgas K, Yamada T, Teasdale RD. Conserved modularity and potential for alternate splicing in mouse and human Slit genes. *Int. J. Dev. Biol.* 2002;46(4):385-91.
199. Ko J. The leucine-rich repeat superfamily of synaptic adhesion molecules: LRRTMs and Slitrks. *Mol. Cells* 2012;34(4):335-340. doi:10.1007/s10059-012-0113-3.
200. Leung E, Hong J, Fraser A, Krissansen GW. Splicing of NOD2 (CARD15)

RNA transcripts. *Mol. Immunol.* 2007;44:284-294. doi:10.1016/j.molimm.2006.03.009.

201. Williams KL, Taxman DJ, Linhoff MW, Reed W, Ting JP. Cutting Edge: Monarch-1: A Pyrin/Nucleotide-Binding Domain/Leucine-Rich Repeat Protein That Controls Classical and Nonclassical MHC Class I Genes. *J. Immunol.* 2003;170:5354-5358. doi:10.4049/jimmunol.170.11.5354.
202. Hoffman HM, Mueller JL, Broide DH, Wanderer a a, Kolodner RD. Mutation of a new gene encoding a putative pyrin-like protein causes familial cold autoinflammatory syndrome and Muckle-Wells syndrome. *Nat. Genet.* 2001;29(3):301-5. doi:10.1038/ng756.
203. Ellis JD, Barrios-Rodiles M, Çolak R, et al. Tissue-Specific Alternative Splicing Remodels Protein-Protein Interaction Networks. *Mol. Cell* 2012;46(6):884-892. doi:10.1016/J.MOLCEL.2012.05.037.
204. Gutierrez-Arcelus M, Ongen H, Lappalainen T, et al. Tissue-Specific Effects of Genetic and Epigenetic Variation on Gene Regulation and Splicing. Brown CD, ed. *PLOS Genet.* 2015;11(1):e1004958. doi:10.1371/journal.pgen.1004958.
205. Katz Y, Wang ET, Silterra J, et al. Quantitative visualization of alternative exon expression from RNA-seq data. *Bioinformatics* 2015;31(14):2400-2402. doi:10.1093/bioinformatics/btv034.
206. Hansen KD, Brenner SE, Dudoit S. Biases in Illumina transcriptome sequencing caused by random hexamer priming. *Nucleic Acids Res.* 2010;38(12):1-7. doi:10.1093/nar/gkq224.
207. Cai G, Liang S, Zheng X, Xiao F. Local sequence and sequencing depth dependent accuracy of RNA-seq reads. *BMC Bioinformatics* 2017;18(1):1-12. doi:10.1186/s12859-017-1780-z.
208. Laehnemann D, Borkhardt A, McHardy AC. Denoising DNA deep sequencing data-high-throughput sequencing errors and their correction. *Brief. Bioinform.* 2016;17(1):154-179. doi:10.1093/bib/bbv029.
209. Hu J, Boritz E, Wylie W, Douek DC. Stochastic principles governing alternative splicing of RNA. *PLoS Comput. Biol.* 2017;13(9):1-20. doi:10.1371/journal.pcbi.1005761.
210. Connor WO, Harton JA, Zhu X, Linhoff MW, Ting JP. Cutting Edge: CIAS1/Cryopyrin/PYPAF1/NALP3/ CATERPILLER 1.1 Is an Inducible Inflammatory Mediator with NF- κB Suppressive Properties. *J. Immunol.* 2003;12(171):6329-6333. doi:10.4049/jimmunol.171.12.6329.
211. Marinov GK, Williams BA, Mccue K, et al. From single-cell to cell-pool

transcriptomes : Stochasticity in gene expression and RNA splicing. *Genome Res.* 2014;24:496-510. doi:10.1101/gr.161034.113.Freely.

212. Sharif O, Bolshakov VN, Raines S, Newham P, Perkins ND. Transcriptional profiling of the LPS induced NF-kappaB response in macrophages. *BMC Immunol.* 2007;8:1. doi:10.1186/1471-2172-8-1.
213. Kubista M, Dreyer-Lamm J, Stalberg A. The secrets of the cell. *Mol. Aspects Med.* 2017. doi:10.1016/j.mam.2017.08.004.
214. Paixão T, Carvalho TP, Calado DP, Carneiro J. Quantitative insights into stochastic monoallelic expression of cytokine genes. *Immunol. Cell Biol.* 2007;(May). doi:10.1038/sj.icb.7100057.
215. Eckersley-Maslin MA, Spector DL. Random monoallelic expression : regulating gene expression one allele at a time. *Trends Genet.* 2014;30(6):237-244. doi:10.1016/j.tig.2014.03.003.
216. Shalek AK, Satija R, Adiconis X, et al. Single-cell transcriptomics reveals bimodality in expression and splicing in immune cells. *Nature* 2013;498(7453):236-40. doi:10.1038/nature12172.
217. Guilliams M, Malissen B. A Death Notice for In-Vitro-Generated GM-CSF Dendritic Cells? *Immunity* 2015;42(6):988-990. doi:10.1016/j.immuni.2015.05.020.
218. Helft J, Böttcher J, Chakravarty P, et al. GM-CSF Mouse Bone Marrow Cultures Comprise a Heterogeneous Population of CD11c+MHCII+ Macrophages and Dendritic Cells. *Immunity* 2015;42(6):1197-1211. doi:10.1016/j.immuni.2015.05.018.
219. Sander J, Schmidt S V, Cirovic B, et al. Cellular Differentiation of Human Monocytes Is Regulated by Time-Dependent Interleukin-4 Article Cellular Differentiation of Human Monocytes Is Regulated by Time-Dependent Interleukin-4 Signaling and the Transcriptional Regulator NCOR2. *Immunity* 2017;47:1051-1066. doi:10.1016/j.immuni.2017.11.024.
220. Jéru I, Hayrapetyan H, Duquesnoy P, Sarkisian T, Amselem S. PYPAF1 nonsense mutation in a patient with an unusual autoinflammatory syndrome: role of PYPAF1 in inflammation. *Arthritis Rheum.* 2006;54(2):508-14. doi:10.1002/art.21618.
221. Zhou J, Zhao S, Dunker AK. Intrinsically Disordered Proteins Link Alternative Splicing and Post-translational Modifications to Complex Cell Signaling and Regulation. *J. Mol. Biol.* 2018. doi:10.1016/J.JMB.2018.03.028.
222. Hornbeck P V., Zhang B, Murray B, Kornhauser JM, Latham V, Skrzypek E. PhosphoSitePlus, 2014: mutations, PTMs and recalibrations. *Nucleic Acids*

Res. 2015;43(D1):D512-D520. doi:10.1093/nar/gku1267.

223. Corey DR. Nusinersen, an antisense oligonucleotide drug for spinal muscular atrophy. *Nat. Neurosci.* 2017;20(4):497-499. doi:10.1038/nn.4508.
224. Lim KR, Maruyama R, Yokota T. Eteplirsen in the treatment of Duchenne muscular dystrophy. *Drug Des. Devel. Ther.* 2017;Volume11:533-545. doi:10.2147/DDDT.S97635.

11. Acknowledgements

Ganz besonders bedanken möchte ich mich bei meinem Doktorvater **Prof. Dr. Eicke Latz**, der mir in seinem Labor ein fantastisches und nahezu unbegrenztes Forschungsumfeld geboten hat, mir maximal Freiheit in der Entwicklung des Projekts gelassen hat und dabei immer an den Erfolg geglaubt hat. Danke für deine Motivation und Unterstützung, deinen wissenschaftlichen Input und für die Möglichkeiten die du mir eröffnet hast.
Ebenfalls bedanken möchte ich mich bei **Prof. Dr. Joachim Schultze**, dafür dass er das Zweitgutachten meiner Doktorarbeit übernommen hat, sowie allen weiteren Mitgliedern der **Prüfungskommission**.

Herzlich bedanken möchte ich mich auch bei **allen Latzis** für ihre Unterstützung und ungezählte Diskussionen ohne die dieses Projekt nicht möglich gewesen wäre, aber auch für viele gemeinsame Stunden auf die ich gerne zurückblicken werde. Mein ganz besonderer Dank gilt in diesem Zusammenhang **Rainer** für die Hilfe bei allen erstellten Plasmiden, **Guddi und Olivia** für ihre Unterstützung wann immer ich eine zusätzliche Hand im Labor gebraucht habe, **Alena, Christina, Juan und Christian** für regelmäßiges Feedback und viele Projektdiskussionen, **Mario** für seine Unterstützung und Freundschaft seit dem ersten Semester und **Andrea** für die Einführung in die Welt des NLRP3 Inflammasomes, ihre ständige Hilfsbereitschaft und nicht zuletzt für das Korrekturlesen dieser Arbeit.

Ein großes Dankeschön gilt auch allen Kooperationspartnern die diese Projekt ermöglicht haben: Allen voran **Prof. Dr. Hal Hoffman und James Mueller** ohne deren initialen Experimente dieses Projekt nie entstanden wäre, außerdem **Prof. Dr. Matthias Geyer und Rebecca Brinkschulte** die mich bei allen strukturbiologischen Fragen unterstützt haben, **Dr. Stefan Canzar und Dr. Francisca R. Ringeling** für ihr bioinformatischen Analysen, **Dr. Gerald Seifert** für seine Hilfe bei der Etablierung der single-cell PCRs, den Mitarbeitern der **FACS core facility** für die Hilfe bei der Entwicklung des FACS ASC-Speck Assays sowie **Moritz Gaidt und Veit Hornung** für die Bereitstellung der BLaER1 Zellen.

Zuletzt möchte ich mich bei meiner **Familie** und meiner Frau **Katharina** für ihre Bedingungslose Unterstützung und die schönen Stunden außerhalb des Labors bedanken.

12. Appendix

12.1. NLR LRR alignments

>NLRP1

PTMVVL**F**RWVP**V**TDAYWQI**L**FSV**L**KVTR
N**L**KE**L**D**L**SGNS**L**SHSAVKS**L**CKT**L**RRPRC
L**L**ET**L**R**L**AGCG**L**TAEDCKD**L**AFG**L**RANQ
T**L**TE**L**D**L**SFNV**L**TDAGAKH**L**CQR**L**RQPSC
K**L**QR**L**Q**L**VSCG**L**TSDCCQD**L**ASV**L**SASP
S**L**KE**L**D**L**QQNN**L**DDVGVRL**L**CEG**L**RHPAC
K**L**IR**L**G**L**DQTT**L**SDEMRQE**L**RALEQEKPQLLIFSR

>NLRP2

N**L**QK**M**S**L**QVIKENLPENVTASESDAEVER
SQDDQHMLPFWTD**L**CSI**F**GSNK
D**L**MG**L**A**I**NDSF**L**SASLVRI**L**CEQ**I**ASDTC
H**L**QR**V**V**F**KNISPA DAHRN**L**CLA**L**RGHK
T**V**TY**L**T**L**QGNDQD DMFPA**L**CEV**L**RHPEC
N**L**RY**L**G**L**VSCSATTQQWAD**L**SLA**L**EVNQ
S**L**TC**V**N**L**SDNE**L**LDEGAKL**L**YTT**L**RHPKC
F**L**QR**L**S**L**ENCH**L**TEANCKD**L**AAV**L**VVSR
E**L**TH**L**C**L**AKNP**I**GNTGVKF**L**CEG**L**RYPEC
K**L**QT**L**V**L**WNCD**I**TSDGCCD**L**TKL**L**QEKS
S**L**LC**L**D**L**GLNH**I**GVKGMKF**L**CEA**L**RKPLC
N**L**RC**L**W**L**WGCS**I**PPFSCED**L**CSA**L**SCNQ
S**L**VT**L**D**L**GQNP**L**GSSGVKM**L**FET**L**TCSSG
T**L**RT**L**R**L**KIDD**F**NDELNK **L**LEE**I**EEKNPQLIIDTEKHHPWAERPSSHDFMI*

>NLRP3

SQQ**I**R**L**E**L**LKWIEVKAKAKK**L**QIQ
PSQ**L**E**L**FYCLYEMQEEDF**V**QRA**M**DYF
PK**I**E**I**N**L**STRMDHMVSSFC**I**ENCH
R**V**ES**L**S**L**GFLHNMPKEEEEEEKEGRHLDM**V**QCV**L**PSSSH
AACS**H**G**L**VNSH**L**TSSFCRG**L**FSV**L**STSQ
S**L**TE**L**D**L**SDNS**L**GDPGMRV**L**CET**L**QHPGC
N**I**RR**L**W**L**GRCG**L**SHECCFD**I**SLV**L**SSNQ
K**L**VE**L**D**L**SDNA**L**GDFGIRL**L**CVG**L**KHLLC
N**L**KK**L**W**L**VSCC**L**TSACCQD**L**ASV**L**STSH
S**L**TR**L**Y**V**GENA**L**GDSGVAI**L**CEK**A**KNPQC
N**L**QK**L**G**L**VNSG**L**TSVCCSA**L**SSV**L**STNQ
N**L**TH**L**Y**L**RGNT**L**GDKGIKL**L**CEG**L**LHPDC
K**L**QV**L**E**L**DNCN**L**TSHCCWD**L**STL**L**TSSQ
S**L**RK**L**S**L**GNND**L**GDLGVMM**F**CEV**L**KQQSC
L**L**QN**L**G**L**SEMY**F**NYETKSA**L**ETLQEEKP
E**L**TV**V**FEPSW*

>NLRP4

S**L**RK**L**C**F**SVQN**V**FKKEDE
HSSTSDYSLICWHH**I**CSV**L**TTSG
H**L**RE**L**Q**V**QDST**L**SESTFVTWCNQ**L**RHPSC
R**L**QK**L**G**I**NNVS**F**S GQSVL**L**FEV**L**FYQP
D**L**KY**L**S**F**TLTK**L**SRDDIRS**L**CDA**L**NYPAG
N**V**KE**L**A**L**VNCH**L**SPIDCEV**L**AGL**L**TNNK
K**L**TY**L**N**V**SCNQ**L**DT GVPL**L**CEA**L**CSPDT
V**L**VY**L**M**L**AFCH**L**SEQCCEY**I**SEM**L**LRNK

SVRYLDLSANVLKDEGLKTLCEALKHPDC
CLDSLCLVKCFITAAGCEDLASALISNQ
NLKILQIGCNEIGDVGVQLLCRALTHTDC
RLEILGLEECGLTSTCCKDLASVLTCSK
TLQQLNLTLNTLDHTGVVVLCEALRHPEC
ALQVLGLRKTDFDEETQALLTAEEERNP
NLTITDDCDTITRVEI*

>NLRP5

IASSFCLQHCPYLRKIRVDVKGIFPRDESAEAC
PVVPLWMRDKTLIEEQWEDFCSMLGTHP
HLRQLDLGSSILTERAMKTLCAKLRHPTC
KIQTLMFRNAQITP GVQHLWRIVMANR
NLRSLNLGGTHLKEEDVRMACEALKHPKC
LLESLRLDCCGLTHACYLKISQILTTSP
SLKSLSLAGNKVTDQGVMPLSDALRVSQC
ALQKLILEDCGITATGCQSLASALVSNR
SLTHLCLSNNSLGNEGVNLLCRSMRLPHC
SLQRLMLNQCHLDTAGCGFLALALMGNS
WLTHLSLSMNPVEDNGVKLLCEVMREPSC
HLQDLELVKCHLTAACCESLSCVISRSR
HLKSLDLTDNALGDGGVAALCEGLKQKNS
VLARLGLKACGLTSDCCEALSLALSCNR
HLTSLNLVQNNFSPKGMMKLCSAFACPTS
NLQIIGLWKWQYPVQIRKLLEEVQLLKPRVVIDGSWHSFDEDDRYWWKN*

>NLRP6

VKQEALRWVQGQGQGCPGVAPEVTEGAKGLEDTEEPEEEEEGEEPNY
PLELLYCLYETQEDAFVRQALC
RFPELALQRVRFCRMDVAVLSYCVRCCP
AGQALRLISCRLVAAQEKKKKSLGKRLQASLGGG
SSSQGTTKQLPASLLHPLFQAMTDPLC
HLSSLTLSHCKLPDAVCRDLSEALRAAP
ALTELGLLHNRLSEAGLRMLSEGLAWPQC
RVQTVRVQLP DPQRGLQYLVGMLRQSP
ALTTLDLSGCQLPAPMVTYLCAVLQHQGC
GLQTLSLASVELSEQSLQELQAVKRAKPDLVITHPALDGHPQPPKELISTF*

>NLRP7

DLQKLSLQVAKGVFLENY
MDF ELDIEFERCTYLTIPNWARQDLRSLRLWTDFCSLFSSNS
NLKFLEVKQSFLSDSSVRILCDHVTRSTC
HLQKVEIKNVTP DTAYRDFCLAFIGKK
TLTHLTLAGHIEWERTMMLMLCDLLRNHKC
NLQYLRLGGHCATPEQWAEFFYVLKANQ
SLKHLRLSANVLLDEGAMLLYKTMTRPKH
FLQMLSLENCRLTEASCKDLAAVLVVSK
KLTHLCLAKNPIGDTGVKFLCEGLSYPDC
KLQTLVLQQCSITKLGCRYLSEALQEAC
SLTNLDLSINQIAR GLWILCQALENPNC
NLKHLRLWSCSLMPFYCQHLGSALLSNQ
KLETLDLGQNHLWKSGIIKLFGVLRQRTG
SLKILRLKTYETNLEIKKLLEEVKEKNP
KLTIDCNASGATAPPCCDFFC*

>NLRP8

TLNFMNVWKLSSSSHPGSE
APESNGLHRWWQDLCSVFATND
KLEVLTMTNSVLGPPFLKALAAALRHPQC
KLQKLLLRRVNSTMLNQDLIGVLTGNQ
HLRYLEIQHVEVESKAVKLLCRVLRSPRC

RLQCLRLEDCLATPRIWTDLGNNLQGNG
HLKTLILRKNSLENCGAYYLSVA
QLERLSIENCNLTQLTCESLASCLRQSK
MLTHLSLAENALKDEGAKHIWNALPHLRC
PLQRLVLRKCDLTFNCCQDMISALCKNK
TLKSLDLSFNSLKDDGVILLCEALKNPDC
TLQILELENCLFTSICCQAMASMLRKNQ
HLRHLDLSKNAIGVYGILTLCEAFSSQKK
REEVIFCIPAWTRITSFSPTPHPPDFTGKSDCLSQINP*

>NLRP9

HLTTLRMCVENIFPDDSGCIS
DYNEKLVYWRELCSMFITNK
NFQILDMENTSLDDPSLAILCKALAQPVC
KLRKLIFTSVYFGH DSELFKAVLHNP
HLKLLSLYGTSLSQSDIRHLCETLKHPMC
KIEELILGKCDISSEVCEDIASVLACNS
KLKHLSLVENPLRDEGMTLLCEALKHSHC
ALERLMLMYCCLTSVSCDSISEVLLCSK
SLSLLDLGSNALEDNGVASLCAALKHPGC
SIRELWLMGCFLTSDSCKDIAAVLICNG
KLKTLKLGHNEIGDTGVRQLCAALQHPHC
KLECLGLQTCPITRACCDDIAAALIACK
TLRSLNLDWIALDADAVVVLCEALSHPDC
ALQMLGLHKSGFDEE TQKILMSVEE
KIPHLTISHGPWIDE EYKIRGVLL*

>NLRP10

no LRR domain

>NLRP11

HHMPLFYCLYENREEEFVKTIVDALMEVTVYLQSDKDMMVSLYCLDYCC
HLRTLKLSVQRIFQNKEPLIRPTA
SQMKSLVYWREICSLFYTME
SLRELHIFDNDLNGISERILSKALEHSSC
KLRTLKLSYVSTAS GFEDLLKALARNR
SLTYLSINCTSISLNMFSLLHDILHEPTC
QISHLSLMKCDLRASECEEIASLLISGG
SLRKLTLSSNPLRSDGMNILCDALLHPNC
TLISLVLVFCCLTENCCSALGRVLLFSP
TLRQLDLCVNRLKNYGVLHVTFPLLFPTC
QLEELHLSGCFFSSDICQYIAIVIATNE
KLRSLEIGSNKIEDAGMQLLCGGLRHPNC
MLVNIGLEECMLTSACCRSLASVLTTNK
TLERLNLLQNHLGNDGVAKLLESLISPDC
VLKVVGLPLTGLNTQTQQLLMTVKERKP
SLIFLSETWSLKEGREIGVTPASQPGSIIPNSNLDYMFFKFPRMSAAMRTSNTASRQPL*

>NLRP12

SAQVLHLYGATYSADGEDRARCSAGAH
TLLVQLPERTVLLDAYSEHLAAALCTNP
NLIELSLYRNALGSRGVKLLCQGLRHPNC
KLQNLRLKRCRISSSACEDLSAALIANK
NLTRMDLSGNGVGFPGMMLLCEGLRHPQC
RLQMIQLRKCQLESGACQEMASVLGTNP
HLVELDLTGNALEDLGLRLLCQGLRHPVC
RLRTLWLKICRLTAAACDELASTLSVNQ
SLRELDLSLNELGDLGVLLLCEGLRHPTC
KLQTLRLGICRLGSAACEGLSVVLQANH
NLRELDLSFNDLGDWGLWLLAEGLQHPAC
RLQKLWLDSCGLTAKACENLYFTLGINQ

```
     TLTDLYLTNNALGDTGVRLLCKRLSHPGC
     KLRVLWLFGMDLNKMTHSRLAALRVTKPYLDIGC*

>NLRP13
     EVDLNILEDEELQASSFC LKHCK
     RLNKLRLSVSSHILERDLEIL
          ETSKFDSRMHAWNSICSTLVTNE
     NLHELDLSNSKLHASSVKGLCLALKNPRC
     KVQKLTCKS VTPEWVLQDLIIALQGNS
     KLTHLNFSSNKLGMTV PLILKALRHSAC
     NLKYLCLEKCNLSAASCQDLALFLTSIQ
     HVTRLCLGFNRLQDDGIKLLCAALTHPKC
     ALERLELWFCQLAAPACKHLSDALLQNR
     SLTHLNLSKNSLRDEGVKFLCEALGRPDG
     NLQSLNLSGCSFTREGCGELANALSHNH
     NVKILDLGENDLQDDGVKLLCEALKPHR
     ALHTLGLAKCNLTTACCQHLFSVLSSSK
     SLVNLNLLGNELDTDGVKMLCKALKKSTC
     RLQKLG*

>NLRP14
VKQLERTFNCKMSLKIKSKLLQCMEVLGNSDYSPS
     QLGFLELFHCLYETQDKAFISQAMRCFPKVAINICEKIHLLVSSFCLKHCRC
      LRTIRLSVTVVFEKKILKTSLPTNT
            WDGDRITHCWQDLCSVLHTNE
     HLRELDLYHSNLDKSAMNILHHELRHPNC
     KLQKLLLKFITFPD GCQDISTSLIHNK
     NLMHLDLKGSDIGDNGVKSLCEALKHPEC
     KLQTLRLESCNLTVFCCLNISNALIRSQ
     SLIFLNLSTNNLLDDGVQLLCEALRHPKC
     YLERLSLESCGLTEAGCEYLSLALISNK
     RLTHLCLADNVLGDGGVKLMSDALQHAQC
     TLKSLVLRRCHFTSLSSEYLSTSLLHNK
     SLTHLDLGSNWLQDNGVKLLCDVFRHPSC
     NLQDLELMGCVLTNACCLDLASVILNNP
     NLRSLDLGNNDLQDDGVKILCDALRYPNC
     NIQRLGLEYCGLTSLCCQDLSSALICNK
     RLIKMNLTQNTLGYEGIVKLYKVLKSPKC
     KLQVLGLCKEAFDEEAQKLLEAVGVSNPHLIIKPDCNYHNEEDVSWWWCF*

>NLRC3
     ALAYLLQVSDACAQEANLSLSLSQGVLQSLLPQLL
     YCRKLRLDTNQFQDPVMELLGSVLSGKDC
     RIQKISLAENQISNKGAKALARSLLVNR
     SLTSLDLRGNSIGPQGAKALADALKINR
     TLTSLSLQGNTVRDDGARSMAEALASNR
     TLSMLHLQKNSIGPMGAQRMADALKQNR
     SLKELMFSSNSIGDGGAKALAEALKVNQ
     GLESLDLQSNSISDAGVAALMGALCTNQ
     TLLSLSLRENSISPEGAQAIAHALCANS
     TLKNLDLTANLLHDQGARAIAVAVRENR
     TLTSLHLQWNFIQAGAAQALGQALQLNR
     SLTSLDLQENAIGDDGACAVARALKVNT
     ALTALYLQVASIGASGAQVLGEALAVNR
     TLEILDLRGNAIGVAGAKALANALKVNS
     SLRRLNLQENSLGMDGAICIATALSGNH
     RLQHINLQGNHIGDSGARMISEAIKTNAPTCTVEM*

>NLRC4
     GKSLYINSGNIPDYLFDFFEHLPNCASAL
      DFIKLDFYGGAMASWEKAAEDTGGIHMEEAPETYIPSRAVSLFFNWKQE
```

FRTLEVTLRDFSKLNKQDIRYLGKIFSS
ATSLRLQIKRCAGVAGSLSLVLSTC
KNIYSLMVEASPLTIEDERHITSVT
NLKTLSIHDLQNQRL PGGLTDSLGNLK
NLTKLIMDNIKMNEEDAIKLAEGLKNLK
KMCLFHLTHLSDIGEGMDYIVKSLSSEPC
DLEEIQLVSCCLSANAVKILAQNLHNLV
KLSILDLSENYLEKDGNEALHELIDRMNVLE
QLTALMLPWGCDVQGSLSSLLKHLEEVP
QLVKLGLKNWRLTDTEIRILGAFFGKNPLK
NFQQLNLAGNRVSSDGWLAFMGVFENLK
QLVFFDFSTKEFLPDPALVRKLSQVLSKLT
FLQEARLVGWQFDDDDLSVITGAFKLVTA*

>NLRC5

LPYQLPFHNFPLTCTDLATLTNILEHRE
API HLDFDGCPLEPHCPEALVGCG
QIENLSFKSRKCGDAFAEALSRSLPTMG
RLQMLGLAGSKITARGISHLVKALPLCP
QLKEVSFRDNQLSDQVVLNIVEVLPHLP
RLRKLDLSSNSICVSTLLCLARVAVTCP
TVRMLQAREADLIFLLSPPTETTAELQ
RAPDLQESDGQRKGAQSRSLTLRLQKCQLQVHDAEALIALLQEGP
HLEEVDLSGNQLEDEGCRLMAEAASQLH
IARKLDLSNNGLSVAGVHCVLRAVSACW
TLAELHISLQHKTVIFMFAQEPEEQKGPQERAA
FLDSLMLQMPSELPLSSRRM
RLTHCGLQEKHLEQLCKA LGGSC
HLGHLHLDFSGNALGDEGAARLAQLLPGLG
ALQSLNLSENGLSLDAVLGLVRCFSTLQ
WLFRLDISFESQHILLRGDKTSRDMWATGSLPDFPAAAKFLGFRQRC
IPRSLCLSECPLEPPSLTRLCATLKDCP
GPLELQLSCEFLSDQSLETLLDCLP
QLPQLSLLQLSQTGLSPKSPFLLANTLSLCP
RVKKVDLRSLHHATLHFRSNEEEEGVCCGRFTGCSLSQEHVE
SLCWLLSKCKDLSQVDLSANLLGDSGLRCLLECLPQVP
ISGLLDLSHNSISQESALYLLETLPSCP
RVREASVNLGSEQSFRIHFSREDQ
AGKTLRLSECSFRPEHVSRLATGLSKSL
QLTELTLTQCCLGQKQLAILLSLVGRPA
GLFSLRVQEPWADRARVLSLLEVCAQASG
SVTEISISETQQQLCVQLEFPRQEENP
EAVALRLAHCDLGAHHSLLVGQLMETCA
RLQQLSLSQVNLCEDDDASSLLLQSLLLSLS
ELKTFRLTSSCVSTEGLAHLASGLGHCH
HLEELDLSNNQFDEEGTKALMRALEGKW
MLKRLDLSHLLLNSSTLALLTHRLSQMT
CLQSLRLNRNSIGDVGCCHLSEALRAAT
SLEELDLSHNQIGDAGVQHLATILPGLP
ELRKIDLSGNSISSAGGVQLAESLVLCR
RLEELMLGCNALGDPTALGLAQELPQ
HLRVLHLPFSHLGPGGALSLAQALDGSP
HLEEISLAENNLAG GVLRFCMELP
LLRQIDLVSCKIDNQTAKLLTSSFTSCP
ALEVILLSWNLLGDEAAAELAQVLPQMG
RLKRVDLEKNQITALGAWLLAEGLAQGS
SIQVIRLWNNPIPCDMAQHLKSQEPRLDFAFFDNQPQAPWGT*

>NOD1

RLTVLRLSVNQITDGGVKVLSEELTKYK
IVTYLGLYNNQITDVGARYVTKILDECK

GLTHLKLGKNKITSEGGKYLALAVKNSK
SISEVGMWGNQVGDEGAKAFAEALRNHP
SLTTLSLASNGISTEGGKSLARALQQNT
SLEILWLTQNELNDEVAESLAEMLKVNQ
TLKHLWLIQNQITAKGTAQLADALQSNT
GITEICLNGNLIKPEEAKVYEDEKRIICF*

>NOD2

NVGHLKLTFCSVGPTECAALAFVLQHLR
RPVALQLDYNSVGDIGVEQLLPCLG
VCKALYLRDNNISDRGICKLIECALHCE
QLQKLALFNNKLTDGCAHSMAKLLACRQ
NFLALRLGNNYITAAGAQVLAEGLRGNT
SLQFLGFWGNRVGDEGAQALAEALGDHQ
SLRWLSLVGNNIGSVGAQALALMLAKNV
MLEELCLEENHLQDEGVCSLAEGLKKNS
SLKILKLSNNCITYLGAEALLQALERND
TILEVWLRGNTFSLEEVDKLGCRD
TRLLL*

>NLRX1

SLRQLNLAGVRMTPVKCTVVAAVLGSGRH
ALDEVNLASCQLDPAGLRTLLPVFL
RARKLGLQLNSLGPEACKDLRDLLLHDQC
QITTLRLSNNPLTAAGVAVLMEGLAGNT
SVTHLSLLHTGLGDEGLELLAAQLDRNR
QLQELNVAYNGAGDTAALALARAAREHP
SLELLHLYFNELSSEGRQVLRDLGGAAE
GGARVVVSLTEG
TAVSEYWSVILSEVQRNLNSWDRARVQRHLELLLRDLEDSRGATLNPWRKAQLLRVEGEVRALLEQLGS
SGS*

>NAIP

NLDKFLCLKELSVDLEGNINVFSVIPEEFPNFHHMEKLLIQISAEYDPS
KLVKLIQNSP
NLHVFHLKCNFFSDFGSLMTMLVSCK
KLTEIKFSDSFFQAVPFVASLPNFI
SLKILNLEGQQFPDEETSEKFAYILGSLS
NLEELILPTGDGIYRVAKLIIQQCQ
QLHCLRVLSFFKTLNDDSVVEIAKVAISGGFQ
KLENLKLSINHKITEEGYRNFFQALDNMP
NLQELDISRHFTECIKAQATTVKSLSQC
VLRLPRLIRLNMLSWLLDADDIALLNVMKER
HPQSKYLTILQKWILPFSPIIQK*

CIITA

DLKKLEFALGPVSGPQAFPKLVRILTAFS
SLQHLDLDALSENKIGDEGVSQLSATFPQLK
SLETLNLSQNNITDLGAYKLAEALPSLAA
SLLRLSLYNNCICDVGAESLARVLPDMV
SLRVMDVQYNKFTAAGAQQLAASLRRCP
HVETLAMWTPTIPFSVQEHLQQQDSRISLR*

Figure 12-1 LRR alignments of all NLRs
LRR exons are highlighted in alternating grey values. Each line represents one leucine-rich repeat (LRR). Conserved residues defining the LRR fold are highlighted in bold.

12.2. Mapping statistics of RNAseq reads

	Donor 1	Donor 2	Donor 3	Donor 4	Donor 5
Number of input reads	134943073	16097467	154640058	162862993	176498896
Average input read length	252	252	252	252	252
Uniquely mapped reads	123424533	146198305	144276036	149360709	163061729
Uniquely mapped reads %	91.46%	90.82%	93.30%	91.71%	91.71%
Average mapped length	245.03	245.74	245.49	245.33	244.5
Mismatch rate per base %	0.44%	0.42%	0.42%	0.43%	0.43%
Multi-mapping reads	6119358	9613436	4915572	7108225	5922473
Multi-mapping reads %	4.57%	6.01%	3.21%	4.39%	3.40%
Un-mapped reads %	3.97%	3.16%	3.50%	3.90%	4.21%

Table 12-1 Mapping statistics of RNAseq reads for each donor

12.3. Sashimi plots

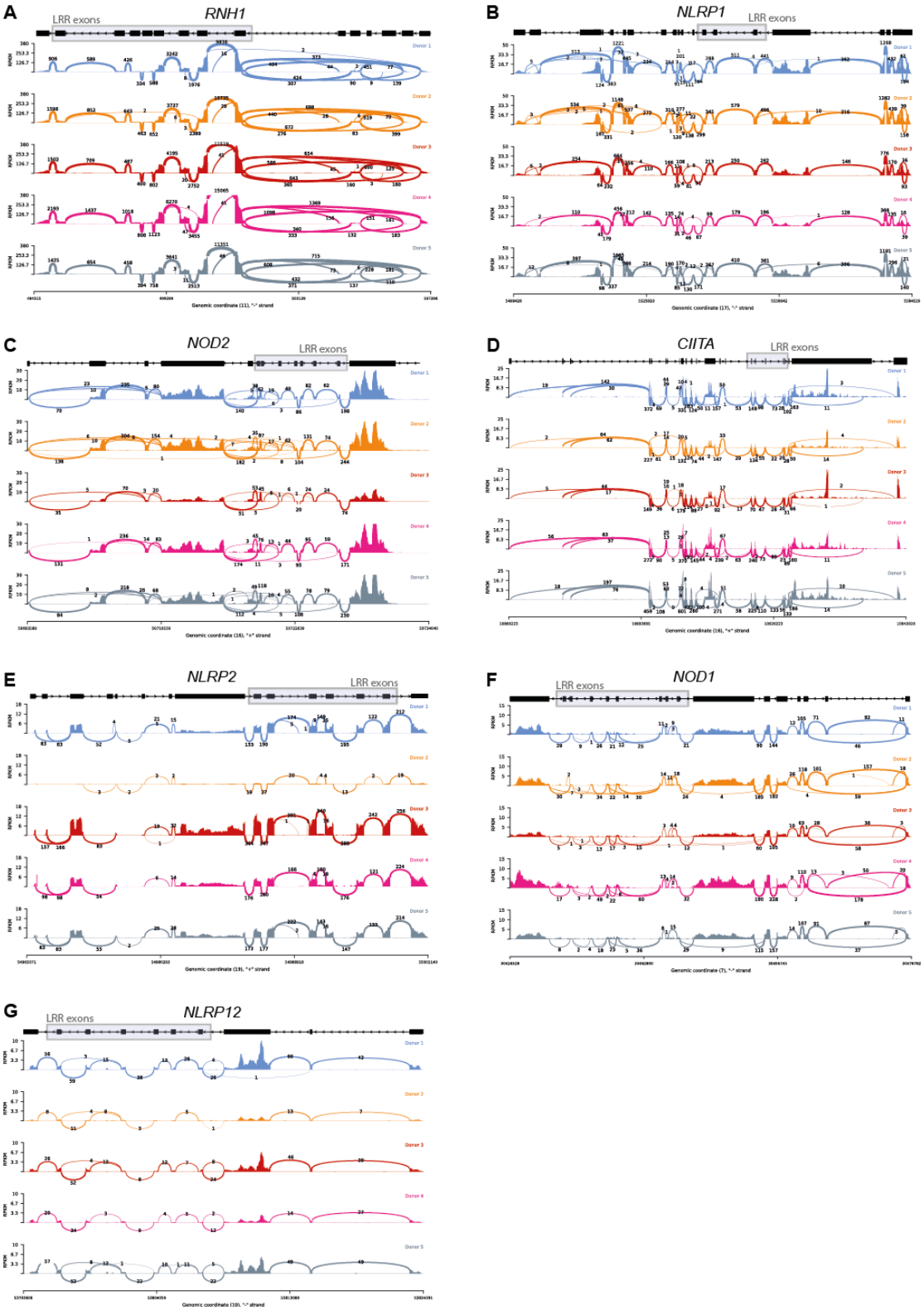

Figure 12-2 Sashimi plots of all expressed genes listed in Error! Reference source not found. **A**
A RNH1, **B** NLRP1, **C** NOD2, **D** CIITA, **E** NLRP2, **F** NOD1 and **G** NLRP12.

12.4. Protein sequences of NLRP3 variants

12.4.1. NLRP3 full-length

MKMASTRCKLARYLEDLEDVDLKKFKMHLEDYPPQKGCIPLPRGQTEKADHVDLATLMIDFN
GEEKAWAMAVWIFAAINRRDLYEKAKRDEPKWGSDNARVSNPTVICQEDSIEEEWMGLLEY
LSRISICKMKKDYRKKYRKYVRSRFQCIEDRNARLGESVSLNKRYTRLRLIKEHRSQQEREQ
ELLAIGKTKTCESPVSPIKMELLFDPDDEHSEPVHTVVFQGAAGIGKTILARKMMLDWASGTL
YQDRFDYLFYIHCREVSLVTQRSLGDLIMSCCPDPNPPIHKIVRKPSRILFLMDGFDELQGAF
DEHIGPLCTDWQKAERGDILLSSLIRKKLLPEASLLITTRPVALEKLQHLLDHPRHVEILGFSEA
KRKEYFFKYFSDEAQARAAFSLIQENEVLFTMCFIPLVCWIVCTGLKQQMESGKSLAQTSKTT
TAVYVFFLSSLLQPRGGSQEHGLCAHLWGLCSLAADGIWNQKILFEESDLRNHGLQKADVS
AFLRMNLFQKEVDCEKFYSFIHMTFQEFFAAMYYLLEEEKEGRTNVPGSRLKLPSRDVTVLL
ENYGKFEKGYLIFVVRFLFGLVNQERTSYLEKKLSCKISQQIRLELLKWIEVKAKAKKLQIQPS
QLELFYCLYEMQEEDFVQRAMDYFPKIEINLSTRMDHMVSSFCIENCHRVESLSLGFLHNMP
KEEEEEEKEGRHLDMVQCVLPSSSHAACSHGLVNSHLTSSFCRGLFSVLSTSQSLTELDLS
DNSLGDPGMRVLCETLQHPGCNIRRLWLGRCGLSHECCFDISLVLSSNQKLVELDLSDNAL
GDFGIRLLCVGLKHLLCNLKKLWLVSCCLTSACCQDLASVLSTSHSLTRLYVGENALGDSGV
AILCEKAKNPQCNLQKLGLVNSGLTSVCCSALSSVLSTNQNLTHLYLRGNTLGDKGIKLLCEG
LLHPDCKLQVLELDNCNLTSHCCWDLSTLLTSSQSLRKLSLGNNDLGDLGVMMFCEVLKQQ
SCLLQNLGLSEMYFNYETKSALETLQEEKPELTVVFEPSW

12.4.2. NLRP3 ∆ exon 5

MKMASTRCKLARYLEDLEDVDLKKFKMHLEDYPPQKGCIPLPRGQTEKADHVDLATLMIDFN
GEEKAWAMAVWIFAAINRRDLYEKAKRDEPKWGSDNARVSNPTVICQEDSIEEEWMGLLEY
LSRISICKMKKDYRKKYRKYVRSRFQCIEDRNARLGESVSLNKRYTRLRLIKEHRSQQEREQ
ELLAIGKTKTCESPVSPIKMELLFDPDDEHSEPVHTVVFQGAAGIGKTILARKMMLDWASGTL
YQDRFDYLFYIHCREVSLVTQRSLGDLIMSCCPDPNPPIHKIVRKPSRILFLMDGFDELQGAF
DEHIGPLCTDWQKAERGDILLSSLIRKKLLPEASLLITTRPVALEKLQHLLDHPRHVEILGFSEA
KRKEYFFKYFSDEAQARAAFSLIQENEVLFTMCFIPLVCWIVCTGLKQQMESGKSLAQTSKTT
TAVYVFFLSSLLQPRGGSQEHGLCAHLWGLCSLAADGIWNQKILFEESDLRNHGLQKADVS
AFLRMNLFQKEVDCEKFYSFIHMTFQEFFAAMYYLLEEEKEGRTNVPGSRLKLPSRDVTVLL
ENYGKFEKGYLIFVVRFLFGLVNQERTSYLEKKLSCKISQQIRLELLKWIEVKAKAKKLQIQPS
QLELFYCLYEMQEEDFVQRAMDYFPKIEINLSTRMDHMVSSFCIENCHRVESLSLGFLHNMP
KEEEEEEKEGRHLDMVQCVLPSSSHAACSHGLGRCGLSHECCFDISLVLSSNQKLVELDLS
DNALGDFGIRLLCVGLKHLLCNLKKLWLVSCCLTSACCQDLASVLSTSHSLTRLYVGENALG
DSGVAILCEKAKNPQCNLQKLGLVNSGLTSVCCSALSSVLSTNQNLTHLYLRGNTLGDKGIKL
LCEGLLHPDCKLQVLELDNCNLTSHCCWDLSTLLTSSQSLRKLSLGNNDLGDLGVMMFCEV
LKQQSCLLQNLGLSEMYFNYETKSALETLQEEKPELTVVFEPSW

12.4.3. NLRP3 2x exon 6

MKMASTRCKLARYLEDLEDVDLKKFKMHLEDYPPQKGCIPLPRGQTEKADHVDLATLMIDFN
GEEKAWAMAVWIFAAINRRDLYEKAKRDEPKWGSDNARVSNPTVICQEDSIEEEWMGLLEY
LSRISICKMKKDYRKKYRKYVRSRFQCIEDRNARLGESVSLNKRYTRLRLIKEHRSQQEREQ
ELLAIGKTKTCESPVSPIKMELLFDPDDEHSEPVHTVVFQGAAGIGKTILARKMMLDWASGTL
YQDRFDYLFYIHCREVSLVTQRSLGDLIMSCCPDPNPPIHKIVRKPSRILFLMDGFDELQGAF
DEHIGPLCTDWQKAERGDILLSSLIRKKLLPEASLLITTRPVALEKLQHLLDHPRHVEILGFSEA
KRKEYFFKYFSDEAQARAAFSLIQENEVLFTMCFIPLVCWIVCTGLKQQMESGKSLAQTSKTT

TAVYVFFLSSLLQPRGGSQEHGLCAHLWGLCSLAADGIWNQKILFEESDLRNHGLQKADVS
AFLRMNLFQKEVDCEKFYSFIHMTFQEFFAAMYYLLEEEKEGRTNVPGSRLKLPSRDVTVLL
ENYGKFEKGYLIFVVRFLFGLVNQERTSYLEKKLSCKISQQIRLELLKWIEVKAKAKKLQIQPS
QLELFYCLYEMQEEDFVQRAMDYFPKIEINLSTRMDHMVSSFCIENCHRVESLSLGFLHNMP
KEEEEEEKEGRHLDMVQCVLPSSSHAACSHGLGRCGLSHECCFDISLVLSSNQKLVELDLS
DNALGDFGIRLLCVGLKHLLCNLKKLWLGRCGLSHECCFDISLVLSSNQKLVELDLSDNALGD
FGIRLLCVGLKHLLCNLKKLWLVSCCLTSACCQDLASVLSTSHSLTRLYVGENALGDSGVAIL
CEKAKNPQCNLQKLGLVNSGLTSVCCSALSSVLSTNQNLTHLYLRGNTLGDKGIKLLCEGLL
HPDCKLQVLELDNCNLTSHCCWDLSTLLTSSQSLRKLSLGNNDLGDLGVMMFCEVLKQQSC
LLQNLGLSEMYFNYETKSALETLQEEKPELTVVFEPSW

12.4.4. NLRP3 exon 5 surface to exon 6

MKMASTRCKLARYLEDLEDVDLKKFKMHLEDYPPQKGCIPLPRGQTEKADHVDLATLMIDFN
GEEKAWAMAVWIFAAINRRDLYEKAKRDEPKWGSDNARVSNPTVICQEDSIEEEWMGLLEY
LSRISICKMKKDYRKKYRKYVRSRFQCIEDRNARLGESVSLNKRYTRLRLIKEHRSQQEREQ
ELLAIGKTKTCESPVSPIKMELLFDPDDEHSEPVHTVVFQGAAGIGKTILARKMMLDWASGTL
YQDRFDYLFYIHCREVSLVTQRSLGDLIMSCCPDPNPPIHKIVRKPSRILFLMDGFDELQGAF
DEHIGPLCTDWQKAERGDILLSSLIRKKLLPEASLLITTRPVALEKLQHLLDHPRHVEILGFSEA
KRKEYFFKYFSDEAQARAAFSLIQENEVLFTMCFIPLVCWIVCTGLKQQMESGKSLAQTSKTT
TAVYVFFLSSLLQPRGGSQEHGLCAHLWGLCSLAADGIWNQKILFEESDLRNHGLQKADVS
AFLRMNLFQKEVDCEKFYSFIHMTFQEFFAAMYYLLEEEKEGRTNVPGSRLKLPSRDVTVLL
ENYGKFEKGYLIFVVRFLFGLVNQERTSYLEKKLSCKISQQIRLELLKWIEVKAKAKKLQIQPS
QLELFYCLYEMQEEDFVQRAMDYFPKIEINLSTRMDHMVSSFCIENCHRVESLSLGFLHNMP
KEEEEEEKEGRHLDMVQCVLPSSSHAACSHGLGRSGLSHEFCFGLSLVLSTSQKLVELDLS
DNALGDFGMRVLCVTLKHPLCNIKKLWLGRCGLSHECCFDISLVLSSNQKLVELDLSDNALG
DFGIRLLCVGLKHLLCNLKKLWLVSCCLTSACCQDLASVLSTSHSLTRLYVGENALGDSGVAI
LCEKAKNPQCNLQKLGLVNSGLTSVCCSALSSVLSTNQNLTHLYLRGNTLGDKGIKLLCEGL
LHPDCKLQVLELDNCNLTSHCCWDLSTLLTSSQSLRKLSLGNNDLGDLGVMMFCEVLKQQS
CLLQNLGLSEMYFNYETKSALETLQEEKPELTVVFEPSW

12.4.5. NLRP3 2x exon 6 surface rescue

MKMASTRCKLARYLEDLEDVDLKKFKMHLEDYPPQKGCIPLPRGQTEKADHVDLATLMIDFN
GEEKAWAMAVWIFAAINRRDLYEKAKRDEPKWGSDNARVSNPTVICQEDSIEEEWMGLLEY
LSRISICKMKKDYRKKYRKYVRSRFQCIEDRNARLGESVSLNKRYTRLRLIKEHRSQQEREQ
ELLAIGKTKTCESPVSPIKMELLFDPDDEHSEPVHTVVFQGAAGIGKTILARKMMLDWASGTL
YQDRFDYLFYIHCREVSLVTQRSLGDLIMSCCPDPNPPIHKIVRKPSRILFLMDGFDELQGAF
DEHIGPLCTDWQKAERGDILLSSLIRKKLLPEASLLITTRPVALEKLQHLLDHPRHVEILGFSEA
KRKEYFFKYFSDEAQARAAFSLIQENEVLFTMCFIPLVCWIVCTGLKQQMESGKSLAQTSKTT
TAVYVFFLSSLLQPRGGSQEHGLCAHLWGLCSLAADGIWNQKILFEESDLRNHGLQKADVS
AFLRMNLFQKEVDCEKFYSFIHMTFQEFFAAMYYLLEEEKEGRTNVPGSRLKLPSRDVTVLL
ENYGKFEKGYLIFVVRFLFGLVNQERTSYLEKKLSCKISQQIRLELLKWIEVKAKAKKLQIQPS
QLELFYCLYEMQEEDFVQRAMDYFPKIEINLSTRMDHMVSSFCIENCHRVESLSLGFLHNMP
KEEEEEEKEGRHLDMVQCVLPSSSHAACSHGLVNCHLTSSCCRDIFSVLSSNQSLTELDLSD
NSLGDPGIRLLCEGLQHLGCNLRRLWLGRCGLSHECCFDISLVLSSNQKLVELDLSDNALGD
FGIRLLCVGLKHLLCNLKKLWLVSCCLTSACCQDLASVLSTSHSLTRLYVGENALGDSGVAIL
CEKAKNPQCNLQKLGLVNSGLTSVCCSALSSVLSTNQNLTHLYLRGNTLGDKGIKLLCEGLL
HPDCKLQVLELDNCNLTSHCCWDLSTLLTSSQSLRKLSLGNNDLGDLGVMMFCEVLKQQSC
LLQNLGLSEMYFNYETKSALETLQEEKPELTVVFEPSW

12.5. Physico-chemical properties of NLRP3 isoforms and artificial variants

	full-length	∆ exon 5	2x exon 6	exon 5 with exon 6 surface	2x exon 6 surface rescue
Sizes (bp)	3108	2937	3108	3108	3108
No. of amino acids	1036	979	1036	1036	1036
Molecular weight (Dalton)	118172.58	111884.42	118181.9	118170.86	118183.62
^No. of − ve charged residue	134	129	135	134	135
No. of + ve charged residue	122	118	124	124	122
Theoretical pI	6.22	6.24	6.28	6.33	6.17
Instability index	45.6	45.1	43.53	43.89	46
Aliphatic index	92.88	92.61	94.86	94.01	93.73
GRAVY	-0.203	-0.213	-0.177	-0.182	-0.198

Table 12-2 Physico-chemical properties of NLRP3 isoforms and artificial variants
Physico-chemical characteristics of the NLRP3 full-length, ∆ exon 5 and the three artificial hybrids containing a doubled exon 6 but no exon 5, a duplication of all exon 6 surface amino acids on to exon 5 or a rescue of all surface amino acids of exon 5 on the doubled exon 6 backbone. Values were calculated with the ExPASy ProtParam tool.